Department of Energy
Office of Civilian Radioactive Waste Management
Yucca Mountain Site Characterization Office
P.O. Box 364629
North Las Vegas, NV 89036-8629

QA: N/A

AUG 2 9 2002

Distribution

DISTRIBUTION OF THE IGNEOUS CONSEQUENCES PEER REVIEW PANEL INTERIM REPORT

Reference: Ltr, Dyer to Distribution, dtd 8/15/02

Enclosed is the Igneous Consequences Peer Review Panel's Interim Report. The Panel will present the results of their Interim Report on September 5, 2002, from 8 a.m. to 5 p.m. at the JW Marriott Las Vegas, 221 North Rampart Drive, as previously announced in the referenced letter.

If you have questions, please contact Eric T. Smistad at (702) 794-5073 or Jean L. Younker at (702) 295-5497.

J. Russell Dyer
Project Manager

OPE:ETS-1685

Enclosure:
As stated

YMP-5

Margaret Chu, DOE/HQ (RW-1), FORS
R. B. Murthy, DOE/OQA (RW-3), Las Vegas, NV
R. M. Latta, NRC, Las Vegas, NV
J. R. Schlueter, NRC, Rockville, MD
J. S. Trapp, NRC, Rockville, MD
R. K. Major, ACNW, Rockville, MD
Budhi Sagar, CNWRA, San Antonio, TX
W. D. Barnard, NWTRB, Arlington, VA
David Franklin, Naval Reactors, Las Vegas, NV
Jerry Reynoldson, Senator Harry Reid's Office,
    Las Vegas, NV
Sonia Joya, Senator John Ensign's Office,
    Las Vegas, NV
Kevin Kirkeby, Senator John Ensign's Office,
    Carson City, NV
Judy Ray, Congressman Jim Gibbon's Office,
    Las Vegas, NV
B. J. Gerber, Congressman Jim Gibbons's Office,
    Reno, NV
Tod Story, Congresswoman Shelley Berkley's Office,
    Las Vegas, NV
R. I. Holden, National Congress of American Indians,
    Washington, DC
Allen Ambler, Nevada Indian Environmental
    Coalition, Fallon, NV
R. R. Loux, State of Nevada, Carson City, NV
Marjorie Paslov-Thomas, Legislative Counsel
    Bureau, Carson City, NV
Irene Navis, Clark County, Las Vegas, NV
Alan Kalt, Churchill County, Fallon, NV
George McCorkell, Esmeralda County, Goldfield, NV
Leonard Fiorenzi, Eureka County, Eureka, NV
Andrew Remus, Inyo County, Independence, CA
Mickey Yarbro, Lander County, Battle Mountain, NV
Lola Stark, Lincoln County, Caliente, NV
Arlo Funk, Mineral County, Hawthorne, NV
L. W. Bradshaw, Nye County, Pahrump, NV
Josie Larson, White Pine County, Ely, NV
J. N. Pegues, City of Las Vegas, Las Vegas, NV
S. A. Orrell, BSC/SNL, Las Vegas, NV
F. V. Perry, BSC/LANL, Los Alamos, NM
K. G. Hess, BSC, Las Vegas, NV

D. W. Pearman, Jr., BSC, Las Vegas, NV
CMS Coordinator, BSC, Las Vegas, NV
S. J. Cereghino, BSC, Las Vegas, NV
T. E. Rodgers, BSC, Las Vegas, NV
M. D. Voegele, BSC, Las Vegas, NV
N. H. Williams, BSC, Las Vegas, NV
R. C. Murray, MTS, Las Vegas, NV
Bruce Parks, USGS, Denver, CO
R. J. Budnitz, Future Resources Associates, Inc.,
    Berkeley, CA
Abigail Johnson, Abigail C. Johnson Consulting,
    Carson City, NV
Steve Kraft, NEI, Washington, DC
R. C. Perman, Geomatrix, Oakland, CA
J. H. Kessler, EPRI, Palo Alto, CA
Chris Binzer, Robison-Seidler, Henderson, NV
Rex Massey, RMA Research, Reno, NV
Mike Baughman, Intertech Services, Corporation,
    Carson, City, NV
J. R. Dyer, DOE/YMSCO, Las Vegas, NV
D. G. Horton, DOE/YMSCO, Las Vegas, NV
W. J. Boyle, DOE/YMSCO, Las Vegas, NV
Stephan Brocoum, DOE/YMSCO, Las Vegas, NV
S. H. Hanauer, DOE/YMSCO, Las Vegas, NV
G. W. Hellstrom, DOE/YMSCO, Las Vegas, NV
A. V. Gil, DOE/YMSCO, Las Vegas, NV
S. P. Mellington, DOE/YMSCO, Las Vegas, NV
A. E. Van Luik, DOE/YMSCO, Las Vegas, NV
J. D. Ziegler, DOE/YMSCO, Las Vegas, NV

Yucca Mountain Igneous Consequences Peer Review Panel

Robert J. Budnitz, Future Resources Associates Inc. (Chair)

Emmanuel M. Detournay, University of Minnesota

Larry Mastin, U.S. Geological Survey

J.R. Anthony Pearson, Schlumberger Cambridge Research, UK

Allan M. Rubin, Princeton University

Frank J. Spera, University of California at Santa Barbara

Interim Report

23 August 2002

Yucca Mountain Igneous Consequences Peer Review Panel

Robert J. Budnitz, Future Resources Associates Inc. (Chair)

Emmanuel M. Detournay, University of Minnesota

Larry Mastin, U.S. Geological Survey

J.R. Anthony Pearson, Schlumberger Cambridge Research, UK

Allan M. Rubin, Princeton University

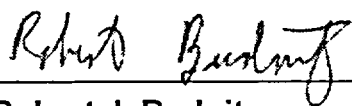Frank J. Spera, University of California at Santa Barbara
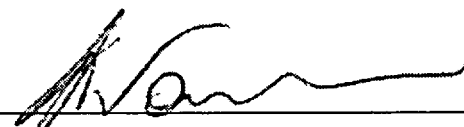
Interim Report

23 August 2002

Yucca Mountain Igneous Consequences
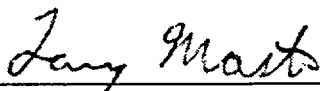# Peer Review Panel

SIGNATURE PAGE (Panel Members)

Robert J. Budnitz

Emmanuel M. Detournay

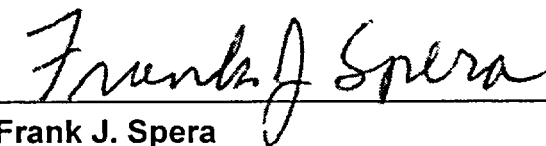Larry Mastin

J.R. Anthony Pearson

Allan M. Rubin

Frank J. Spera

Table of Contents

Chapter 0

Introduction

0.1   Background

For several years, the issue of whether volcanic/igneous events are an important contributor to overall risk from the U.S. Department of Energy's proposed Yucca Mountain Repository has been under consideration both within the Yucca Mountain Project ("the Project") itself and within the staff and contractors of the U.S. Nuclear Regulatory Commission (NRC). Other interested parties such as the State of Nevada and the U.S. Nuclear Waste Technical Review Board have also given the issue important consideration. Much technical work has been done to examine and evaluate this issue, and more is underway and planned.

In early 2002, at the request of the U.S. Department of Energy's Office of Civilian Radioactive Waste Management, Bechtel SAIC Company LLC formed the "Igneous Consequences Peer Review Panel", to review the technical basis used to analyze the consequences of igneous events that might impact the repository and to recommend any additional tasks that would significantly strengthen the program. As part of the Panel's initial instruction, BSC charged it with examining a set of eight questions, which are displayed in Table 0-1 (see next page).

The Panel was formed in the spring of 2002. Its membership consists of six individuals, selected by the Project's senior management. These individuals are working under contractual agreements with the Project, and the Project is also providing administrative support (for setting up meetings and conference calls, for document dissemination, etc.), but otherwise the Panel is working entirely independently of the Yucca Mountain Project.

0.2 Panel membership

The Panel's membership is as follows (see Table 0-2 for addresses, etc.):

Robert J. Budnitz, Future Resources Associates Inc. (Chair)
Emmanuel M. Detournay, University of Minnesota
Larry G. Mastin, U.S. Geological Survey
J.R. Anthony Pearson, Schlumberger Cambridge Research, UK
Allan M. Rubin, Princeton University
Frank J. Spera, University of California at Santa Barbara

TABLE 0-1

Questions for the Igneous Consequences Peer Review Panel

1. Conceptual Model:
   a. Is the conceptual model adequate for framing the analysis?
   b. Does the conceptual model allow for consideration of the key physical processes that are likely to significantly influence magma/drift interactions?
   c. Have any key processes or parameters been omitted that should be accounted for in the model?

2. What level of analysis (e.g., hand calculations versus code calculations) is "sufficient" to capture the nature of magma/drift interactions, given the uncertainties inherent in the input parameters (e.g., magma properties, repository environment)?

3. Quantitative modeling:
   a. Are the software codes chosen for the analysis adequate to model the anticipated physical processes?
   b. Will the modeling adequately account for all significant fluid dynamic processes expected to occur during a transient or sustained magma/drift interaction?
   c. Will the modeling adequately account for rock-mechanics processes that may affect magma/drift interactions and subsequent magma pathways and eruption characteristics?
   d. Are the physical parameters necessary to model magma/drift interactions likely to be sufficiently constrained to produce results with a "reasonable" level of confidence?
   e. Are the assumptions underlying the models appropriate?

4. What alternatives to the modeling approach are feasible, including experimental alternatives?

5. What is the appropriate role of analog studies for understanding magma/drift interactions? (e.g., literature review of historic volcanoes to understand analogous magmatic processes or examples of magmatic intrusions that have interacted with geologic or human-engineered structures)

6. Will the planned modeling provide results that reasonably and realistically represent magma/drift interaction in terms of drift temperature, pressure, and magma inflow and outflow?

7. Will the uncertainties of the models be readily quantifiable? Will it be possible to easily discriminate uncertainties resulting from uncertainties in input parameters versus uncertainties in understanding of complexities of physical processes? To what extent should the uncertainties be quantified, given the intended use of the model outputs to constrain issues such as waste package damage and the possibility that the presence of the repository will influence magma pathways to the surface?

8. Are the methods proposed for use in validating the modeling models adequate?

Table 0-2

**Roster of the
Yucca Mountain Igneous Consequences Peer Review Panel**

Robert J. Budnitz – Chair
Future Resources Associates, Inc.
2039 Shattuck Avenue, Suite 402
Berkeley, CA 94704
Phone: (510) 644-2700, Fax: (510) 644-1117; e-mail: budnitz@pacbell.net

Emmanuel M. Detournay
Professor, Department of Civil Engineering
University of Minnesota
160 Civ E
500 Pillsbury Dr SE
Minneapolis, MN 55455
Phone: (612) 625-3043; e-mail: detou001@umn.edu

Larry G. Mastin
U.S. Geological Survey
Cascades Volcano Observatory
1300 SE Cardinal Court, Bldg 10, Suite 100
Vancouver, WA 98661
Phone: (360) 993-8925; Fax: (360) 993-8980; e-mail: lgmastin@usgs.gov

J. R. Anthony Pearson
Schlumberger Cambridge Research
High Cross, Madingley Road
Cambridge CB3 0EL, UK
Phone: 011 44 1223 3509276 (w); 011 44 1223 350927
e-mail: anthonypearson1@ntlworld.com

Allan M. Rubin
Professor, Department of Geosciences
Princeton University
Princeton, NJ 08544
Phone: (609) 258-1506; Fax: (609) 258-1274; e-mail: arubin@princeton.edu

Frank J. Spera
Professor, Department of Geological Sciences
2118 Webb Hall
University of California
Santa Barbara, CA 93106
Phone: (805) 893-4880; Fax: (805) 893-2314; e-mail: spera@geol.ucsb.edu

0.3 Panel's *modus operandi*

The *modus operandi* of the Panel has been and will continue to be to gather relevant information, to discuss the issues among the Panel's membership, to perform analysis needed to support tentative Panel positions, and finally to develop two reports (this "Interim Report" and a "Final Report" due in December 2002), aimed at addressing the questions in the Panel charter (Table 0-1). The Panel's work has thus involved both the *review of previous work* and also the *performance of original work* -- original calculations, development of original conceptual models of the phenomena, etc.

The information-gathering aspect has taken many different forms, including receiving and reading reports and memoranda from the Project, from NRC contractors, and from the general public. The Panel has also been active in seeking information from colleagues throughout the world where appropriate, and in interacting with them.

The Panel began its work with a public meeting held in Las Vegas on May 21-22, 2002. The objective of that kick-off meeting was strictly information-gathering --- the agenda included presentations by several experts working for the Project as well as by experts working for the NRC. The agenda was established through discussions between the Panel's chairman and members of the Yucca Mountain Project staff. During the meeting, opportunities to speak were also afforded to the general public. In addition, a general public appeal was made during that meeting to send the Panel any relevant information, in the form of reports or memoranda, from anywhere worldwide. (Subsequently, numerous pieces of information in the form of reports, memoranda, and telephone calls were in fact received from experts and from members of the public, and this information has greatly assisted the Panel.)

During the evening after the two-day public meeting, the Panel met in executive session to plan its work, and on the next day members took a one-day field trip to visit the Yucca Mountain site (above and below ground) and also the nearby Lathrop Wells cinder cone. Accompanying the Panel on that field trip were various volcanism experts selected by the Project with the Panel chairman's concurrence.

Since that May meeting and field trip, the Panel's work has consisted of studying various reports; of interacting not only with experts within the Project and within NRC's contractor group but also experts outside; and of interactions within the Panel itself. A good deal of preliminary analysis was performed by Panel members, along with a large number of speculative and exploratory discussions by telephone and email, as the Panel members worked to assess what the important issues are, and why, and which information gathered or sent in is important (or not), and why. This sorting process is, of course, the essence of what technical experts do when confronted by a new and difficult problem.

The number of technical topics to be covered was large, and so the Panel "assigned" one or two of its members to take a "lead" role for each topic, so that each Panel member could concentrate on his own areas of special expertise. This "lead role" also carried with it the assignment to write the first draft of one or more sections of this Interim Report. However, despite the specialization, each Panel member took care to inform all of the others of nearly all of his thinking as it progressed, which made for a mountain of correspondence for everyone to sort through, but also led to important insights from all of the various members on the full set of topics.

0.4 The nature of this "Interim Report"

One major caveat is in order here. Specifically, this is an "Interim Report", and as such it makes no pretense of representing the Panel's final position on any of the technical subjects covered. It is a "snapshot in time" of the Panel's views as of the time of its release, and is to be understood as a *work-in-progress*, nothing more nor less.

First is the issue of scope. This Interim Report does not cover each of the issues raised by the Panel's sponsors and shown in Table 0-1 --- some of the issues have not yet been addressed adequately, although the Panel expects that they will be before the Final Report is completed.

Second, the way this Interim Report was developed, by individual Panel members writing draft sections for circulation to the others, but *without sufficient opportunity for interaction among the whole Panel working together*, means that this report must be considered a "bottoms-up" piece of work, assembled into a whole from its pieces, rather than a "top-down" piece of work, assembled by starting with overall consideration of the major issues and then writing the technical report from that perspective. The Panel recognizes that this Interim Report is therefore defective to that extent. This "reductionist" character is clearly recognizable to the reader; it represents the way individual scientists go about their work. The Panel recognizes that this Interim Report suffers because not enough effort has yet been devoted to the other way of approaching the Panel's charge, which is an "integrationist" approach.

One example of this is that not enough advantage is taken (by cross-referencing in the other chapters) of the wealth of technical information in Chapter 1, and conversely not enough cross-referencing to later chapters can be found in Chapter 1. A second example is that the so-called "dog-leg" scenario, in which magma comes up a dike, goes down one or more drifts, and then breaks through and continues upward to the surface at a distance from where it originally broke through into the drift. This scenario is discussed, in terms of both its likelihood and the associated phenomena, in several different chapters, and from different

perspectives. In an integrated approach, which the Panel expects to take in its Final Report, the "dog-leg" issue would be treated more comprehensively in one integrated discussion. In this Interim Report, the scattered nature of the "dog-leg" discussions, arising from the way the various chapters were written without the opportunity for enough integration, has perhaps obscured the Panel's main message (which is that this issue requires significantly more work before it will be well-enough understood).

This report is also defective to the extent that *every position taken here is subject to reconsideration and reevaluation* as the remainder of the Panel's work proceeds.

Furthermore, not all of the technical topics requiring examination have been covered well enough during this initial period. Some important topics within the Panel's charter are absent here or are dealt with in only a preliminary or tentative way.

Despite the caveats above, the Panel does of course stand fully behind this report, if it is understood for what it is and what it is not. Specifically, the findings, conclusions, and recommendations contained herein should be of value to the Interim Report's readers because they describe the Panel's thinking as of now, and they can perhaps be particularly useful to those now working on the volcanism issue as they continue their ongoing work, but *they are tentative.*

0.5   This Interim Report's principal findings/conclusions and recommendations

This Interim Report contains many findings, conclusions, and recommendations. As mentioned just above, the spirit in which these are offered is that they are tentative, and subject in every case to reconsideration as the Panel continues with its work over the four-month period before its Final Report is due in late December 2002.

At first, the plan had been to gather the most of these into a "summary section", where they could be listed and given prominence. However, all too many of the most important ones are embedded in a section of text where the surrounding text provides the context and the explanatory background for the finding, conclusion, or recommendation.

Therefore, as a convenience for the authors and we hope as an aid to the reader, the principal findings, conclusions, and recommendations have been left in the

text where they arise, but are highlighted to assist the reader. Specifically, <u>each principal finding or conclusion can be found in underlined text</u> and **each principal recommendation can be found in bold text.** The text of this Interim Report is, therefore, literally sprinkled throughout by <u>underlined text</u> and **text in bold type**, to call out to the reader where a finding, conclusion, or recommendation is to be found. Also, the "header" at the top of each page will continually remind the reader of this <u>underlining</u> and **bold-text** technique. (See the "header" at the top of this page and also at the top of each subsequent page.)

0.6   Acknowledgments

The Panel wishes to thank Jean Younker and Thomas Rodgers of Bechtel SAIC Company for their assistance in expediting the Panel's work. The resolution of numerous issues, both technical and administrative, was accomplished through the fine work of these two individuals. The Panel also wishes to acknowledge the outstanding support of Mark Board of BSC, Frank Perry of Los Alamos National Laboratory, and Peter Swift of Sandia National Laboratories.

The Panel's work has been carried out under a set of individual contracts with Bechtel SAIC Company LLC, which in turn is under contract to the Office of Civilian Radioactive Waste Management of the U.S. Department of Energy.

Chapter 1

Magma Properties

The purpose of this chapter is to review and establish the essential thermodynamic and transport properties of magma relevant to potential magma-drift interactions at the proposed Yucca Mountain Repository (YMR). Although the probability of igneous disruption at YMR is low [1.6×10^{-8} yr^{-1} or 1 chance in 6250 over 10,000 years (SSPA)], this value exceeds the NRC criterion of 1 chance in 10,000 over 10,000 years and, consequently, igneous disruption is deemed a credible risk [10 CFR 63.114(d, e, f)]. The consequences of igneous disruption must therefore be fully explored. Knowledge of the composition and properties (thermodynamic and transport) of magma relevant to potential igneous disruption is essential in order to characterize the complex dynamics and thermal consequences of magma-drift interaction.

1.1   Synopsis of volcanic history in Crater Flats region

The following summary of the volcanic history of the Yucca Mountain area is provided for geological context and to establish the likely composition and crystallinity of magma of relevance to potential igneous disruption of the potential Yucca Mountain Repository (YMR). Details of this summary are drawn mainly from *LA-13478, Volcanism Studies: Final Report for Yucca Mountain Project* (December 1998), and include other literature sources as well. Additional information from F. Perry and B. Hill in the timeframe May-August, 2002, in the form of private communications, was also evaluated.

Miocene silicic volcanism in the Yucca Mountain region was succeeded by late Miocene-Quaternary basaltic volcanic activity. The basaltic activity can be divided into two major episodes: basalt of the silicic episode (BSE) that occurred during the waning stage of silicic volcanism (>8Ma) and Postcaldera basalt (PB) from ~9 million years (Ma) to the Quaternary. The Postcaldera episode can be further subdivided into the Older Postcaldera basalts (OPB) which outcrop north and northeast of Yucca mountain and the Younger Postcaldera basalts (YPB) which crop out west, southwest and south of Yucca mountain. The OPB ages range from ~ 9 Ma (basalt of Pahute Mesa) to ~6.3 Ma (basalt of Nye Canyon); a crude estimate of the total eruptive volume of the OPB cycle is ~ 1 km^3. There is a volcanic hiatus of about 2.5 Ma (from 7.2 Ma to 4.7 Ma) in the Yucca Mountain region that separates the Older Post-caldera Basalts (OPB) and the Younger Post-caldera Basalts (YPB).

The YPB have been studied more intensely in the field and laboratory (geochronology and geochemistry) compared to the older BSE and OPB volcanic rocks because, <u>it is argued</u> in *LA-13478, Volcanism Studies: Final Report for Yucca Mountain Project* <u>that the YPB part of the post-caldera magmatic record provides the critical basis for forecasting future possible magmatic activity at YMR. The Panel agrees with this assessment. Basaltic rather than silicic magmatism represents the most likely igneous event in the Yucca Mountain region in the next 10 ka and the record of the Quaternary volcanic history of the Crater Flat Volcanic Zone (CFVZ) is most relevant to possible activity in the future.</u> From a geologic perspective it is impossible to unequivocally rule out other types of magmatism *a priori*. However, the 'recent' past (i.e., the past million years or the Quaternary) is the best guide to the future.

In order of decreasing age, the basalts of the YPB include the basalt of Thirsty Mesa, the basalt of Amargosa Valley, the Pliocene basalt of southeast Crater Flat, the basaltic andesite of Buckboard Mesa, the Quaternary basalt of Crater Flat, the basalt of Sleeping Butte and the Lathrop Wells basalt. Except for the basaltic andesite of Buckboard Mesa, all YPB products lie within a narrow northwest-trending zone located west and south of Yucca Mountain termed the Crater Flat Volcanic Zone (CFVZ) by Crowe and Perry (1989). Information on the age, petrographic characteristics, volume and composition of the Younger Post-caldera Basalts of the CFVZ are summarized in Table 1-1 which is based upon Tables 2.1, 2.A and 2.B in *LA-13478, Volcanism Studies: Final Report for Yucca Mountain Project* (December 1998) and Table 1 (eruptive volume estimates) from TDR-NBS-GS-000016 REV 00 *Data Qualification Report: Data Related to Characterization of eruptive Processes for Use on the Yucca Mountain Project* (May 2000).

TABLE 1 - 1
VOLCANIC HISTORY of CRATER FLATS VOLCANIC ZONE

YPB Unit	Age ± 2σ (Ma)	Volume (km³)	Phenocrysts	Composition
Thirsty Mesa	4.88(±0.04) 4.68(±0.03)	3	Sparse olivine	Potassic trachybasalt
Amargosa Valley	3.85 ±0.05	~ 0 8 not exposed at surface		
Pliocene basalt of southeast Crater Flat	3 75 ±0.04 3.69 ±0.06 3.65 ±0.06	0.68	ol>plag>cpx (Σ ~ 15 vol %)	
Buckboard Mesa	3.15 ±0.08 3.08 ±0.04	1	Olivine & sparse amphibole	Trachyandesite
Quaternary basalts of Crater Flat (Little Cones, Red Cone, Black Cone, and Makani Cone)	Little Cones 0.77 ±0.02 0,83 ±0.16 1.02 ±0.10	0.002	Olivine & sparse amphibole at Red Cone & Little Cones	Potassic trachybasalt
	Red Cones 0.92 ±0.06 1.05 ±0.14 1.08 ±0.04	0.105		
	Black Cone 0.94 ±0.05 0.96 ±0.15 1.05 ±0.08 1.05 ±0.14 1.10 ±0 05	0.105		
	Makani Cone 1.16 ±0.10 1.17 ±0.06	0 006		
Sleeping Butte	Hidden Cone 0.56 ±0.10 0.32 ±0.03	0.03	Sparse amphibole	potassic trachybasalt
	Little Black Peak 0.39 ±0.03 0.36 ±0.04	0.03		
Lathrop Wells Cone	~ 0.075 ±0.10	0.14	Sparse olivine	potassic trachybasalt to subalkaline basalt

Cumulative eruptive volume versus time data based upon Table 1-1 is graphically portrayed in Figure 1-1. The integrated volumetric eruption rate averaged over the past 4.78 Ma is 1.22 km^3Ma^{-1} or 0.012 km^3 per 10,000 years. The integrated rate over the past 1 Ma is 0.43 km^3 Ma^{-1} or 0.004 km^3 per 10,000 years. The integrated rate over the past 100 ka is 1.4 km^3 Ma^{-1} or 0.014 km^3 per 10,000 years.

────●──── Volume (cubic km)

cum vol vs time YMR
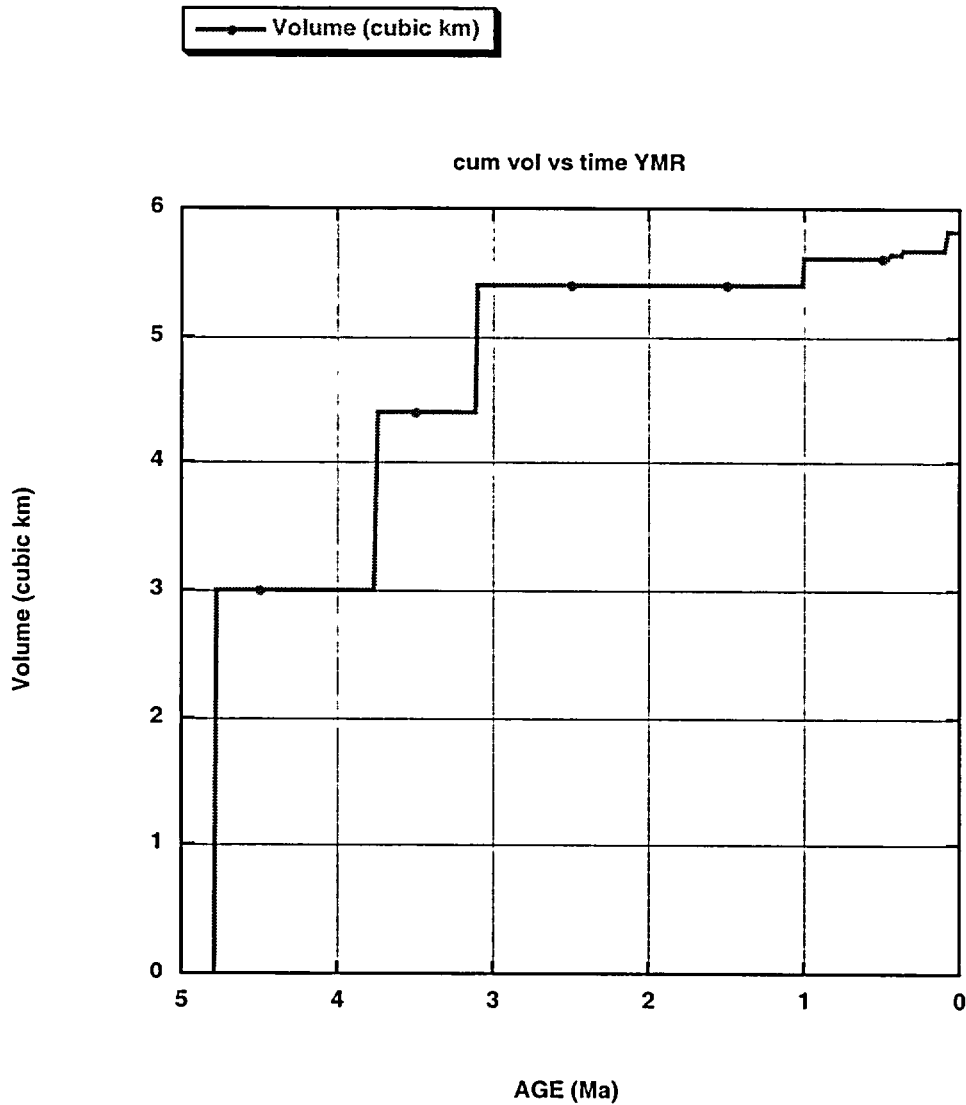
Figure 1-1

Cumulative Eruptive Magma Volume vs. Age in Ma (Million Years Before Present) (see Table 1-1)

1.2   Key aspects of volcanic history relevant to magma properties

The salient aspects of Pliocene to Quaternary volcanism in the CFVZ relevant to previous and future analyses of potential igneous disruption at YMR can be summarized:

(1) <u>The most likely magma composition of potential renewed magmatism in the CFVZ is a potassic trachybasalt</u> (IUGS classification). This is in agreement with conclusions expressed in *ANL-MGR-GS-000002, REV 00, ICN 01 CHARACTERIZE ERUPTIVE PROCESSES AT YUCCA MOUNTAIN, NEVADA* (Dec. 2001) where an average of ~ 45 compositions from Lathrop Wells (LW) was used to define a representative bulk composition for use in dynamical models. Rather than calculate a volume-weighted mean composition of all Pliocene to Quaternary basalts from the CFVZ, choosing solely Lathrop Wells eruptive products makes sense because: (a) LW is the youngest volcanism in the Yucca Mountain Region; (b) Based on the dispersal pattern of LW tephra, LW volcanism was probably at least as or more explosive than other Quaternary events at CFVZ. <u>Hence analysis of ash dispersal relevant to TSPA is conservative</u> based on behavior at LW; and (c) The LW eruption of volume 0.14 km^3 is the most voluminous eruption in the CFVZ within the last 3 Ma. A representative devolatilized mean reference composition used in further property and dynamical calculations is given in Table 1-2. We consider this a reasonable composition of a potential Disruptive Yucca Mountain Basalt (DYMB).

TABLE 1-2

Estimated DYMB reference composition (dry)

Oxide	Percent by Mass
SiO_2	48.99
TiO_2	1.95
Al_2O_3	16.91
Fe_2O_3	1.76
FeO	8.99
MnO	0.17
MgO	5.89
CaO	8.69
Na_2O	3.57
K_2O	1.86
P_2O_5	1.23
TOTAL	100.00

(2) Based on the observed phenocryst content of Quaternary CFVZ eruptive products, the phenocryst content of potential magma relevant to igneous disruption at YMR is small (~ few modal percent). The presence of sparse olivine phenocrysts (with or without spinel inclusions) suggests that the Quaternary eruptive products at CFVZ were not undergoing cotectic crystallization at depth before eruption. Coexistence of groundmass olivine, plagioclase, clinopyroxene and magnetite suggests that the Quaternary basalts of Crater Flats and the Lathrop Wells basalt did reach multiple saturation (cotectic crystallization) upon decompression in the very near surface. <u>Hence, melt viscosity estimates based on aphyric melts of LW composition are appropriate below the depth of volatile saturation.</u>

(3) The presence of sparse phenocrysts of amphibole in some of the Quaternary basalts of Crater Flat and at Hidden Cone (basalt of Sleeping Butte) puts a constraint on the pre-eruptive dissolved H_2O content of some magmas of the CFVZ. In addition, the petrographically-inferred sequence of crystallization at Lathrop Wells, with olivine (ol) and spinel (sp) as liquidus phases followed by monoclinic pyroxene (cpx) and anorthitic plagioclase (plag) puts constraints on the dissolved H_2O content of the melt at the time of crystal growth.

(4) The presence of significant basaltic tephra at Lathrop Wells indicates that the volume fraction of supercritical fluid (θ), composed mainly of components H-O-C-S-Cl-F by analogy with other basaltic systems, exceeded the critical volume fraction (θ_{crit}) associated with the rheological transition from bubbly flow to pyroclast flow. The important issues for igneous consequences include:

      (a) composition (speciation) of the vapor evolved during shallow-level decompression;

      (b) dependence of the fragmentation depth (pressure) on the temperature, mass fraction and bulk composition of volatiles in the two-phase magmatic (melt plus coexisting vapor) mixture.

1.3   Volatile content of possible disruptive magma at YMR

<u>The devolatilized bulk composition developed in *ANL-MGR-GS-000002, REV 00, ICN 01 Characterize Eruptive Processes at Yucca Mountain, Nevada* (hereafter referred to as CEPYM) is considered representative.</u> The ascent and eruption dynamics is intimately related to the composition and abundance of the volatiles. *Precise* information on the volatile content of magmas is generally difficult to establish even when eruptive products are available for study. Predicting *a priori* the precise abundance of volatiles is virtually impossible. <u>However, the abundance of magmatic volatiles *can* be estimated within certain bounds and</u>

these bounds then used to quantify the properties of possible Disruptive Yucca Mountain Basalt (DYMB) magma.

The presence of amphibole, a hydroxyl-bearing phase can in principle constrain the water fugacity (f_{H2O}) and hence dissolved H_2O content of melt. Experiments or detailed calculations taking account of potential magma composition, oxygen fugacity and presence of dissolved CO_2 and SO_2 were not carried out or cited in CEPYM. Instead, a literature survey was undertaken and it was concluded that a H_2O content between 1 and 3 weight per cent (wt%) is most likely. This estimate is based on (1) measured H_2O contents of basaltic magmas worldwide and (2) the experimental observation of amphibole saturation in basaltic melts similar in bulk composition to LW and the Quaternary basalts of Crater Flat containing 2 to 5 wt% dissolved H_2O.

In order to examine this issue further, calculations were undertaken using the MELTS algorithm (Ghiorso, 1997, 1999) for the bulk composition presented in Table 1 (this report). This is a model calculation because activity-composition relations for Ti-bearing amphibole are not available. At 50 MPa and 1220 °C there is no water content that causes saturation with amphibole. At 50 MPa the dry liquidus temperature is 1182 °C on the QFM oxygen fugacity buffer and the liquidus phase is olivine (Fo_{81}). The minimum chemical affinity for phase saturation of amphibole at 1220 °C and 50 MPa occurs at 2.5 wt % H_2O. At higher pressures of 100 MPa and 300 MPa the dry liquidi are 1186 °C and 1200 °C, respectively and the minimum chemical affinity for amphibole phase saturation occurs at 2.5 wt % H_2O. Thermochemical calculations suggest that amphibole is not stabilized at any pressure at ~ 1200 °C. Additional calculations reveal that at 100 MPa amphibole saturation occurs with 2.2 wt % H_2O at 1010 °C. Because the amphibole activity-composition model used in MELTS does not incorporate the effects of TiO_2, these results can not be considered definitive. However, based on the H_2O content of the melts at which amphibole does attain its minimum chemical affinity and allowing for the probable effects of TiO_2 on the stability of amphibole, we estimate that the maximum stability of amphibole occurs at a H_2O content of ~ 2.5 wt %. Multiple phase saturation of amphibole, olivine, clinopyroxene, plagioclase and Fe-Ti oxides (magnetite crystalline solution) occurs at temperature in the range 1025-1100 °C at 100 MPa based on the estimated effects of Ti in stabilizing amphibole in a potassic trachybasalt bulk composition. The results of these thermochemical computations are broadly consistent with the conclusions in "CEPYM" pertaining to likely H_2O contents of potential DYMB. Note that the LW basalts do not contain amphibole and that the Fluorine (F) content of amphibole present in older CF basalts has not been determined to our knowledge. **Some effort should be directed to studying the composition and abundance and phase relations of the amphibole-bearing CF basalts; this is relatively inexpensive. The Halogen content of the vapor site occupied by (OH, F, O, Cl) in amphibole phenocrysts should be determined and further systematic thermochemical computations be undertaken to attempt to further refine the constraint imposed by**

amphibole presence in some CF basaltic rocks. D/H ratios can be determined in the amphibole as well.

Because the Lathrop Wells basalts do not contain amphibole, it is important to consider constraints on the dissolved water content imposed by examination of the sequence of crystallization of anhydrous phases present as phenocrysts and microphenocrysts. Isobaric (100 MPa) simulations of fractional crystallization of DYMB composition (Table 1-2) (above) plus varying amounts of H_2O (dry, 1 wt %, 2 wt %, 3 wt %, 4 wt %) using the MELTS algorithm (Ghiorso, 1997) and comparison with Lathrop Wells basalts suggests dissolved H_2O contents were between 2 to 4 wt % H_2O at the time of phenocryst growth. At $<\sim2$ wt % dissolved H_2O, plagioclase is the liquidus phase in contradiction with observations; between about 2.5 wt % and 4 wt % H_2O, spinel and olivine are on the liquidus and monoclinic pyroxene and plagioclase saturate about 60 K below the liquidus. This is qualitatively consistent with petrographic observation. **The conclusion is that DYMB may contain circa 2.5 to 4 wt% dissolved H_2O.**

There are few constraints on the CO_2 content of potential DYMB. One approach is to argue by analogy using measured, estimated or inferred CO_2 concentrations from studies on other potassic trachybasalts worldwide. Estimates of dissolved CO_2 concentrations from other mildly alkaline basalts generally fall in the range 0.2- 0.6 wt%. Another approach is to examine glass and possible fluid inclusions within olivine, pyroxene and plagioclase phenocrysts from the Quaternary potassic trachybasalts basalts of Crater Flat. Although these data would not provide an unambiguous assessment, they would provide some information regarding total volatile contents and the $H_2O:CO_2$ ratios. The significance of including CO_2 explicitly is that the solubility of H_2O, the primary magmatic volatile, is affected by the concentration of CO_2 in the system. Because the solubility of CO_2 in basaltic melts is considerably smaller than H_2O solubility, even small amounts of CO_2 in the system lead to formation of a vapor phase. This vapor phase will contain H_2O even at conditions of temperature, pressure and total H_2O content inconsistent with H_2O exsolution in the absence of CO_2. Consequently, the depth at which exsolution of vapor and eventually magma fragmentation occurs can be influenced by the concentration of CO_2 in the magma. Dynamical models for the ascent and decompression of potential DYMB, should include the effects of mixed volatiles. **Although inclusion of S-bearing species (H_2S, SO_2, H_2S) would be optimal, at the least mixed H_2O-CO_2 volatiles should be taken into account.**

In order to study in more detail the effects of mixed volatiles, the mixed volatile model of Papale (1999) has been used to compute the dissolved volatile content of potential DYMB (composition presented in Table 1-1) for a range of temperatures, pressures, total volatiles, and different $H_2O: CO_2$ ratios. Because of inherent uncertainty in the total (H_2O+CO_2) volatile content of DYMB, calculations were carried out for total magma (volatile-saturated melt plus vapor) $H_2O + CO_2$ contents of 1, 2, 3 and 4 wt% with (in each case) a $H_2O:CO_2$ ratio of

2:1, 4:1 and 6:1. Values for the density of melt, vapor and two-phase (melt plus vapor) magma, the mass fraction, volume fraction and composition of the vapor phase and melt viscosity as a function of pressure in the range 0.1-100 MPa for temperatures of 1080 °C, 1150 °C and 1220 °C were computed. These results are too extensive to present in this Interim Report. Instead results are presented for the single case of 3 wt % total volatiles, a H_2O: CO_2 ratio of 6 and a temperature 1423 K (1150 °C). The total system H_2O and CO_2 are 2.6 wt % and 0.4 wt %, respectively. These results can be compared to Figures 1 and 2 in CEPYM. The main differences are as follows:

(a) The depth at which volatile exsolution begins is deeper than that estimated in CEPYM because of inclusion of CO_2. **Future comprehensive models should include mixed volatiles explicitly including CO_2. The effects that S-bearing species might have on exsolution and magma fragmentation depths should also be considered.**

(b) **The fragmentation depth is similarly affected by the presence of mixed H_2O+CO_2 volatiles and could be modeled quantitatively using more recent thermodynamic (e.g., Papale, 1999) and transport models (e.g., Mastin, 2002) including a more detailed treatment of the separated flow regime.**

(c) **Melt, magma and vapor properties, necessary input for dynamical models, should be computed self-consistently once a thermodynamic solubility model is adopted using the latest algorithms to compute melt isobaric heat capacity, density and melt viscosity.**

The Panel does not believe that any of these factors would produce qualitatively different results from those presented in CEPYM; however, until such work is done one cannot be certain and the investment in time and effort is relatively modest. A critical parameter is the variation of the volume fraction of vapor (θ) with pressure and translation of that pressure to depth given the ambient stress field and notions of the fracture mechanics associated with magma transport in the shallow crust beneath Yucca Mountain, as outlined elsewhere in this Interim Report (mainly in Chapter 2). One may anticipate distinct consequences of magma-drift interaction depending on the state of the magma at the time of drift breaching. Is magma an 'incompressible' (melt-dominated) viscous flow or a quasi-homogeneous melt + bubble mixture or a separated flow of volatile-saturated melt and vapor each with a distinct mean velocity? Complexity arises because all three and possibly other regimes may be applicable at different times and different locations in the drift system during a disruptive event.

Another approach to study magmatic volatiles is to carry out experiments on an DYMB composition with careful control of water, oxygen and carbon dioxide fugacity, temperature and pressure. The composition of all crystalline products could be determined to assess the effects of volatiles and other thermodynamic variables on the compositions of phenocrysts and groundmass crystalline

phases. Although such an experimental program would improve estimates of the precise volatile content of potential DYMB, it is not expected that the estimate of ~2 to 3.5 wt% H_2O and 0.2 to 0.5 wt% CO_2 (the dominant volatile constituents) would markedly change. In other words, uncertainties associated with the choice of devolatilized starting materials and the laboratory control of experimental variables probably fall within the range of volatile contents given above. Experimental petrological studies of DYMB to better characterize magmatic volatile contents are assigned a secondary level of importance at least until more through thermochemical modeling is accomplished.

VAPOR COMPOSITION

$T = 1150\ ^{0}C$

$Z^{0}_{H_2O} + Z^{0}_{CO_2} = 3\ wt\ \%$

Ratio $H_2O:CO_2 = 6:1$

w_{H2O}^{v}
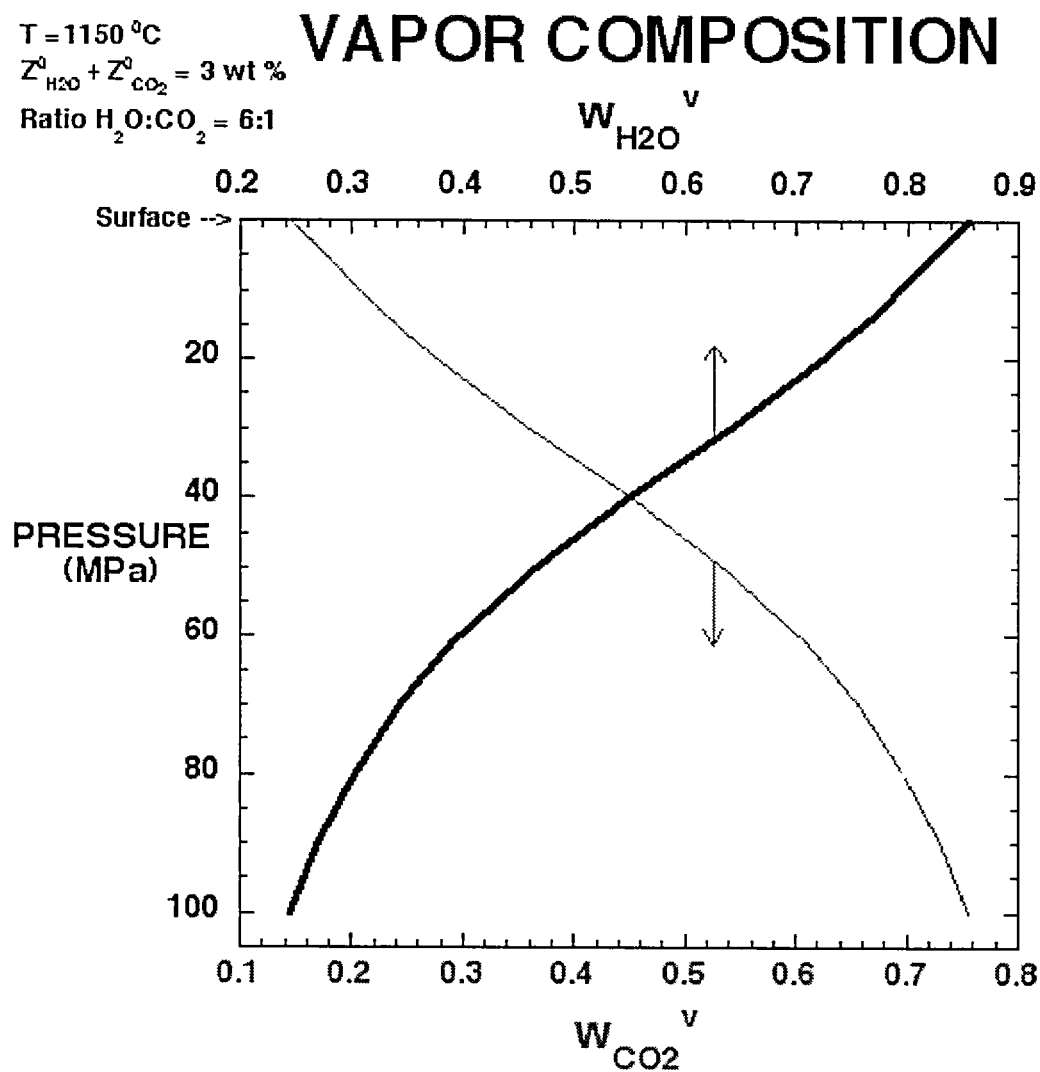
w_{CO2}^{v}

PRESSURE (MPa)

FIGURE 1-2a

Mass fraction of H_2O (w_{H2O}^{v}) and CO_2 (w_{CO2}^{v}) in vapor phase vs. pressure for Disruptive Yucca Mountain Basalt (DYMB) composition for total water (Z_{H2O}^{0}) and carbon dioxide (Z_{CO2}^{0}) content of 2.6 wt % and 0.4 wt %, respectively at temperature (T) 1150 °C

MELT COMPOSITION

$T = 1150\,^{\circ}C$

$Z^{0}_{H2O} + Z^{0}_{CO_2} = 3\ wt\%$

Ratio $H_2O + CO_2 = 6{:}1$
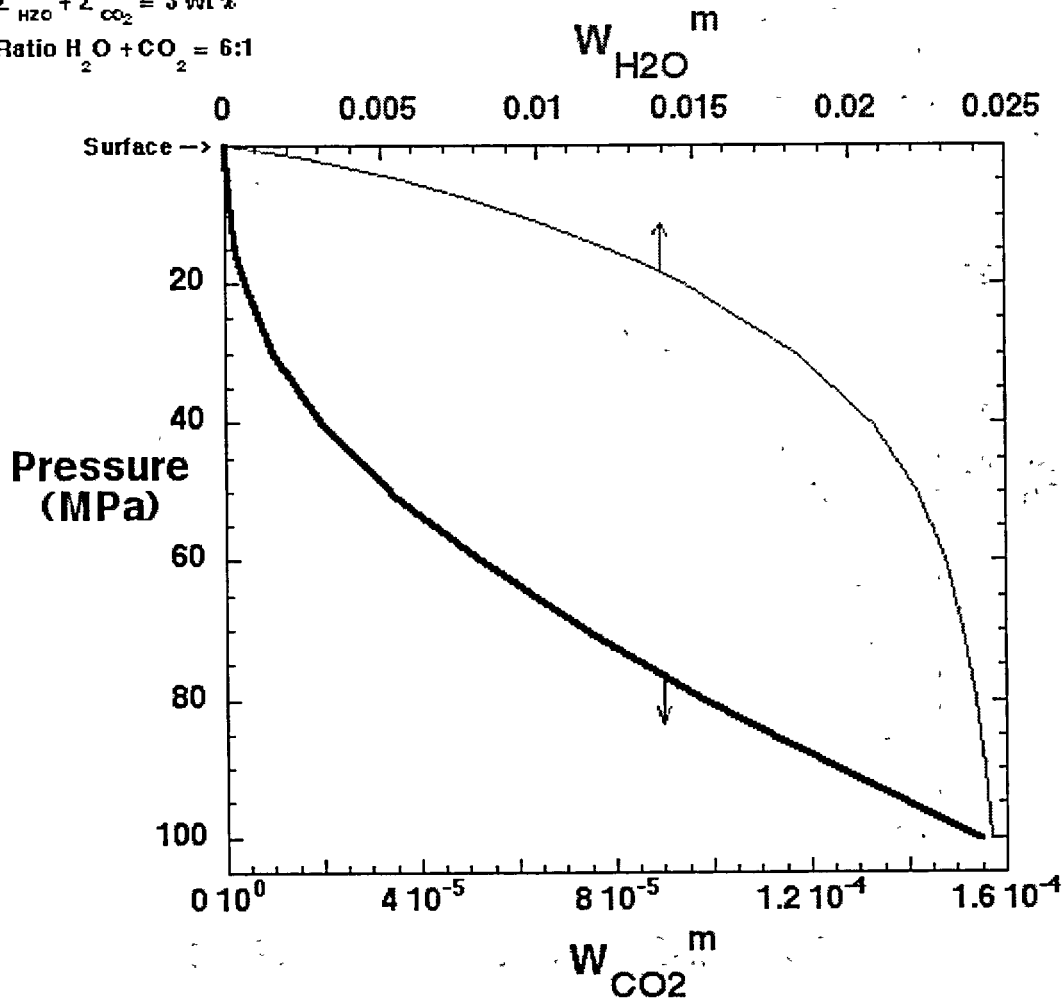
W_{H2O}^{m}

FIGURE 1-2b

Mass fraction of dissolved H_2O (w_{H2O}^{m}) and CO_2 (w_{CO2}^{m}) in melt phase vs. pressure for Disruptive Yucca Mountain Basalt (DYMB) composition for total water (Z_{H2O}°) and carbon dioxide (Z_{CO2}°) content of 2.6 wt % and 0.4 wt %, respectively at temperature (T) 1150 °C

$T = 1150\,^{0}C$

$Z^{0}_{H2O} + Z^{0}_{CO_2} = 3\ wt\%$

Ratio $H_2O:CO_2 = 6:1$

MASS FRACTION VAPOR (ϕ)

| 0.005 | 0.01 | 0.015 | 0.02 | 0.025 | 0.03 |

Surface -->

PRESSURE (MPa)

20
40
60
80
100

0   0.2   0.4   0.6   0.8   1

VOLUME FRACTION VAPOR (θ)
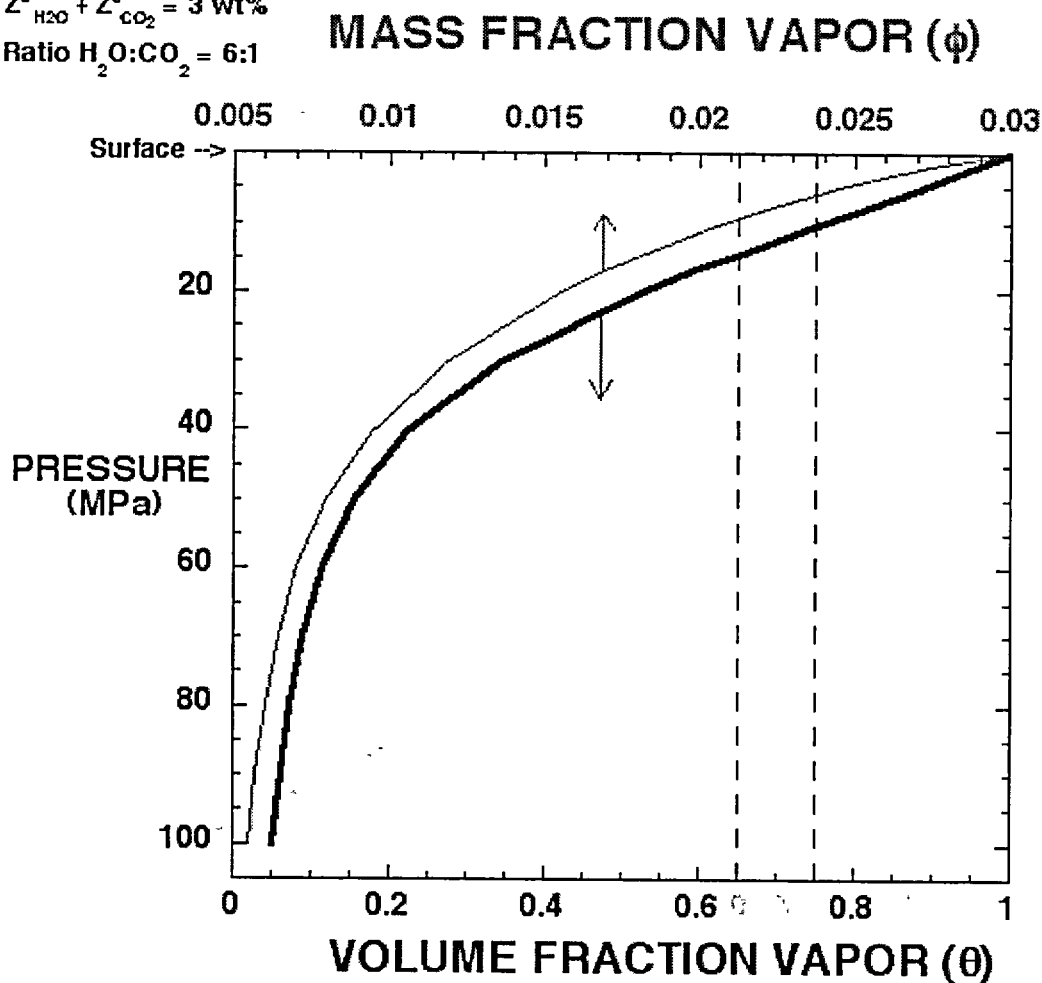
FIGURE 1-2c

Mass fraction (ϕ) and volume fraction of vapor (θ) in Disruptive Yucca Mountain Basalt (DYMB) for total water (Z_{H2O}^{0}) and carbon dioxide (Z_{CO2}^{0}) content of 2.6 wt % and 0.4 wt %, respectively at temperature (T) 1150 °C. The vertical dashed lines show the probable values of the volume fraction of vapor (θ) at which vapor becomes the continuous phase upon magma decompression. The critical value, denoted θ_{crit} is approximately 0.7±0.05; its precise value depends on a host of factors beyond the scope of the Interim Report.

$T = 1150\ ^{0}C$

$Z^{0}_{H2O} + Z^{0}_{CO_2} = 3\ wt\%$

Ratio $H_2O + CO_2 = 6{:}1$

VAPOR & MELT DENSITY

VAPOR DENSITY, ρ_V (kg m^{-3})

MELT DENSITY, ρ_m (kg m^{-3})
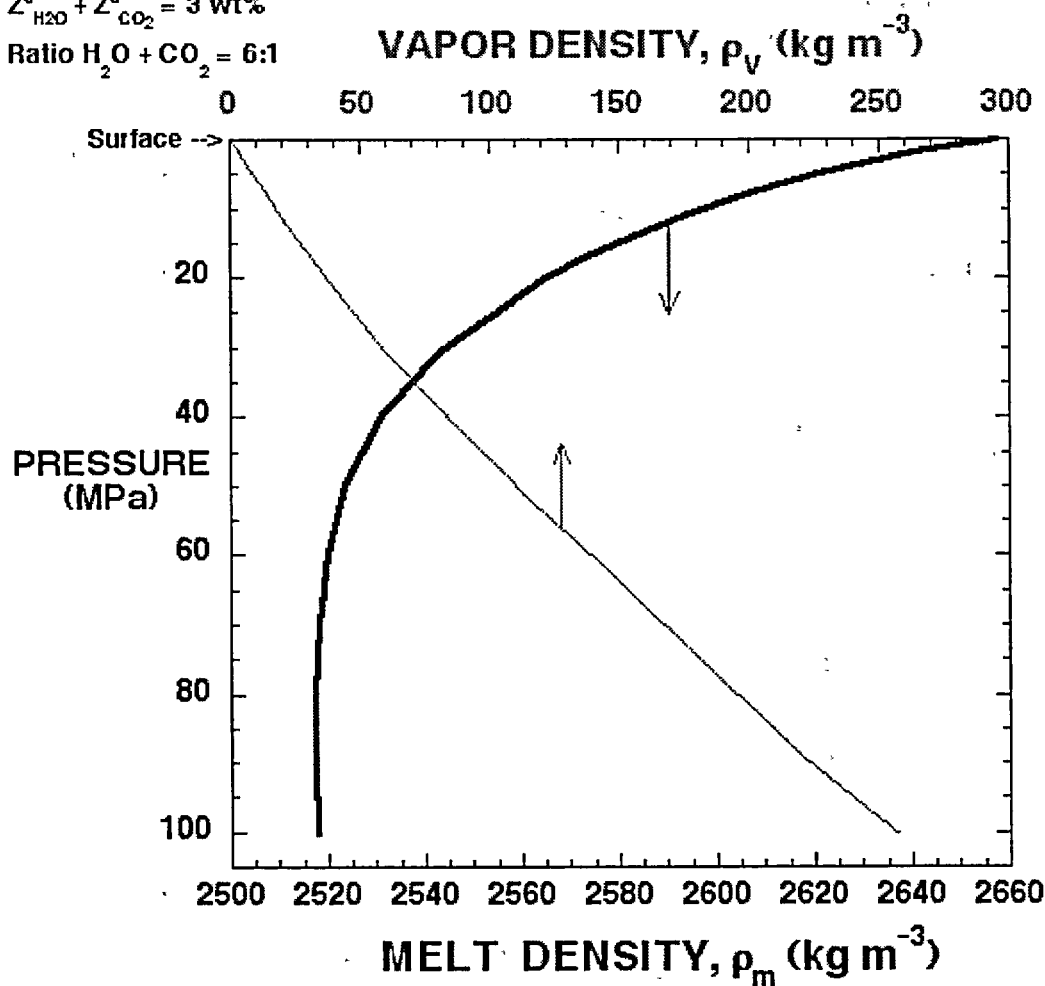
FIGURE 1-2d

Density of vapor (ρ_v) and volatile-saturated melt (ρ_m) vs. pressure for Disruptive Yucca Mountain Basalt (DYMB) composition for total water (Z_{H2O}^{0}) and carbon dioxide (Z_{CO2}^{0}) content of 2.6 wt % and 0.4 wt %, respectively at temperature (T) 1150 °C. Note that the melt density increases upon decompression because the dissolved volatile content drops sharply upon decompression along the 1150 °C isotherm.

T = 1150°C
Total Magma $H_2O + CO_2 = 3$ wt%
Magma $H_2O:CO_2$ ratio = 6:1
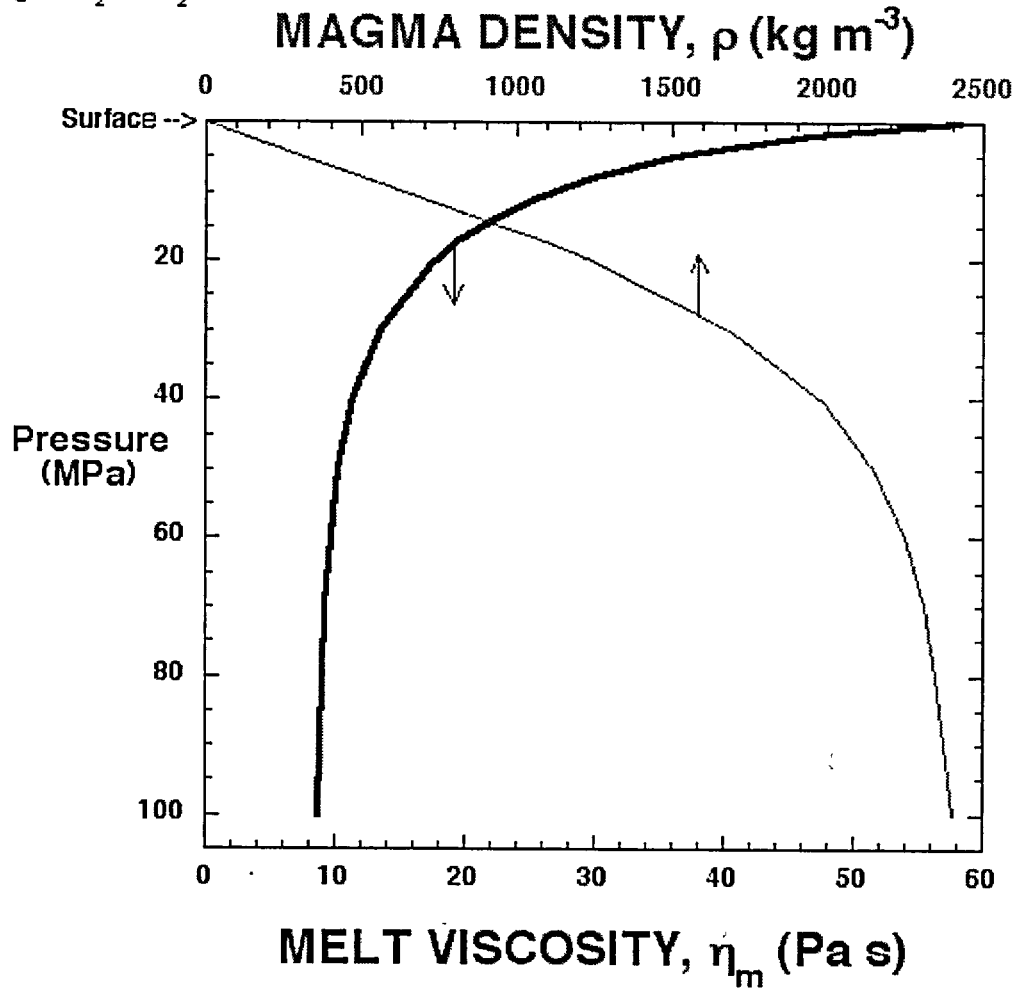
FIGURE 1-2e

Density of magma (ρ) (i.e., two-phase mixture) and shear viscosity of melt (η_m) vs. pressure for Disruptive Yucca Mountain Basalt (DYMB) composition for total water ($Z_{H2O}°$) and carbon dioxide ($Z_{CO2}°$) content of 2.6 wt % and 0.4 wt %, respectively at temperature (T) 1150 °C. Note that the magma density decreases rapidly upon decompression because of the exsolution of volatiles from coexisting melt.

1.4 Corrosive properties of magmatic volatiles

The concentration of magmatic gas species (i.e., mole fractions of H_2O, CO_2, SO_2, CO, CH_4, H_2, H_2S, HCl, HF) is a predictable function of temperature, pressure, bulk composition of the vapor phase (H:O:C:S:Cl:F) and oxygen fugacity (f_{O2}) which is buffered by constituents in coexisting silicate melt phase. The composition of magmatic gases in CEPYM (p.29-30) took the approach of compiling volcanic gases from mafic volcanic centers and computing an appropriate mean. While this is a reasonable first-order approach, species abundance presented in Table 3 of CEPYM pertain to a total pressure at or close to 100 kPa and species in small concentration, that may play a role in canister stability, are neglected. The composition of corrosive magmatic gases can be computed from existing thermodynamic sources and appropriate Gibbs free-energy minimization algorithms that are widely available. **If magmatic gas corrosion studies are carried out, the effects of pressure and temperature changes should be considered in evaluating the starting composition of magmatic vapors relevant to waste container reactivity.**

Regarding the reactivity of magmatic volatiles and HLW canisters, we note that the speciation of magmatic gases depends rather sensitively on pressure temperature and oxygen fugacity for fixed bulk composition. It is beyond the purview of this panel to address in detail the reactivity and corrosion of waste packages, specifically Stainless Steel Type 316NG and Ni-based Alloy 22 with respect to magmatic gases. **If such studies are to be of value, a range of magmatic vapor compositions should be addressed that encompass the range of conditions expected at depth.**

1.5 Transport properties

1.5.1 Shear viscosity

Magma viscosity is perhaps the most important physical property to quantify in any dynamical model of DYMB-drift interaction. Melt viscosity is most sensitive to temperature and dissolved H_2O at the shallow depth of magma-drift interaction. The variation of melt viscosity is given for a range of temperatures and dissolved water contents in the Figures presented above. In addition to changes in the melt viscosity, the effects of vapor bubbles in two-phase magma must also be considered. The effect of bubbles on the viscosity of DYMB was not addressed in CEPYM; the analysis provided below suggests that bubbles can change the shear viscosity of potential DYMB by up to an order of magnitude. Bubbles also impart significant non-Newtonian characteristics to magma and this can affect the dynamics and heat transfer characteristics of magma-drift and magma-waste-canister interaction.

Two cases can be differentiated. If the bubble Stokes ascent rate ($u_b = 2/9$ $gr_b^2\Delta\rho/\eta$) is large compared to the mean magma vertical velocity (U), bubbles will efficiently escape to form a vapor-rich cap and may be removed entirely from rising magma by percolation into permeable country rock if volatile saturation occurs at a deep enough level. Alternatively, if the magma ascent rate is fast compared to bubble Stokes rise rates, the mixture can be treated as a homogeneous bubbly flow with an effective mixture viscosity. For typical parameters ($r_b \approx 5$ mm, $\Delta\rho \approx 1800$ kg/m^3, $\eta \approx 50$ Pa s and U ≈ 1m/s), one finds u_b/U to be of order 10^{-3}. This implies that the melt-bubble magmatic suspension can be treated as a homogeneous bubbly flow. Naturally, at very shallow depths when the volume fraction of vapor is close to unity u_b/U will approach and perhaps exceed unity. There is a flow regime change at this point from quasi-homogeneous bubbly flow to separated slug flow.

There is a large literature on the shear viscosity of bubbly flows that extends from the pioneering work of G.I. Taylor in the early part of the last century (1932) to the present (e.g., Frankel and Acrivos, 1970; Stein and Spera, 1992; Bogdassarov and Dingwell, 1992; Manga et al, 1998; Lejeune et al, 1999; Martel et al, 2000; Spera and Stein, 2000; Spera, 2000; Lensky et al, 2001; Blower et al, 2001; Pal, 2001a,b,c; Manga and Loewenberg, 2001; Rust and Manga, 2002; Llewellin et al, 2002; Stein and Spera, 2002). For magmatic flows relevant to Yucca mountain, the bubble Reynolds number ($Re_b \equiv \rho Gr_b^2/\eta_m$ where G, the mean shear rate $\approx U/d$, d is the dike thickness, and η_m is the melt viscosity) is small, which means that from the point of view of the bubble viscous forces outweigh inertial ones. The shear viscosity of a magmatic two-phase pseudofluid mixture (η_p) is given by

$$\eta_p = f(\eta_m, \theta, Ca),$$

where η_m is the shear viscosity of the melt (a function of pressure, temperature and composition including dissolved volatiles, θ is the volume fraction of bubbles, and Ca is the Capillary number defined as $Ca \equiv Gr_b\eta_m/\sigma$ where G is a mean macroscopic shear rate, r_b is a typical bubble radius, and σ is the melt-vapor interfacial energy. It is convenient to discuss the relative viscosity (η_r) defined as the ratio of the pseudofluid (mixture) viscosity to the viscosity of the single-phase melt: $\eta_r \equiv \eta_p/\eta_m$ and so $\eta_r = g(\theta, Ca)$.

There are three relevant regimes based on the magnitude of Ca. At low Ca (say, Ca < 0.1,) bubbles are little deformed from spheres and η_r is a monotonically *increasing* function of the bubble volume fraction θ and independent of the shear rate (or Ca number). In the dilute limit, $\eta_r = 1 + \theta$. For higher bubble fractions, there are a number of empirical relations of the form $\eta_r = h(\theta)$ where $h(\theta)$ is a monotonically increasing function of the bubble loading (θ). In this regime, the viscosity of the two-phase mixture exceeds that of the melt and Newtonian behavior is observed. In contrast, for 0.1 < Ca <10, a transitional power-law

25

regime exists such that η_r decreases as Ca increases at fixed θ. In the power law regime, the relative viscosity decreases as the volume fraction of vapor increases. Finally for Ca > 10 η_r is independent of Ca and again a monotonically decreasing function of θ.

The key factor is the magnitude of the Capillary number, Ca = G $r_b\eta_m/\sigma$. For application to magma transport beneath Yucca Mountain, $\eta_m \approx 50$ Pa s and $\sigma \approx$ .2 N/m. For a dike 1 m thick and magma ascent rate 1 m/s one finds for $r_b = 1$, 3 and 10 mm, Ca ≈ 0.3, 0.8, and 3, respectively. If the magma ascent rate is 10 m/s then G = 10 s^{-1} and one finds Ca ≈ 3, 8 and 30, respectively. <u>The conclusions are that (1) the flow of DYMB straddles the range within which shear rate dependence of the shear viscosity is important and (2) DYMB can be characterized by a shear viscosity up to a factor of five to ten times less than that of melt at the same conditions of temperature and pressure.</u> Representative results for the variation of relative viscosity as a function of Capillary number for various melt-bubble mixtures is presented in the graph below. Note that θ is the volume fraction of vapor bubbles in the (homogeneous) mixture. This simple model assumes a monodisperse suspension of single-sized bubbles; the effects of polydispersity (i.e., a range of bubble sizes) can be accounted for although the relations depicted below apply strictly to a monodisperse homogeneous mixture of bubbles plus melt.

Relative Viscosity
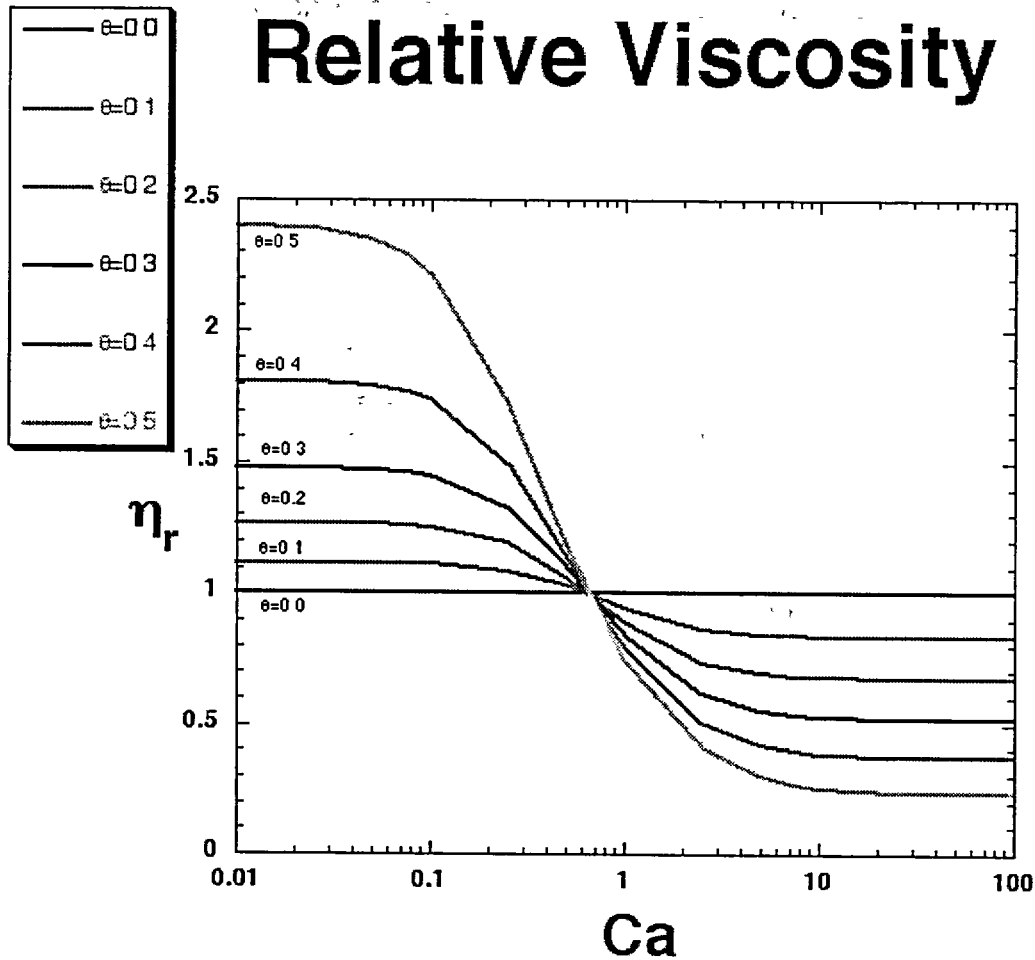
FIGURE 1-3

Relative viscosity of magma (η_r) as a function of Capillary number (Ca) for various volume fraction of vapor (θ) values. The definition of both relative viscosity and the Capillary number are noted in the text. Note that in the high Ca regime applicable to Disruptive Yucca Mountain magmatism, the shear viscosity of magma is up to a factor of 5 smaller than for that of melt alone at the same conditions of temperature and pressure. In contrast, at low Ca, the magmatic mixture is more viscous than that of single-phase melt at the same conditions of temperature and pressure.

1.5.2 Thermal conductivity

There is analysis of magma-drift interaction, specifically solidification of (incompressible) magma flowing down a drift in *ANL-WIS-MD-000015 REV00, ICN1 Dike Propagation Near Drifts.* The value cited on p. 36 of that document is couched in unfamiliar units of J/kg s °C rather than the usual units of thermal conductivity: J/m s K or W/m K.

For analysis of heat transport of magma-drift and magma canister interaction, the total thermal conductivity (k_T) of magma is needed. The total thermal conductivity represents the sum of two terms: the lattice or phonon conductivity (k_P) and the radiative conductivity (k_R). The relative magnitude of the phonon and radiative contributions to melt thermal conductivity are currently the source of contention in the literature. Some background discussion may be found in Gable and Shankland (1984), Snyder et al (1994) and in a recent review (Spera (2000). A major issue involves the variation of melt opacity with the concentration of transition metals and dissolved water.

When opacity is large, the k_R contribution is small and the phonon conductivity (k_P) is the appropriate thermal property. From measurements on Hawaiian basaltic melts, there is a factor of two decrease in k_P as temperature increases in the range 1150 °C to 1350 °C. Based on values reported in the literature (e.g., Butter et al, 2000; Snyder et al, 1994) it is estimated that the phonon thermal conductivity at 1100 °C is in the range 0.7-1.1 W/m K for DYMB (potassic trachybasalt melt). For two-phase magma a value could be calculated based on mixture theory using the thermal conductivity of melt and coexisting vapor. Thermal conductivity is one of the most poorly known physical properties of silicate melts and magmatic mixtures. <u>For the purpose of magma-drift interaction thermal modeling, a constant value around 1 W/m K is adequate as a first approximation. However, if more accurate magma-drift thermal evolution is required, a more through literature survey and perhaps laboratory experiments should be undertaken for a DYMB composition. There are virtually no measurements of the effects of dissolved water on the phonon thermal conductivity of natural basaltic compositions that the Panel is aware of. One approach is to use Molecular Dynamics simulation (MD) to compute phonon thermal conductivity of analog basaltic melt (e.g., $CaMgSi_2O_6$-$CaAl_2Si_2O_8$-H_2O) as an adjunct to laboratory experiments.</u>

1.6   References for Chapter 1

Buttner, R; Zimanowski, B; Lenk, C; Koopmann, A; and others. Determination of thermal conductivity of natural silicate melts. Applied Physics Letters, **77** ,1810-1812 (2000)

Gable, CW and TJ Shankland, Radiative Heat transfer in molten and glassy Obsidian, Jour of Geophysical Research, **89**, 7107-7110,. 1984

Ghiorso, MS, On the stability relations of hydrous minerals in water-undersaturated magmas, American Mineralogist, **84,** 1506-1511, 1999.

Ghiorso, MS, Thermodynamic models of igneous processes. Annual Review of Earth and Planetary Sciences, **25**, 221-241, 1997.

Mastin, LG, Insights into volcanic conduit flow from an open-source numerical model, Geochemistry Geophysics Geosystems, **3**, 1-18, 2002.

Papale, P, Modeling of the solubility of a two-component $H_2O + CO_2$ fluid in silicate liquids, American Mineralogist, **84**, 477-492, 1999.

Lejeune, AM, Y Bottinga, TW Trull, P Richet, Rheology of bubble-bearing magmas, Earth Planet. Sci. Lett. 166 (1999) 71-84.

F.J. Spera, D.J. Stein, Comment on "Rheology of bubble-bearing magmas" by Lejeune et al., Earth Planet. Sci. Lett. 175 (2000) 327-331.

D.J. Stein, F.J. Spera, Rheology and microstructure of magmatic emulsions: theory and experiments, J. Volcanol. Geotherm. Res. 49 (1992) 157-174.

M. Manga, J. Castro, K.V. Cashman, M. Loewenberg, Rheology of bubble-bearing magmas, J. Volcanol. Geotherm. Res. 87 (1998) 15-28.

M. Manga, M. Loewenberg, Viscosity of magmas containing highly deformable bubbles, J. Volcanol. Geotherm. Res. 105 (2001) 19-24.

N.S. Bogdassarov, D.B. Dingwell, A rheological investigation of vesicular rhyolite, J. Volcanol. Geotherm. Res. 50 (1992) 307-322.

D.J. Stein, F.J. Spera, Shear viscosity of rhyolite – vapor emulsions at magmatic temperatures by concentric cylinder rheometry, J. Volcanol. Geotherm. Res. 113

A.C. Rust, M. Manga, Bubble shapes and orientations in low Re simple shear flow, J. Colloid Interface Sci. 249 (2002) 476-480.

N.G. Lensky, V. Lyakhovsky, O. Mavon, Radial variations of melt viscosity around growing bubbles and gas overpressure in vesiculating magmas, Earth Planet. Sci. Lett. 186 (2001) 1-6.

J.D. Blower, H.M. Mader, S.D.R. Wilson, Coupling of viscous and diffusive controls on bubble growth during explosive volcanic eruptions, Earth Planet. Sci. Lett. 193 (2001) 47-56.

C. Martel, D.B. Dingwell, O. Spieler, M. Pichavant, M. Wilke, Fragmentation of foamed silicic melts: an experimental study, Earth Planet. Sci. Lett. 178 (2000) 47-58.

R. Pal, Evaluation of theoretical viscosity models for concentrated emulsions at low capillary numbers, Chem. Eng. J. 81 (2001) 15-21.

R. Pal, Novel viscosity equations for emulsions of two immiscible liquids, J. Rheol. 45 (2001) 509-520.

R. Pal, Single-parameter and two-parameter rheological equations of state for nondilute emulsions, Ind. Eng. Chem. Res. 40 (2001) 5666-5674.

E.W. Llewellin, H.M. Mader, S.D.R. Wilson, The rheology of a bubbly liquid, Proc. R. Soc. Lond. A 458 (2002) 987-1016.

G.I. Taylor, The viscosity of a fluid containing small drops of another liquid, Proc. R. Soc. Lond. A 138 (1932) 41-48.

N.A. Frankel, A. Acrivos, The constitutive equation for a dilute emulsion, J. Fluid Mech. 44 (1970) 65-78.

Spera, F. J., Physical Properties of Magma. In: Encyclopedia of Volcanoes, H. Sigurdsson, Ed. (Academic Press, New York, 2000), p. 171-190.

Snyder, D., Gier, E., and Carmichael, I., 1994. Experimental determination of the thermal conductivity of molten $CaMgSi_2O_6$, and the transport of heat through magmas. J. of Geophy. Res., 99, 15503-15516.

Chapter 2

Dike Propagation in the Absence of a Repository

[NOTE: While this chapter is meant to be self-contained, much of it is condensed from a more technical Appendix 2. The interested reader can find more detail in that Appendix.]

2.1   Introduction

A major challenge for the analysis under discussion in this report is the influence of the repository on dike propagation and magma ascent. However, several aspects of dike propagation relevant to a hazards assessment at Yucca Mountain are poorly understood even in the absence of a repository. These include the questions of what controls the lateral extent of dikes rising from the mantle, what controls the pressure within the magma-less region behind the dike tip, and the implications of both magma degassing and distributed inelastic deformation of the host rock as the dike tip approaches the surface. The purpose of this chapter is to summarize existing work and present the results of new analyses and suggestions designed to address these questions.

Although observations of fissure eruptions and eroded dikes provide important constraints on dike propagation, many important aspects of dike ascent from the mantle to the surface are inaccessible to direct observation and must be deduced from continuum mechanical models. These models have tended to treat the host rock as linear elastic and the magma as incompressible and linear viscous (Lister and Kerr, 1991; Rubin, 1995a) (Figures 2-1 and 2-2). Under these conditions a Poiseuille flow or lubrication approximation, in which the fluid pressure is taken to be uniform across the dike thickness, is appropriate. A minimum necessary additional ingredient is a rock fracture criterion. Magma freezing (and subsequent remelting, for sufficiently robust dikes) has also been considered, often at the expense of simplifying other aspects of the problem (Bruce and Huppert, 1990; Rubin, 1993a, 1995b; Lister, 1994; Lister and Dellar, 1996; Fialko and Rubin, 1998). Because of the difficulty of coupling the fluid flow to the solid deformation (i.e., the evolving pressure field within the dike must satisfy both local mass balance within the fluid and long-range elasticity within the host rock) while simultaneously satisfying a fracture criterion, most models couple only 1-dimensional (1-D) magma flow with equations for 2-D elastic deformation of the crack walls. These are referred to here as 2-D models. A few 3-D problems have been approximated by using mass balance to "marry" separate 2-D models in vertical and horizontal cross-sections (Lister and Kerr, 1991).
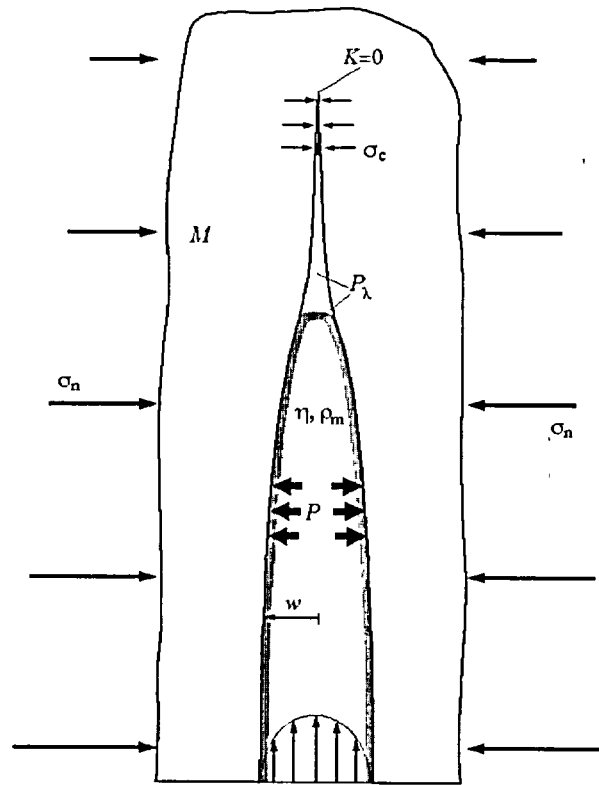
Figure 2-1

Cartoon depiction of a basic 2-dimensional mechanical model of a vertically-propagating dike

The dike is intruded into host rock with an elastic stiffness $M \equiv G/(1-v)$, where G is the elastic shear modulus and v is Poisson's ratio. The dike plane is subjected to an ambient normal stress σ_n that increases with depth. Magma with a viscosity η and density ρ_m is injected with a specified pressure or flux history at depth. A constant pressure $P_\lambda < \sigma_n$ acts within the tip cavity and is continuous with the magma pressure at the magma front; in principal this pressure should be determined as part of the solution. The rock fracture properties may be represented by a nonzero stress intensity factor K at the dike tip, or by $K=0$ and an internal cohesive stress σ_c that acts over a crack-wall separation δ_c at the dike tip. For rock fracture toughnesses even considerably in excess of lab values the rock fracture properties may be neglected (most of the resistance to propagation comes from the confining pressure acing over the tip cavity). Elastic thicknesses depend only upon the difference $\Delta P \equiv P - \sigma_n$. Parameters to be solved for are the magma pressure P and dike thickness w as functions of position and time, and (for a given P_λ) the location of the magma front and dike tip as functions of time.

32
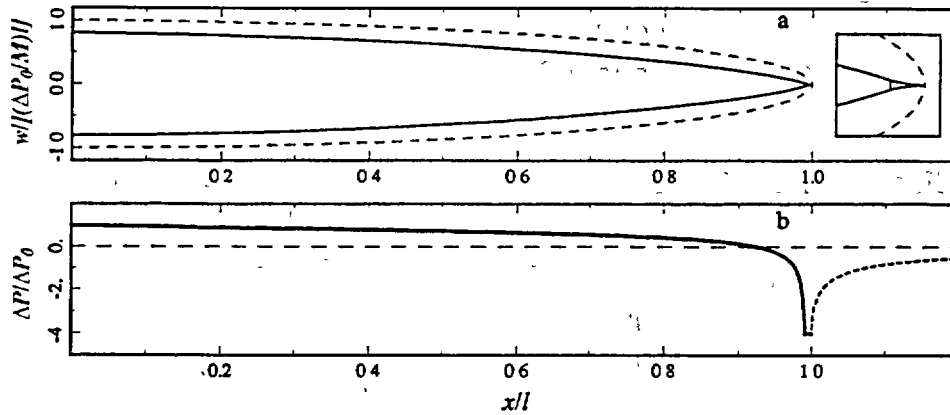
Figure 2-2

Example of a dike propagation calculation

Example of a dike propagation calculation illustrating the distribution of (a) dike thickness w and (b) excess pressure ΔP as a function of normalized distance along the dike x/L, where L is the dike length. The 2-D dike grows horizontally under plane strain conditions from a source of constant pressure. The ratio $\Delta P_\lambda/\Delta P_0$, the underpressure within the tip cavity ΔP_λ normalized by the excess pressure at the magma source ΔP_0, equals 4; in this case the tip cavity occupies ~1% of the dike length. Thicknesses in (a) are normalized by $(\Delta P_0/M)L$, where M is the elastic stiffness. The dashed profile shows the elliptical dike shape that would result from a uniform excess pressure equal to ΔP_0. The inset shows the tip region enlarged by a factor of 5; the vertical line indicates the magma front. Pressures in (b) are normalized by the excess source pressure ΔP_0. Most of the pressure drop near the tip occurs on a length scale comparable to the cavity length. The dashed curve for $x/L > 1$ shows the change in normal stress ahead of the dike tip.

33

2.2   Dike ascent through the mantle and crust

Importance:
i. The lateral extent of near-surface dikes affects the probability of an igneous event impacting the repository.
ii. The characteristics of dike ascent provide a "bottom boundary condition" for modeling interaction of a dike with the repository.

There is currently no published model capable of explaining how mantle-derived dikes can have strike lengths as short as 1-2 km near the surface, as is inferred from analog dikes. Estimates of the strike length based on an approximate analysis, and assuming a constant flux from a source at depth of 30-100 km and a constant magma buoyancy, are an order of magnitude larger and quite insensitive to reasonable variation in the values of the governing parameters (mass flux, magma viscosity, etc.) (Lister, 1990a). The state of stress in regions undergoing tectonic extension is such that unvesiculated magma is expected to be "effectively negatively buoyant" from the surface down to the brittle/ductile transition, at a depth of perhaps 10-12 km in the Basin and Range (e.g., Hickman, 1991). Because alkali basalts with 1-4 wt% H_2O are not expected to reach the bubble fractions of ~40% necessary to become "effectively buoyant" except at much shallower depth, this stress state would be expected to further increase the strike length of mantle-derived dikes (Rubin, 1995a).

Sections C and D of Appendix 2 describe some processes that might help account for the short observed strike lengths of analog dikes. Some of these rely on the 3-D nature of the problem as the curved dike top approaches either the earth's surface or the depth at which the dike-normal stress equals the pressure at which the magma/gas mixture would become effectively buoyant. **Although an understanding of this issue could impact a TSPA for the proposed repository, we do not currently recommend a program of devoted numerical calculations designed to address this difficult 3-D problem. Instead, we recommend that the uncertainty in the relevant "bottom boundary condition" be accounted for by allowing for a reasonable variation of boundary conditions (dike length and excess magma pressure or magma flux) in 2-D models, as dictated by observations of and inferences from analog dikes.**

One issue that must be faced in conducting such a modeling program is that the relevant 2-D cross section to model the approach to the surface is a vertical section, while the relevant dike length for controlling the thickness appears only in a horizontal section (assuming the strike length to be less than the dike height). **A reasonable 2-D approach is to carry out calculations in a vertical cross-section in which the dike height (in the case of a finite crack) or other relevant length scale (in the case of a semi-infinite crack with a specified flux; see, e.g., Appendix 1) is taken to be roughly the inferred lateral extent of analog dikes. Such calculations can be supplemented by 3-D elastic**

calculations in which the coupling to (perhaps 1-D, i.e. vertical) magma flow is approximated to various degrees, and which are designed specifically to gain insight into how the 3-D world might change the nature of the processes under consideration.

Real-world data could also be very useful. **A field program to investigate the degree of lateral vs. vertical crack propagation and subsequent magma flow in analog dikes (from offset dike margins, flow lineations, or anisotropy of magnetic susceptibility) might shed some light on the poorly-constrained geometry of the dikes at greater depth.** For example, Delaney and Gartner (1997) suggest that lateral propagation is pervasive in mantle-derived dikes of <2 km lateral extent on the Colorado Plateau, and that the dikes appear to shorten and thicken upward (estimated depths of erosion are 0.5-1.5 km).

2.3   The dike tip cavity

Importance:
The gap between the crack tip and the magma front is the first part of the dike to intersect the repository. The pressure within this lag zone determines the explosivity, and its length the duration, of this initial interaction.

It is widely accepted that at the tip of a dike propagating in largely elastic rock there is a "tip cavity", or "magma lag zone", where magma cannot reach (Barenblatt, 1962; Lister, 1990b; Rubin, 1993b; Garagash and Detournay, 2000) (Figure 2-1). The lag zone arises because of the large pressure drop required to force a viscous fluid through a slot of ever-decreasing thickness. This region may be filled at some low pressure by either pore fluids infiltrating from the adjacent host rock or by volatiles exsolving from the magma. Beneath Yucca Mountain the water table is ~300 m below the proposed repository, and the likely magma is H_2O-rich, so we expect the lag zone in the vicinity of the proposed repository to be filled by H_2O vapor. Because the viscosity and density of this vapor is very low, the pressure within the lag zone may be taken as ~constant. For rock fracture toughnesses comparable to laboratory values and even up to 1-2 orders of magnitude larger, the pressure within the lag zone must be less than the dike-normal stress if the dike tip is to propagate at less than elastic wave speeds (Lister and Kerr, 1991).

In published models of dike propagation, either the lag zone pressure or length is specified and the other is determined as part of the solution. In general, these solutions show that in order to satisfy the rock fracture criterion the lag length increases as the underpressure within the lag zone decreases (e.g., Figure 2-3). These models also indicate that the lag underpressure does not significantly affect global properties such as the dike thickness or propagation velocity, provided the lag zone occupies only a small fraction of the dike length.
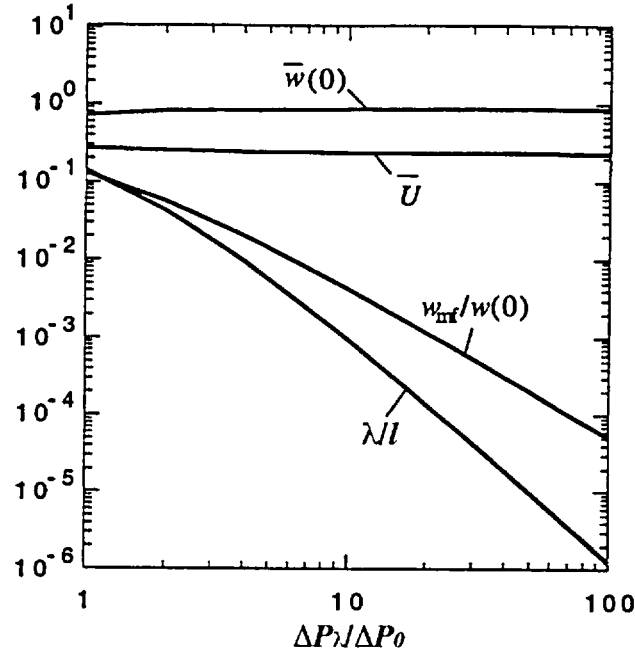
Figure 2-3

Various attributes of a 2-D dike growing horizontally under plane strain conditions from a source of constant pressure, as a function of the ratio $\Delta P_\lambda/\Delta P_o$

Various attributes of a 2-D dike growing horizontally under plane strain conditions from a source of constant pressure, as a function of the ratio $\Delta P_\lambda/\Delta P_0$, the underpressure within the tip cavity or magma lag zone ΔP_λ normalized by the excess pressure at the magma source ΔP_0. Curves are for λ/l, the tip cavity or lag zone length λ normalized by the dike length l; $w_{mf}/w(0)$, the dike thickness at the magma front w_{mf} normalized by the thickness at the source $w(0)$; U overbar, the propagation velocity normalized by a dimensional estimate of the velocity $(1/3\eta)(\Delta P_0{}^3/M^2)l$, where η is the magma viscosity and M is the elastic stiffness; and $w(0)$ overbar, the thickness at the origin normalized by a dimensional estimate of the thickness $l(\Delta P_0/M)$. Note that the ratio λ/l varies by orders of magnitude for modest changes in $\Delta P_\lambda/\Delta P_0$, while $w(0)$ and U are largely unaffected. With some quantitative changes these results carry over to the case of vertical propagation.

Ideally, one should determine both the lag length and the lag pressure from mass balance considerations. Paragraphs 7-19 of section E, Appendix 2, are designed to develop a self-consistent model of the lag zone. An approximate expression is derived for the quasi-steady-state pressure that would result from balancing the gas flux into the lag zone (from bubble-bearing magma that reaches the magma front) with that out of the lag zone (by diffusion into the adjacent host rock). The adopted diffusion analysis is deficient in that the large density variations of the gas phase are not accounted for in the mass flux equation. However, the preliminary conclusion is that the measured Yucca Mountain tuff permeabilities of 10^{-12}–10^{-13} m^2 are sufficient for volatiles to leak out of the lag zone easily, such that the lag pressure is only very slightly larger than the pore pressure in the adjacent host rock (i.e., 1 atmosphere or 0.1 MPa). A corollary is that the assumption of a well-defined magma front with (isolated) bubble-bearing magma upstream and gas downstream is physically unrealistic. Instead, at the large gas fractions expected at near atmospheric pressure, there must be a permeable magma foam in the vicinity of the magma front and a pressure drop along this foam. This complicates the problem considerably, in that there is no well-defined flow law for such foams. In addition, one would need to specify the pressure at which the magma/bubble mixture becomes permeable to gas flow, and the fractional surface area within the foamy region that is available for gas flux into the host rock. It is unlikely that these parameters can be defined with any confidence in the foreseeable future.

In view of the above, one can envision a hierarchy of 2-D calculations:

(1) Steady-state and time-dependent incompressible, linear viscous flow models of the sort that have been carried out to date (see, e.g., Appendix 1).

(2) Time-dependent models that include the effects of volatile exsolution and compressibility (to be derived from an equation of state for the magma) in the fluid mass balance equation, but that do not solve for gas leak-off explicitly.

In view of the above-mentioned results regarding the steady-state lag pressure, it can be assumed that the lag pressure is atmospheric. A choice would have to be made between the following (end-member) scenarios:

(a) No segregation between the gas and liquid phases, including no venting of volatiles into the tip cavity. Bubbles that reach the magma front are simply carried to the dike wall, at which point they experience increasing pressure (magma near the wall moves slower than the dike tip) and partial gas resorption. This is the simplest case to model in that the fluid density as a function of pressure (and hence distance along the dike) can be taken directly from the equation of state. It is the approach implicit in this report's Appendix 1. It overestimates the dike volume for a given magma mass because there is no gas leak-off, but if the low-pressure region is short enough this may not be a concern.

(b) All of the gas reaching the magma front (see paragraph 11, section E, Appendix 2) is expelled into the tip cavity and immediately leaks into the host rock. This scenario is more realistic but would require keeping track of the fraction of degassed vs. undegassed magma at every position along the dike (because the dike is so thin near the magma front, in any cross-section most of the magma would be undegassed).

Whichever of the options (a) or (b) is adopted, a choice would have to be made between two unphysical boundary conditions at the tip — a continuous pressure across the magma front, in which case the magma bubble fraction behind the magma front would be unreasonably large, or a discontinuous pressure across the magma front, in which case the magma bubble fraction could be (arbitrarily) made reasonable but the pressure jump would be unphysical. The two choices could be compared and the difference used to judge how important it would be to carry out a more complete computation.

Before following this strategy, the calculation for a steady-state lag pressure should be repeated with a more complete (numerical) description of gas diffusion into the host rock, and with accounting for how a pressure drop across the magma front or down a (variable thickness) foamy region would increase the gas flux into the lag zone (at the low confining pressures expected at repository depths, differences in the lag pressure of a few atmospheres could be significant).

The viscosity in these models could be assumed constant and linear, or variable and nonlinear, depending upon the availability of approximate constitutive laws based on the computed magma bubble fraction and strain rate, and anticipated bubble size (see Chapter 1).

(3) Time-dependent models that compute the gas flux into and out of the lag zone at each timestep. This would make sense in conjunction with a complete description of the foamy region, including the pressure at the two ends and the gas flux from the foam into the host rock. **Such calculations seem advisable only if (1) the different scenarios outlined under (2) above produce very different results, or (2) gas expansion at shallow depths occurs so rapidly that the steady-state estimate of the lag pressure becomes grossly inaccurate.**

2.4   Approach to the surface

Importance:
As the dike tip approaches the surface several poorly understood processes become potentially important. These include dynamic instability of the dike tip, increased likelihood of inelastic deformation at low confining pressure, and the possible transition to hydrodynamic flow.

2.4.1 Dike tip instability

For a confining pressure that increases ~linearly with depth, the underpressure in the lag zone decreases ~linearly from the magma front to the dike tip. As the lag length increases, this will ultimately result in unstable propagation of the dike tip.

An approximate analytical solution (paragraphs 3-4, section F, Appendix 2) suggests that the dike tip will go unstable when the underpressure at the tip is 1/2 that at the magma front. In the context of Yucca Mountain, where the host rock permeability suggests a lag pressure near atmospheric (so that the underpressure equals the local dike-normal stress), this implies that the dike tip might go unstable when its depth is ~1/2 that of the magma front. 2-D steady-state calculations that do not include the mechanical influence of the free surface, and 2-D and 3-D calculations that include the influence of the free surface but not viscous pressure losses within the dike, suggest that for dikes about 2 km long and a compressive stress at repository depths of 3.6 MPa (i.e., a gradient of 12 MPa/km), the tip will go unstable while the magma front is deeper than 300 m if the excess magma pressure exceeds ~1–2.5 MPa. For reasonable values of the in-situ elastic shear modulus of the host rock this would give rise to dike thicknesses of order 1 m. Thus, in elastic rock it seems entirely plausible that the dike tip could reach the surface before magma reached drifts at 200-300 m depth. If, on the other hand, thermal stresses increased the dike-normal stress at repository depths to 10-20 MPa, reasonable lag lengths might be only 1-10 m (Fig. 2-3).

Thus, a full spectrum of ~atmospheric-pressure lag lengths at repository depths, from <1 m to hundreds of meters, seems possible. The associated range of thicknesses at the magma front varies from <1% to >20% of the maximum dike thickness. **These ranges should be considered in models of dike/drift interaction.**

2.4.2 Inelastic deformation

Inelastic deformation at shallow depth (e.g., slip on a pre-existing fault that cuts one wall of the lag zone) becomes more likely at shallow depth (Rubin and Gillard, 1998) and might reduce the lag zone length or temporarily block or divert the magma flow, thus altering the pressure/time/dike thickness history seen by the drifts. Such inelastic deformation is difficult to incorporate with confidence in numerical models of magma flow in dikes. **Field observations of analog dikes, particularly in near-vertical cross sections, might shed useful light on this issue.**

2.4.3 The transition to hydrodynamic flow

The transition from subsurface dike propagation (with typical velocities of 1-10 m/s) to gas-dominated eruption through a more-or-less cylindrical vent (with typical velocities of ~100 m/s), has not been addressed theoretically to date. It is conceivable that the transition to high-speed gas-charged flow occurs in the shallow subsurface, prior to eruption or development of a cylindrical vent, for sufficiently water-rich (and as-yet undegassed) magmas. **A sensible approach would be to begin with the "standard" dike propagation equations with no inertial terms (see, e.g., Appendix 1) and monitor the flow velocity and sound speed of the bubbly magma until mass acceleration is deemed important.**

Limited observations bear on the transition from fissure-flow to more equidimensional or plug-flow. This may occur subsequent to the dike breaching the surface (as is typically the case for gas-poor basalts, e.g. in Hawaii and Iceland), after the dike "tip cavity" reaches the surface but before any liquid flows up that crack (e.g. Paricutin); and while the parent crack remains hundreds of meters to a few kilometers beneath the surface (for highly gas-charged kimberlites and diatremes). In all cases the equidimensional conduit is thought to be initiated by mechanical erosion of the host rock, although for long-duration eruptions thermal erosion becomes an important agent of conduit enlargement.

2.5 Inelastic deformation before dike arrival

Importance:
i. In the tectonic environment of the proposed repository, inelastic deformation is virtually certain to occur before the dike reaches the drifts. This deformation may be the first to directly impact the repository.
ii. Normal faulting ahead of the dike is likely to increase the horizontal compressive stress at the depth of the repository, thus shortening the lag zone and damping possible instability of the tip.
iii. There is a chance that significant cracks will grow downward from the surface into the repository even before magma arrives at repository depths, setting up a potential magma pathway up the dike, through the drifts, and up the cracks to the surface.

2.5.1 Normal faulting

Earthquakes are ubiquitous during dike propagation. Historically; in any particular tectonic setting the maximum size of the earthquakes accompanying intrusion tends to increase with elapsed time since the last intrusion, reaching magnitude 5.5-6 in some cases in Iceland (Rubin and Gillard, 1998). This is consistent with the notion that tectonic extension between intrusions tends to bring the rock closer to failure, while intrusion generally increases the horizontal

stress and moves the rock farther from failure (adjacent to but not beyond the ends of the intrusion). <u>Given that the stress state at Yucca Mountain resides near the failure envelope (Stock et al., 1985), normal faulting is virtually certain to occur in conjunction with a propagating dike.</u> <u>As earthquakes themselves are not expected to present much hazard, the biggest influence of such normal faulting might lie in how it affects dike propagation.</u> Horizontal stress changes in conjunction with normal faulting are spatially variable, but in most regions adjacent to the fault they are compressive (locally they are tensile) and on the length scale of the fault they are on the order of the fault stress drop. Thus, induced normal faulting is an additional mechanism that could reduce the lag zone length. **Because the largest normal faults at Yucca Mountain have been mapped, the range of stress changes they produce upon slip can be sensibly evaluated using elastic methods.**

2.5.2 Paired tensile cracks

Paired tensile cracks or crack sets are often observed to occur parallel to and symmetrically about an eruptive fissure, or to diverge from the ends of an eruptive fissure (Pollard et al., 1983; Mastin and Pollard, 1988). These cracks are inferred to grow down from the surface at maxima in the dike-induced horizontal tensile stress. Numerical and experimental studies indicate that the depth of the dike top at the time of crack formation might be half (or more) of the separation between the crack sets for a quasi-uniform excess magma pressure, but 1/4 to 1/5 the separation between the crack sets for a magma pressure distribution more appropriate for lateral dike propagation (paragraph 10, section G, Appendix 2). The largest system of paired crack sets of which we are aware surround an eruptive fissure in the King's Bowl lava field on the Snake River Plain (Greeley et al., 1997). These crack sets are separated by ~1.6 km, suggesting that the dike top might have been more than 300 m deep when they formed. <u>If comparable fissures at Yucca Mountain could grow to depths greater than 200-300 m, then a potential "dogleg" pathway could be set up in which magma ascends up a dike, along many drifts for hundreds of meters, and up the tensile cracks to the surface.</u> The depth to which such fractures might extend can be estimated using 2-D and 3-D boundary element models. 2-D calculations that are rather favorable for crack growth, in that (a) the fracture toughness is assumed to be zero and (b) the cracks are assumed to initiate just before the dike tip goes unstable, show that such cracks might grow to 160 m depth a few hundred meters from the dike plane. 3-D calculations for a 2-km dike reduce this to 130 m. <u>While a larger variety of calculations can be carried out, at present it seems unlikely that such cracks would grow to repository depths.</u>

41

2.6   Magma freezing

Importance:
i. Freezing near the dike tip will effect the pressure/thickness/time history seen by the drifts.
ii. Long-term freezing will determine how long magma can flow from the dike into the drifts.

Magma freezing is an important but difficult issue that has been addressed only approximately in the published literature. The Panel is considering appropriate methods for including thermal effects in future calculations.

Independent of the details of such calculations, one can imagine two time periods at which freezing might be important - at early times near the (very thin) tip, which would retard dike propagation, and long after the passage of the magma front, when freezing may be responsible for shutting off the flow. Two mechanisms for freezing are available: conduction out the dike walls, which should be important over most of the dike ascent path and which is most effective near the dike walls, and raising of the liquidus temperature due to volatile exsolution, which might always be important at the dike tip but which becomes important over a larger and larger portion of the dike as the tip shallows (and which affects magma across the entire dike thickness). Mechanisms for retarding freezing are viscous dissipation and (for constant composition) decreasing the liquidus temperature with decreasing pressure, as well as latent heat release.

Observations of the eruption of m-wide dikes in Iceland and Hawaii indicate that fissure eruptions tend to localize to one or more plugs in a matter of hours to days. This is consistent with theoretical estimates of the thermal lifetime of such dikes (Delaney and Pollard, 1982). At early times, conduction of heat out the dike walls is the dominant thermal process and the thermal lifetime increases as the square of the dike thickness. Conductive heat loss decreases with time as the thermal diffusion length increases, so for sufficiently wide dikes the influx of (hot) magma from the source may exceed conductive heat loss and lead to meltback of the previously-frozen margin and eventually the wall rock. The lifetime of such dikes is determined by magma availability from the source. Theoretical estimates of the "critical" thickness that will ultimately allow meltback are generally 1-2 m (Bruce and Huppert, 1990; Lister and Dellar, 1996). This appears to be somewhat smaller than the thickness of dikes that show clear evidence of meltback, perhaps because the assumed fluxes are too large. **Analog dikes should be examined for signs of meltback, but if these are typical of m-wide dikes elsewhere such signs are most likely absent.**

Freezing near the tip at shallow depth might help explain why eruptions that ultimately produce >0.1 km^3 of magma appear to have such slow "starts" (e.g.,

42

Paricutin (Foshag and Gonzales, 1956)). <u>It is not clear that dike propagation calculations that neglect freezing are capable of reproducing this behavior.</u>

2.7 References for Chapter 2

Barenblatt, G.I., The mathematical theory of equilibrium cracks in brittle fracture, *Adv. Appl. Mech.*, *7*, 55-129, 1962.

Bruce, P.M., and Huppert, H.E., Solidification and melting along dikes by the laminar flow of basaltic magma, in *Magma Transport and Storage*, ed. by M.P. Ryan, pp. 87-101.

Delaney, P.T., and Gartner, A.E., Physical processes of shallow mafic dike emplacement near the San Raphael Swell, Utah, *Geol. Soc. Am. Bull.*, *109*, 1177-1192, 1997.

Fialko, Y.A., and Rubin, A.M., 1998, Thermodynamics of lateral dike propagation: Implications for crustal accretion at slow spreading mid-ocean ridges, *J. Geophys. Res.*, *103*, 2501-2514.

Foshag, W., and Gonzalez, J., Birth and development of Paricutin volcano, U.S. Geol. Surv. Bull. D 965, 355-485, 1956.

Garagash, D, and Detournay, E., The tip region of a fluid-driven fracture in an elastic medium, *J. Appl. Mech.-T. ASME*, *67*, 183-192, 2000.

Greeley, R., Thelig, E., and King, J.S., Guide to the geology of the King's Bowl Lava Field, in Volcanism of the Eastern Snake River Plain, Idaho: A Comparative Planetology Guidebook, R. Greeley and J.S. King, eds., Washington, DC, NASA, pp. 177-188, 1977.

Hickman, S.H., Stress in the lithosphere and the strength of active faults, *U.S. Natl. Rep. Int. Union Geol. Geophys. 1987-1990, Rev. Geophys.*, *29*, 759-775, 1991.

Lister, JR, Buoyancy-driven fluid fracture: Similarity solutions for the horizontal and vertical propagation of fluid-filled cracks, *J. Fluid Mech.*, *217*, 213-239, 1990a.

Lister, JR, Buoyancy-driven fluid fracture: The effects of material toughness and of low-viscosity precursors, *J. Fluid Mech.*, *217*, 263-280, 1990b.

Lister, JR, The solidification of buoyancy-driven flow in a flexible-walled channel. Part 1. Constant-volume release, *J. Fluid Mech.*, *272*, 21-44, 1994.

Lister, JR, and Dellar, PJ, Solidification of pressure-driven flow in a finite rigid channel with application to volcanic eruptions, *J. Fluid Mech.*, *323*, 267-283, 1996.

Lister, JR, and Kerr, RC, Fluid-mechanical models of dike propagation and their application to magma transport in dykes, *J. Geophys. Res.*, *96*, 10,049-10,077, 1991.

Mastin, L.G., and Pollard, D.D., Surface deformation and shallow dike intrusion processes at Inyo Craters, Long Valley, California, *J. Geophys. Res.*, *93*, 13,221-13236, 1988.

Pollard, D.D., Delaney, P.T., Duffield, W.A., Endo, E.T., Okamura, A.T, Surface deformation in volcanic rift zones, *Tectonophys*, *94*:, 541-584, 1983.

Rubin, A.M., 1993a, On the thermal viability of dikes leaving magma chambers: *Geophys. Res. Lett.*, *20*, 257-260.

Rubin, A.M., 1993b, Tensile fracture of rock at high confining pressure: Implications for dike propagation: *J. Geophys. Res.*, *98*, 15,919-15,935.

Rubin, A.M., 1995a, Propagation of magma-filled cracks: *Ann. Rev. Earth Planet. Sci.*, *23*, 287-336.

Rubin, A.M., 1995b, Getting granite dikes out of the source region: *J. Geophys. Res.*, *100*, 5911-5929.

Rubin, A.M., and D. Gillard, 1998, Dike-induced earthquakes: Theoretical considerations, *J. Geophys. Res.*, *103*, 10,017-10,030.

Stock, J.M., J.H. Healy, S.H. Hickman, and M.D. Zoback, Hydraulic fracturing stress measurements at Yucca Mountain, Nevada, and relationship to the regional stress field, *J. Geophys. Res.*, *90*, 8691-8706, 1985.

Chapter 3

Phenomena: Dike/Crack Approach to the Drift's Disturbed Zone

The ascent of the dike can in principle be influenced by the stress perturbation induced by the presence of the repository in the rock mass. It is convenient to decompose this stress perturbation into a mechanical (M) component and a thermomechanical (TM) component.

The M-perturbation is essentially time-independent (assuming that the rock does not have any "viscosity") and is limited to a cylindrical zone around each drift which has a thickness of about 5 meters (i.e. about twice the radius of the tunnel). Assuming that the rock is elastic and the dike orthogonal to the drifts, the stress perturbation perpendicular to the dike plane decays as the inverse of the square of the distance from the tunnel axis from a maximum (minimum) of about 2 MPa at the drift wall (it varies as $\cos 2\vartheta$ around the tunnel). In view of the localized nature of the M-perturbation, and also taking into account that the distance between the axes of two adjacent drifts is about 80 m, we can conclude that propagation of the dike will hardly be affected by the mechanical stress perturbation induced by the repository.

The TM-perturbation is time-dependent, both in magnitude and extent. Calculations of the temperature and stress changes due to thermal loading are summarized by Barr (2000) and by Elsworth (2001). Such predictions are judged very reliable because of the relatively small range of variation of the thermal properties among rocks (expansivity, conductivity, heat capacity, and diffusivity), and the well-defined boundary conditions for this class of problems. Furthermore, the mean stress induced by the temperature is, in the system under study, proportional to $\alpha E \Delta T$ at any point (where α is the thermal expansivity, E is Young's modulus, and ΔT the local temperature change), with the constant of proportionality being a function of Poisson's ratio.

During the first few years following the closure of the repository, the thermal stress induced around each drift is unaffected by the heat generated in the other drifts. The maximum compressive stress change takes place at the tunnel wall and is of the order of a few MPa. The perturbation decays with distance from the drift and the zone of influence increases with time (initially as the square root of time, and later more slowly). After a period of about 100 years, the temperature between the drifts becomes more uniform, as thermal interaction between the drifts has taken place. The thermal stresses induced around the repository become progressively more consistent with those that would have been generated by a uniformly distributed heat source across the footprint of the repository. In the "hot" design scenario, the thermal perturbation is large enough

to cause a rotation of the principal stresses in the repository region over a period of about two thousand years (i.e. the horizontal stresses become the maximum compressive stress and could reach approximately 15 MPa, an increase of about 10 MPa over the initial value). After this period, the repository will progressively cool down, with the thermal stresses having essentially vanished after about 100,000 years.

The stress barrier that develops around a "hot" repository during the intermediate period spanning the first two thousand years could cause the dike to be deflected so as to avoid crossing of the repository. <u>Such a protection is time limited, however, and it is therefore conservative to assume that the dike would propagate vertically under all circumstances and would intersect the repository.</u> The major impact of the thermal perturbation would be to reduce significantly the size of the tip cavity ahead of the magma front, and to increase the magma pressure (see Chapter 2). **Assessment of the change in the lag zone and in the magma pressure due to the existence of thermal stresses should be carried out within the framework of the models discussed in Chapter 2 and in Appendices 1 and 2.**

References for Chapter 3

Barr, G.E., 2000, "Dike propagation near drifts", ANL-WIS-MD-000015 REV00, ICN1

Elsworth, D., 2001, "Summary report to NWTRB, The consequences of igneous intrusions at Yucca Mountain. Some rock mechanics aspects of dike-repository interaction"

Chapter 4

Phenomena as the Dike Intersects the Drift - Shock Phenomena, Gaseous Pressurization

When the dike first reaches a drift, it can be regarded as a form of eruption into the atmosphere.[a] Although the drifts are 300 meters below the surface, they are, nevertheless, presumed to be connected to it by other relatively wide tunnels. The total volume of the subsurface excavations envisaged is of order 0.003 km^3 and depends on whether a 'hot' or 'cold' design is adopted. For scale, this volume is sufficient to fill a single cylindrical drift of diameter of 5.5 m for a length of ~125 km. A volume of 0.003 km^3 is a significant fraction of the lower end of the range of eruptive volumes of the 1 Ma Quaternary basaltic volcanics at Crater Flats (e.g., Little Black Peak, Little Cones, Black Cone and Red Cone) and is about 50 times smaller than the 75 ka old eruption at Lathrop Wells of ~ 0.15 km^3. A table (Table 1-1) of eruptive volumes of all Pliocene and Quaternary volcanic products is given in Chapter 1.

In Chapter 2, the mechanics of the rise of a dike in the absence of drifts is discussed and important information regarding the time development of a basaltic eruption is presented. Because volatiles are strongly partitioned into the vapor during magma decompression, the dynamical evolution of rising magma hinges critically on the thermodynamics of magmatic volatile exsolution and the rheological effects of both volatile-saturated melt and magmatic two-phase mixture.. Although the succession or progression of rheological and hence dynamical states remains the same, the depth at which the development takes place varies depending on the abundance of volatile constituents. Some of this development can be expected to arise within the drifts once breached by the dike tip, though there are differences between a surface eruption and an eruption into a drift. Two main differences are that the earth stress tending to close the dike "fracture" will be of order 5 MPa (maybe rather less) rather than atmospheric (100 kPa) and that the dike flow will converge into the limited drift cross-section. **Although it is not obvious that either of these would imply a qualitative alteration in behavior, the dynamical consequences should be considered in on-going modeling studies.**

---

[a] This will not be true if the drifts are back filled. However, discussed here is potentially a worst case, and hence is conservative or pessimistic. If back-filling is partial but drifts are properly sealed at their ends, then equilibration of pressure within the drifts at the value relevant for the dike flow at their intersection with the dike(s) will take place along the whole of the drifts. This final condition is included in what follows. The only essential change is the time taken to reach a fully pressured state.

The work by Woods *et al.* (*Geophys. Res. Letters* 29, 2002, 19 – 1 to 19 – 4) reported by Brittain Hill at the May 21-22, 2002 Panel Meeting in Las Vegas (NRC Perspective on Magma-Repository Interactions...) and other work reported by Edward Gaffney at the same Meeting (Modelling of Magma/Gas-Drift Interactions) are not inconsistent with this view. <u>However, we take issue with some of the details of the model, especially with some of the assumed initial and boundary conditions. Most simply put, we do not believe that there will necessarily be an explosive decompression of magma leading to significant shock waves when the dike reaches the drift. The pressure within the dike at or near the dike tip is not expected to be equal to the local earth stress as discussed extensively in sections two and three of this Interim Report.</u> This reduction of pressure near the tip is well known to arise in hydraulic fracturing even in impermeable rocks. At the proposed Yucca Mountain Repository (YMR) site, the silicic volcanic tuff near the drifts is unsaturated and quite permeable ($\sim 10^{-12}$-10^{-13} m^2). <u>We therefore expect magma rising in the dike to be at least partially decompressed near the magma front due to 'bleed off' into permeable tuff as it reaches the drift. We expect that a quasi-steady state may be reached such that the evolution of vapor from behind the magma front would lead to a bubbly two-phase flow near the vapor cavity (however small the latter might be).</u>

The shear viscosity of this bubbly mixture is considered in Chapter 1. <u>The concept of magma with a pressure exceeding the dike-normal stress being coincident with the dike tip, *i.e.*, no vapor cavity or low-pressure two-phase region, is unlikely in the Panel's view.</u> Once the drift is reached, it is however reasonable to assume that there would be some acceleration of the decompressive process in the magma and consequent extension downwards into the dike of the two-phase flow region, just as happens when a dike first erupts, although the magnitude of the effect would be less than in the case of magma at 10-20 MPa pressure breaching a drift or system of drifts. **A more comprehensive calculation of the flow of magma-drift interaction given these initial conditions and magma properties, which forms part of the Woods *et al.* study and of Gaffney's work, is entirely justified. Indeed, such calculations are required if any of the scenarios described by Hill are to be investigated.**

It seems sensible to adopt the simplification of neglecting the presence of canisters and other obstructions in the drifts, and of regarding the walls as rigid and the drifts as infinitely long, when carrying out initial fluid mechanical calculations for magmatic flow into drifts. **Such calculations should provide the basis for deciding whether the dike tip arriving at a drift would continue upwards above the drift (discussed in more detail in the next Chapter) so that the drift becomes a side channel, whether the drift would fill up to its ends and whether cracks/fissures/faults some way along the drift would open up thus further diverting the magmatic flow.**

The key variable in making such estimates would appear to be the local pressure in the magmatic flow. (This is the context in which the term "lubrication approximation" should be viewed; even though there will be a vertical pressure gradient in a horizontal [or subhorizontal] drift, such pressure variations across the drift will be largely insignificant compared with variations along the flow lines). Simple arguments show that in general pressure will decrease along flow lines. As argued in the next Chapter, drifts can be regarded as hydrodynamic 'sinks', which 'steal' magma locally from the rising dike flow. This implies that vertical streamlines in a dike rising below the drifts will be distorted towards the drifts once the drifts are intersected by the dike. <u>From the simple argument that pressure decreases along flow lines, there will be a local minimum of pressure at the entry to drifts with respect to pressure elsewhere in the dike. Furthermore, while there is flow along the drift away from the point where it intersects the dike, the pressure will decrease away from the entrance. Indeed if vapor can continue to escape from the drift ahead of the flowing magma, the pressure will fall to near atmospheric at the limit of magma intrusion. Thus if the rock above the drift is in a uniform state as far as position along the drift is concerned, the dike can be expected to continue upwards after reaching the drift, and not anywhere else along the drift. A significant exception to this would only occur if a sealed end of the drift were reached, in which case the pressure would rapidly equilibrate along the whole length of the sealed portion of the drift, and if, in addition, the rock stresses above the drift were very non-uniform along the length of that sealed portion of the drift.</u> **This is the so-called dog-leg scenario, which needs further careful study.**

Estimates of canister transport/entrainment of waste by magmatic (one- or two-phase) flow, dealt with in Chapters 6 and 7 below, can then be based on the simplified fluid-mechanical solutions carried out neglecting the presence of waste. The simplified calculations are in principle straightforward, even if complicated by a need to include dike propagation, heat transfer, vapor evolution, and possibly non-Newtonian viscosity. What matters crucially is whether the flow past the canisters would be a slow melt-dominated magma flow, as in an un-erupted dike far from its tip, or would be a fast low-density relatively compressible multiphase flow with a volatile phase being the continuous phase characteristic of localized slug or pyroclastic conduit flows.

Chapter 5

First (Liquid) Magma Arrives at the Drift

**5.1   Dike propagation following intersection with the drifts/partitioning
        of magma between a dike and drifts**

Importance:
*The degree to which the drifts impede further dike propagation or magma flow up
the parent dike affects the likelihood of ultimately forming a pathway to the
surface along new or pre-existing fractures that may be quite distant from the
parent dike. This could give rise to a scenario in which magma flows up the dike,
along many drifts for considerable distances, and then up to the surface. This
would affect many more canisters than in the "cookie-cutter" model in which only
those canisters within the footprint of a volcanic plug are impacted.*

The possibility of magma breaking out of the drifts at some distance from the
parent dike is considered later in this Chapter. Here we focus on the narrower
questions of (1) the ability of the drifts to impede further dike propagation, and (2)
assuming the parent dike does extend above the drifts, the ratio of the mass flux
up the dike to the mass flux down the drifts. The drifts can influence dike
propagation in the following ways:

1. They can locally increase the ambient compressive stress acting normal to the
dike plane (by tunneling or by thermally-induced stresses).

2. They can locally alter the principal stress directions, for example by making the
least compressive stress vertical, which might promote sill formation.

3. They can act as mass "sinks", spaced about 80 m apart, that suck off magma
or pyroclastic material that otherwise would have been available to pressurize
and promote continued propagation of the parent dike.

Point (2) above is discussed in Chapter 3 and is not considered further here.
The stresses alluded to in point (1) are not computed here but their estimated
range from existing modeling is considered.

*The main focus of this Chapter is to outline our current thinking about how to
quantify point (3). This can be divided in turn into two parts: (a) the ability of the
dike tip to propagate beyond the drifts before magma reaches the drifts, and (b)
assuming the dike continues propagating, the partitioning of magma into the
drifts and up the dike once magma does reach the drifts.*

Consider first a much simpler model problem: A rigid-walled penny-shaped crack filled with a compressible liquid at high pressure, into which (perpendicular to the crack) is drilled a low-pressure hole at the crack center. Relevant parameters are the crack thickness w and radius a, the hole radius R, the fluid viscosity η and compressibility β, and the initial pressure difference between the crack fluid and the hole ΔP. The problem is time-dependent as the low-pressure region diffuses out from the central hole, but provided $a >> R$ the ratio a/R initially plays no role in determining the mass flux. In addition, provided $R >> w$ the viscous pressure drop down the hole is negligible, and one can model the "hole" simply by applying the low-pressure boundary condition within the crack at a distance R from the origin. Under these conditions, the ratio R/w also plays no essential role and the mass flux into the hole (suitably normalized by the crack thickness and fluid viscosity) is determined by two ratios: the ratio of the hole radius R to the diffusion length (until this approaches a), and the ratio $\Delta P/\beta$. For a given crack thickness and material properties η and β, the mass flux out the hole increases with the hole diameter and the initial pressure drop.

Another highly simplified model problem involves an incompressible fluid flowing up a rigid-walled crack in response to an imposed pressure (in excess of hydrostatic) at the base. Assume that the pressure boundary conditions at the top of the crack and in a series of holes drilled orthogonal to the crack at a fixed depth and with a spacing a are atmospheric. Under these conditions a steady-state flow is reached. Increasing the pressure at the base of the crack (or decreasing the fluid viscosity) increases both the flux up the crack and the flux out the holes but leaves the ratio of these fluxes unchanged. In this scenario, the ratio of the flux up the crack to the flux out the holes is determined only by the hole diameter-to-spacing ratio R/a.

The actual problem of interest is of course much more complex because it requires consideration of (1) both fluid compressibility and a bottom boundary condition, (2) the time-dependence of the dike thickness and pressure even in the absence of interaction with the drift, (3) elastic dike thickness changes in response to pressure changes induced by mass loss into the drifts, (4) the possibility of the flow of both pyroclastic material and bubbly magma into the drift, with their different constitutive laws and momentum equations, (5) coupled hydrodynamic (in the fluid) and perhaps elastodynamic (in the crack) effects if decompression is explosive and pyroclastic material enters the drift, and (6) the evolution of the drift in terms of pressure and the nature of the material filling it.

Before embarking on a numerical program to evaluate some or all of these effects, some rules-of-thumb can be derived from the simple model problems discussed above. Flux into the drifts increases with the ratio of the drift diameter to drift spacing, and with the dike/drift pressure differential. The drift diameter/spacing ratio is small (~1:15). Thus, unless the pressure drop from the dike into the drifts is "large" in some sense, the mass loss into the drifts will be of little consequence to the dike. Results discussed in Chapter 2 suggest that the

pressure within the dike tip cavity will be only very slightly greater than that in the drifts. <u>In this case, if the tip cavity is much larger than the 5-meter drift diameter, then the drifts (as opposed to the drift-induced stress field) should be nearly "invisible" to the dike and will exert a negligible influence on propagation.</u> As discussed in Chapter 2, tip cavities much longer than 5 meters are expected for dikes of modest thickness if (1) thermal stresses are small and (2) inelastic deformation does not significantly shorten the tip cavity, relative to the linear elastic calculation.

If thermal stresses increase the dike-normal stress to 10-20 MPa, then for bulk dike excess pressures of one to a few MPa and lengths of one to a few kilometers, tip cavities of only 1-10 m might result (Chapter 2, Figure 2-3). For tip cavities only a few meters long the drifts would see a time-varying pressure before the dike tip extended beyond the drifts. **Computing the initial flux into the drifts under this scenario would require judicious use of numerical models.** However, the first "magma" to intersect the drift would have a pressure that is continuous with the (approximately atmospheric-pressure) tip cavity and would therefore be very frothy, and in addition would occupy a crack that at this point is probably ~millimeters thick. This would make the initial magma/drift interaction very different from that envisioned by Woods et al. (2002), in which at time zero a 1-m-wide dike at 10-20 MPa pressure has intersected the drifts.

As a first pass at computing the mass flux into and pressure history within the drifts, one could imagine using the CFDLIB numerical package discussed by Edward Gaffney at the Peer Review Panel meeting in Las Vegas on May 21, 2002. Instead of the uniform dike pressure/thickness initial condition adopted by Woods et al. (2002), **one could adopt the dike pressure/thickness profile that resulted from a dike propagation calculation in the absence of a repository. This dike thickness profile could then be advected past the drift opening at the (drift-absent) dike propagation velocity.** The result would be a much more gradual pressurization of the drift than in the Woods et al. calculation, because of both the low pressure and the narrow aperture near the dike tip.

The above approach neglects the change in dike thickness brought about by the changing pressure distribution within the dike. Accounting for this would be quite a challenge numerically, particularly in 3-D. **An approximate 2-D approach would be to transform the mass loss from the dike per drift into a mass loss per unit strike length of dike. This mass loss could then be imposed as a point sink at the repository depth in a 2-D dike propagation calculation. As with the approach to the surface (see Chapter 2), the fluid velocity would have to be monitored to determine when it was necessary to include mass acceleration in the momentum equation.** Two end-member results are instructive: If the (strike-normalized) mass loss is negligible compared to the local flux up the dike, propagation is largely unaffected. On the other hand, if the mass loss is sufficient, propagation of the dike tip will cease.

The geologic analogy for the latter would be a diatreme or kimberlite pipe, where (presumably) as the dike tip approached the surface there was sufficient gas escape to erode a plug that was capable of siphoning off a sufficient mass flux to shut down the rest of the dike (mined kimberlite pipes are generally observed to become more tabular and "dike-like" over a depth range of hundreds of meters to kilometers). This is probably not a good analogy for Yucca Mountain magmas because, as was discussed in Chapter 2, gas escape is expected to maintain a near-atmospheric pressure in the tip cavity for basalts with 2-4 wt% H_2O. An additional difference is that the drifts will pressurize with time, whereas the earth's surface remains at atmospheric pressure. However, mechanical erosion of the drift walls at the dike intersection seems likely.

5.2   Phenomenon: magma goes down the drift

The first material to enter the drifts is expected to be pyroclastic. Previous chapters have discussed the importance of keeping track of the gas pressure in the drifts and ways in which this might be done.

Eventually, bubbly magma is likely to enter the drifts. This may occur if (1) the drifts have been pressurized sufficiently to prevent further explosive decompression of the magma (e.g., to perhaps 10 MPa for 2 wt% H2O; see Fig. 6-1), or (2) the drifts fill with partially degassed magma that enters as gas-accelerated spatter from the dike/drift intersection, by the viscous flow of degassed drainback down the dike at some later stage of an eruption, or perhaps by some other mechanism. Given that the initial pressurization of the drifts is expected to be more gradual than in the Woods et al. (2002) calculation, and given the permeable nature of the repository rocks, scenario (1) may be unlikely. However, one could postulate that scenario (2) might give rise to a "dogleg" in which magma flows for considerable distances along one or more drifts prior to eruption.

The Panel recognizes the importance of evaluating this possibility but has not had sufficient time to do so. What follows is a list of issues that have been identified as important, and some preliminary comments on them:

1. What is the pressure of the bubbly magma mixture away from the drift? This will be less than the pressure at the dike/drift intersection, assuming that the magma flows away from the dike. If the viscosity of the drift magma is low enough that the flow does not reach the drift roof, then (unless the roof becomes spatter-covered) the permeability of the drift walls to gas ensures that the pressure in the drift will be not much more than that in a standing body of magma 5 m deep. The pressure downdrift must be greater than the compressive stress across any pre-existing fracture that might be hypothesized to act as a pathway to the surface.

2. What is the density of the bubbly magma mixture entering the drift? The ability of magma to erupt through fractures distant from the parent dike requires pressures large

enough to drive the magma to the surface as well as to open those fractures. If the drift fills with dense, partially degassed magma, then it is possible for the magma to open pre-existing fractures at the level of the drift without having sufficient pressure to erupt. Even if the drift pressure is sufficient for eruption, if the static pressure gradient in the magma is greater than the vertical gradient of the horizontal stress normal to the potential fracture (occurring for bubble fractions less than ~50%, for a horizontal stress that increases at 12 MPa/km), magma entering the fracture will preferentially move down, not up. The fraction of the magma that does move up will do so in a narrow fracture and be susceptible to freezing (see point 5 below).

3. What is the viscosity of the magma entering the drift? If this is the same as the viscosity of the magma in the dike, then (assuming the dike thickness to be considerably less than the drift radius) the flow down the drift will have a gentle slope, low pressure, and the opportunity for further degassing and densification. If the viscosity is larger than that in the dike (e.g., a spatter-fed flow from a gas-charged dike) but most of the dike flow goes straight up, the scenario might be the same. If the viscosity is larger than that in the dike and a large fraction of the dike flow is initially channeled into the drift, the drift flow might rise to the drift roof and a substantial pressure gradient might arise within the drift. While the dike flow remains gas-charged, however, it seems likely that this would quickly reduce further flux from the dike into the drift. **The question of the viscosity of the drift flow might be addressed by looking at the slopes and estimated cooling times of analog Lathrop Wells flows.**

4. What is the velocity of the magma flow within the drift? If this is low enough, then magma will tend to freeze onto the canisters (or exposed waste material, if damaged by earlier pyroclastic flows) and this frozen rind will only increase with time. If the velocity is large enough, however, this initial chilled margin can be remelted by continued flow and waste material may contact magma.

5. What is the thermal fate of the flow up the distant fractures? The drift is fed by some fraction R (0%<R<100%) of the flow up a robust parent dike. This fraction must then feed a new dike, for the dogleg to occur. If R is low enough, then the new dike will be more susceptible to freezing than the parent dike (particularly if the magma is more viscous than the parent dike, or "effectively negatively buoyant" because it has less than ~50% bubble fraction).

6. What is the explosivity of the "dogleg" magma upon eruption? This should be considerably less than that of the parent dike, if it is correct that bubbly magma flows down the drift not because the drift pressure is large but because the magma is partially degassed. This would give rise to considerably lower eruption column heights, and perhaps the eruption of a larger fraction of contaminated magma rather than contaminated ash.

7. How does the magma flow degrade the canisters/incorporate the waste? This issue is discussed to some extent in subsequent chapters.

5.3 Split fraction: magma breaks through at original dike, vs. breaks through elsewhere, vs. never breaks through

We now examine various scenarios of magma breaking out of the drifts, once the repository has been filled with hot magma. We consider separately two situations: Case 1 where the horizontal stresses are larger than the vertical stress, and Case 2 where the vertical stress remains the maximum compressive stress. (Note that the horizontal and vertical stresses are contrasted at the repository scale, not at the drift scale.)

Case 1 (the horizontal stresses are larger than the vertical stress): This situation arises within the period spanning approximately a few hundred years to a few thousand years following closure of the repository, in the hot design scheme. To first order, the pressure in the drift system will be equal to the horizontal stress perpendicular to the dike (i.e. the original *in situ* stress augmented by the thermal component). Under these conditions, the drifts would more likely break at mid-height and a system of horizontal fractures (that could possibly link) would form. This magma eruption from the drifts would lead in effect to the propagation of sills. Outside the repository area, where the vertical stress becomes again the major compressive stress, the magma-filled fracture would either progressively reorient to eventually propagate along vertical planes perpendicular to minimum horizontal stress, or feed magma into pre-existing vertical fractures. (Reorientation of the fractures would be accompanied by multiple break-ups of the crack edge, associated with mode-III fracture propagation.) Note, however, that a significant volume of magma could be held inside the sill, especially when accounting for the increased storage due to bulging of the ground surface, for crack radius to depth ratio exceeding 1. **Calculations should therefore be performed to assess the possibility that the system of drifts and the sills (within the repository footprint) could contain the volume of magma diverted from the main dike.** Appendix 3 outlines the equations to be used to compute the radius of a sill in stable limit equilibrium (i.e. no further propagation takes place), given the volume of magma it contains, the elastic properties of the rock and its toughness.

Case 2 (the vertical stress remains the maximum compressive stress): We consider two mechanisms of magma breakthroughs: (Case 2a) the magma erupts along fractures aligned with the drift axis that have initiated in the crown and in the floor of the tunnel; (Case 2b) the magma erupts along pre-existing fractures that are sub-orthogonal to the drift (and the thus roughly parallel to the dike plane).

- Case 2a is plausible since in the absence of thermal stresses and when the tunnels are not pressurized, the stress concentration around the drifts yields low values of the hoop stress in the crown and in the roof. However, propagation of the fractures beyond a distance approximately equal to the drift diameter causes the fracture to be orthogonal to the

smallest horizontal stress. The energy losses associated with fracture turning imply that these fractures are unlikely to propagate far-beyond the zone of stress concentration. <u>Thus, in this scenario, we can conclude that the magma would erupt along the original dike, even though vertical longitudinal fractures would have initiated along the drifts.</u>

- For <u>Case 2b</u>, we consider the simplified scenario of an existing fracture parallel to the dike. It is expected that the aperture of this fracture would be less than the opening of the dike under most circumstances, since it closed by compressive stress. Although one would infer from static considerations alone that the pre-existing fracture would reopen since the magma pressure in the drift is about the same as the normal stress across the fracture, <u>it is easy to argue using hydrodynamical considerations that the magma would flow in the fracture with the widest opening, i.e. along the pre-existing dike in this case. Nonetheless, eruption of magma along this existing fracture rather than the dike cannot be ruled out entirely. For example, the normal stress across the fracture could be substantially less than across the dike because of the surface topography.</u> **An analysis of the influence of the surface topography and the presence of the dike on the horizontal stress around the repository would shed some light on the possibility of magma eruption from an existing vertical fracture intersecting a drift.**

In summary, if the horizontal stress is more compressive than the vertical stress (approximately during the first few thousands years following sealing of the repository, in the hot design), the magma would escape the drifts via the formation of sills. If the sill extends into the region outside the repository where the vertical stress is again the maximum compressive stress, then the possibility exists that the magma could reach the surface, either by pre-existing vertical fracture or by reorientation of the initially horizontal fracture. If the horizontal stress is less compressive than the vertical stress, the magma would preferentially erupt along the original dike, but it is possible to imagine scenarios where it might erupt along pre-existing vertical fractures intersecting the drifts. Further work is necessary to assess the likelihood or reasonableness of such scenarios.

Chapter 6

Magma Breaks Through at Original Dike (Hence, Eruption)

The effect of an eruption on the annual dose to nearby inhabitants depends on numerous factors: among them, the eruption type, the number of waste packages entrained, the degree to which waste in entrained packages is incorporated into the erupting magma; the dispersal area and grain size of eruptive products, the degree and mode of remobilization of eruptive debris following deposition. These factors are controlled in turn by additional ones; the dispersal area of eruptive products, for example, depends on magma composition, mass eruption rate, and wind velocity, to name just a few.

Table 6-1 lists eruption-related factors deemed most significant in affecting dose to nearby residents. They can be grouped into (1) subsurface processes during eruption (items 1-4), (2) surface processes during eruption (5-6), and (3) remobilization into the biosphere following deposition.

6.1　Subsurface processes during eruption

6.1.1　Probability that an intrusion at repository depth will erupt

As described elsewhere in this report and in reports of the Yucca Mountain Project (e.g. ANL-WIS-MD-000015 REV00, ICN1), the characteristics of an intrusion into the Yucca Mountain region are controlled largely by magma composition, source characteristics (magma flux and volume), host rock properties, state of tectonic stress, and large-scale properties of the Earth's crust in the area. Past eruptions in Pliocene through Recent time consist primarily of alkali basalt (e.g. Crowe et al., 1983), which are thought to have originated from mantle depth and risen to the surface, perhaps with storage and some fractional crystallization at intermediate depths along the way. Basalts generally intrude as fissures oriented parallel to the most compressive horizontal stress direction, S_H, or through pre-existing fractures at an angle to S_H limited by the ratio of horizontal principal stress magnitudes. Repository drifts are oriented perpendicular to this orientation and therefore will likely be intersected at a high angle to the dike. The upward propagation of a dike is controlled primarily by its vertical pressure gradient relative to that of the least horizontal compressive stress (S_h). The vertical gradient in S_h is anomalously low in this area (e.g. Stock et al., 1985; see also Chapter 2 of this report)—probably lower than the vertical pressure gradient in a dike containing less than a few tens of percent vesicles; thus hindering the upward propagation of dikes at depths below that where vesiculation is significant. This factor may partly explain the petrologic evidence for storage and partial crystallization of magma at crustal levels en route to the surface (Crow et al., 1983).

Table 6-1:

Some of the most important factors affecting dose to nearby residents following a volcanic eruption through the waste repository. In the right-hand column is an order-of-magnitude estimate of the uncertainty in these parameters. For example, an uncertainty of 10^{-1} implies an uncertainty of a few tens of percent in the value taken in the TSPA-SR; 10^0 implies that the uncertainty may be a few times less or greater and the value, etc. The uncertainties noted here provide a basis for ranking the importance of each factor.

Factor	Uncertainty
Probability that a dike will erupt once it reaches the repository	10^0

Number of waste packages that contact erupting magma
   i. Number of conduits
   ii. Route(s) followed by magma to the surface (i.e. straight up, or diverted through repository drifts).
   iii. Conduit diameter (10^0) & geometry
      1. Mechanisms of conduit development
	10^1

Fraction of waste in each package that is entrained into erupted material	10^1 [a]
Grain size of entrained waste	10^2 [b]

Deposit thickness in nearest inhabited area
   iv. Magma properties
   v. Mass flow rate
   vi. Host rock properties (e.g. gas permeability)
   vii. Atmospheric properties
      1. Thermal lapse rate
      2. Moisture content of atmosphere
      3. Wind velocity
	10^2 [c]

Concentration of waste in tephra deposit
   i. grain size distribution of tephra
   ii. grain size distribution of waste
   iii. Number of canisters entrained, and disruption of canisters
	10^2 [d]

[a] The TSPA-SR assumes that all of the entrained waste is removed from canisters and incorporated into the magma. It seems plausible, however, that only a small fraction ($<\sim 10^{-2}$) of the waste might be incorporated if fuel rods are not breached.

[b] the grain size of entrained fragments may vary from roughly the size of a waste pellet ($\sim 10^{-2}$ m) to that of the powder ($\sim 10^{-6}$ m).

[c] Based on mapped deposits from analog eruptions, the deposit thickness at 20 kilometers could vary from centimeters to the mean grain size of the deposit at that location ($>\sim 10^{-5}$ m)

[d] The uncertainty in this number reflects primarily the uncertainty in the number of waste packages entrained in the eruption, and, to a lesser extent, the grain size of the waste.

At a depth of roughly 300 meters, and a pressure equal to S_h at that depth (~2 MPa), however, an alkali basalt containing 1-4 wt% H_2O would contain a significant fraction of gas by volume (Fig. 6-1) and, assuming that most of the exsolved gas had not yet escaped, would have a bulk density (ρ) less than half that of the unvesiculated magma (2500-2700 kg/m³). The pressure gradient (ρg, where g is gravitational acceleration) within such a mixture would be comparable to or less than the vertical gradient in S_h (~7,000 to 8,000 Pa/m; Stock et al., 1985). <u>Whether the dike reached the surface or not would depend largely on the degree to which gas could escape from the magma, densifying it and increasing its vertical pressure gradient above that of S_h (see Chapter 2 for details).</u>

The TSPA-SR assumes that the probability of an eruption is a large fraction of 1 once the intrusion has ascended to repository depth. **As a conservative measure, the TSPA could easily assume that the probability of an eruption equals 1 once the dike has ascended to repository elevation.** Assigning a particular probability to eruption (e.g., 0.37) requires some physical justification and is subject to debate. The difference between the value assumed in the TSPA (~0.3-0.7) and 1 is not likely to substantially affect TSPA results.

6.1.2 Number of waste packages contacting magma

The processes of dike intrusion and conduit enlargement would incorporate some number of waste packages from the drifts into the erupting magma-gas mixture. Calculations of waste-package incorporation for the TSPA are based on the well-established observation that basaltic eruptions begin along a linear fissure, then focus into a few central vents (e.g. slide 10, Greg Valentine's talk at the May Panel meting). <u>The number of waste packages incorporated therefore depends on the number of primary conduits, on the size of the conduit and on the mode by which wall rock (and waste packages) are removed from conduit walls.</u>

6.1.2.1 Number of vents, and conduit diameter

The number of possible vents used in the TSPA (up to 5) is consistent with observations from Surtsey (Thorarinsson, 1964), Tolbachik (Doubik and Hill, 1999), Paricutin (Luhr and Simkin, 1993), and Hawaii (e.g. Richter et al., 1970; Wolfe et al., 1987). At the Earth's surface, these vents are circular in plan view. In the subsurface their geometry is more poorly constrained; they are assumed to become increasingly ellipsoidal in cross section with depth and merge with the tabular shape of the dike. The depth interval for the cylindrical-tabular transition is also not well constrained, though it may be related to the fragmentation depth; volatile-rich kimberlites, for example, produce cylindrical diatremes that extend kilometers or more.

Volume fraction gas and density of Yucca Mountain basalt
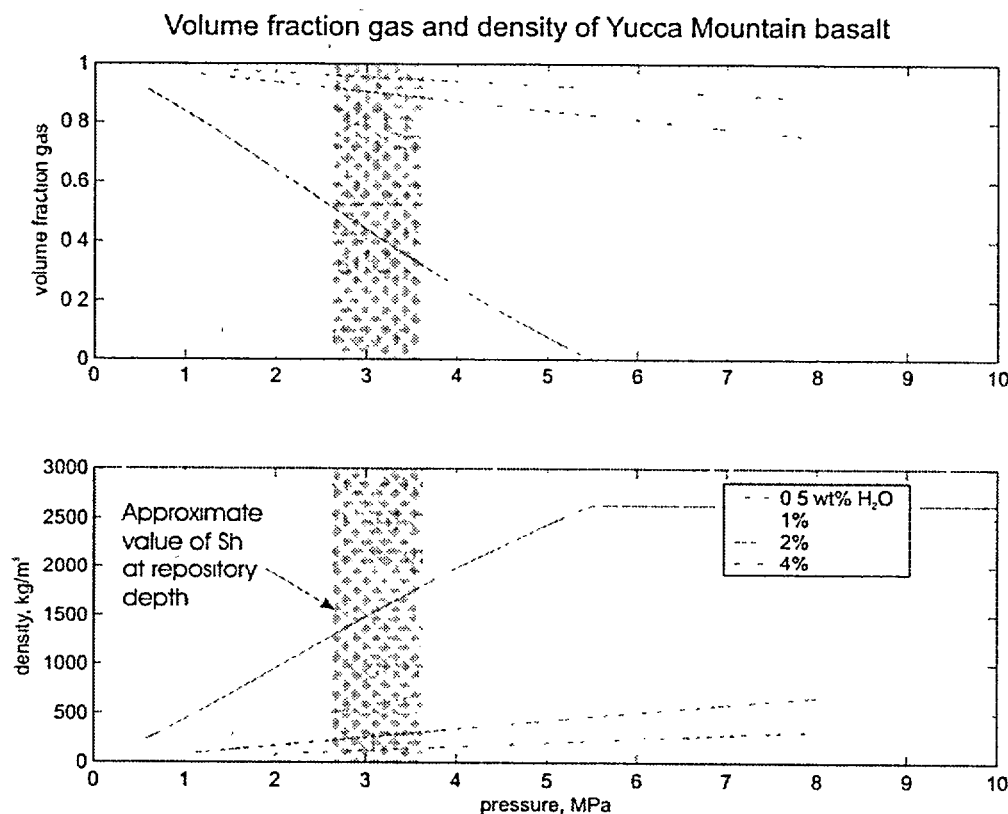
Figure 6-1

Volume-fraction of gas (a) and bulk density (b) of a vesiculated basalt-gas mixture as a function of pressure, for four values of total water (exsolved plus dissolved) in the magma

Calculations were made using Conflow (Mastin and Ghiorso, 2000; Mastin, 2002), which calculates density of basalt using the method of Ghiorso and Sack (1995), the density of the gas phase using thermodynamic relations of Haar et al. (1984), and the solubility of water in melt of this composition by comparing the chemical potential of dissolved water in the melt (calculated using methods of Ghiorso and Sack, 1995) with that of water (calculated using methods of Haar et al., 1984). At saturation, the chemical potential of this species should be the same in both the dissolved and exsolved phases. The calculations ignore the escape of gas during ascent and therefore give maximum values of volume fraction gas, and minimum values of density. At pressure corresponding to S_h at the repository depth (gray shaded area), the magma would be highly vesicular and its bulk density less than half that of the unvesiculated melt (2500-2700 kg/m^3).

Based on surface exposures of eroded basaltic conduits (e.g. WoldeGabriel et al., 1999) and of studies of lithic components of basaltic cinder-cone ejecta (e.g. Doubik and Hill, 1999), the TSPA assumes a diameter distribution ranging from a few meters to 150 m, with a mean of 50 m (e.g. ANL-MGR-GS-000002, REV 00, ICN 01, p. 25-26) Other studies of exposed basaltic dikes and plugs (e.g. Delaney and Pollard, 1981) are consistent with a diameter of tens of meters at a few hundred meters depth. Models of conduit flow, however, suggest that the mass flux associated with a violent Strombolian eruption (10^4-10^6 kg/s) could be delivered through a conduit only a few meters in diameter (Table 6-2). The discrepancy between model results and observed conduits may be reconciled by at least two possibilities: (1) magma flows through only a small fraction of the available conduit cross-sectional area during the most vigorous basaltic eruptions; or (2) conduit enlargement takes place after violent Strombolian activity has ceased. The latter mechanism appears to have occurred at Tolbachik (Doubik and Hill, 1999). In long-lived eruptions that discharge cubic kilometers of magma, conduit enlargement also takes place by thermal erosion (e.g., Pu'u O'o). **In view of the latter mechanism, it may be worth considering that the conduit diameter used in TSPA models be correlated with eruption duration or total volume.** Overall, however, the discrepancy between model results and observations would not seem to warrant a downward revision of the range of conduit diameters (15-150 m) used in the TSPA.

6.1.2.2 En echelon dike segments

One complication mentioned in ANL-MGR-GS-000002, REV 00 (p. 26), though not incorporated into the TSPA, is the possibility that more than one dike segment could intersect each drift. Basalt fissures typically intrude as en echelon segments, with a certain degree of overlap between each segment. A perusal of published maps of exposed basaltic dikes (e.g. Delaney, 1981; Delaney et al., 1986) suggests that adjacent en echelon segments are typically separated by meters to tens of meters, and overlap one another by a similar amount. It also appears that overlaps make up only a few percent of the total length of an en echelon dike array. **More systematic study of published maps, and possibly of exposed dikes in outcrop, would help verify this point.** If the spacing and overlap between adjacent dikes were in fact meters to tens of meters, a small percentage of the drifts in the Yucca Mountain repository would be intersected by more than one dike segment.

It should be noted that thermal stresses may cause dikes to curve near drifts. A vertically propagating dike may rise to an elevation above the repository between drifts, and then connect through the drifts along ragged, en echelon steps. If thermal stresses extend a few drift radii (~10 m) from the drift wall, and if the dike were deflected a few degrees from its average orientation over this distance as it propagated toward the drift from both sides, the dike step through the drift would be on the order of a meter. Thermal effects on dike-drift interaction are discussed in greater detail in Chapter 3.

Table 6-2

Modeling results of mass flux (kg/s) versus conduit diameter for three initial dissolved water contents

These values were calculated using a public, open-source conduit-modeling program (Conflow; Mastin and Ghiorso, 2000), using a magma with the same composition as Lathrop Wells basalt, at 1120 C, with 15% crystals by volume, in a conduit 1 kilometer long. Results in plain (non-bold, non-italic) text are for a pressure of 27 MPa at the base of the conduit; **results in bold** are for a basal pressure of 20 MPa, and *results in italics* are for a basal pressure of 10 MPa.

Conduit Diameter (m)	Mass flux (kg/s)		
	1 wt% H_2O	2 wt% H_2O	4 wt% H_2O
1	9.39E+03	1.54E+04	2.25E+04
2	7.12E+04	1.04E+05	1.28E+05
3	2.22E+05	3.08E+05	3.46E+05
4	4.81E+05	6.47E+05	6.89E+05
5	*2.145E+05*	*4.229E+05*	*4.489E+05*
5	**5.033E+05**	**7.974E+05**	**8.927E+05**
5	8.57E+05	1.13E+06	1.16E+06
6	1.36E+06	1.76E+06	1.78E+06
7	1.98E+06	2.55E+06	2.52E+06
8	2.73E+06	3.50E+06	3.41E+06
9	3.60E+06	4.60E+06	4.44E+06
10	*1.041E+06*	*1.936E+06*	*2.074E+06*
10	**2.568E+06**	**4.011E+06**	**4.205E+06**
10	4.61E+06	5.87E+06	5.62E+06

6.1.2.3   The "dogleg" scenario

For mechanical reasons, the eruption scenario has been envisioned to involve a dike that cuts through the waste repository and continues to the surface. Under this scenario, the number of waste packages directly intersected by a dike or conduit would typically amount to a few per drift (up to perhaps a few dozen, if a 150-m diameter conduit intersected a drift). A less likely scenario is that magma would be diverted through one of the drifts and up a pre-existing shaft, or possibly up a new dike, to the surface. This possibility, considered in some studies (Woods et al., 2002; IRSR, Rev. 2, 1999, pp. 78-81), could entrain hundreds of waste packages in erupting magma depending on the drift length and the number of drifts through which magma flowed. The possibility of such a scenario is considered in Chapter 4 from a mechanical perspective. Here we consider the consequences of such a scenario on eruptive processes and on the entrainment of waste.

Eruption through one of the exhaust or intake airshafts. <u>This scenario would seem plausible only in the 200 or so years prior to permanent closure and sealing of the repository.</u> If the seals on these shafts are engineered and constructed with the possibility of an eruption in mind, their strength should exceed that of the surrounding rock, ensuring that any intrusion proceeds elsewhere. If an intrusion were to take place in the first 200 years of the repository, the magma must either (1) be diverted through the intake air shaft to the surface, or (2) flow downward from the drifts into the exhaust main (see, for example, Figure 2-44 of the Science and Engineering Plan), then along the exhaust main and upward through the exhaust air shaft.

Eruption through a dike that initiates within the repository. Assuming that the east and west mains are backfilled during repository closure, <u>a secondary dike would most likely initiate somewhere within the repository drifts.</u> Small dikes would have to initiate separately at the end of each 5.5 m diameter drift, and then link up between drifts, which are spaced about 80 m apart.

In intact rock, the excess fluid pressure required to propagate a dike decreases with the square root of dike length (e.g. Pollard, 1987). Thus the pressure required to propagate a "starter" dike, within an initial length slightly larger than the 5.5 m drift diameter, would be many times greater than that required to propagate the existing, kilometers-long dike. **Exactly how much additional pressure is required is not known, but could be assessed using numerical models currently available.**

In fractured rock, the propagation of a magma-filled crack from the drift requires only that the magma pressure impose a tensile stress normal to the fracture plane. The magma pressure required to open cracks at the drift wall depends on crack orientation; under the current stress regime, the most favorably oriented cracks would lie parallel to the drift axis at the top and bottom of the drifts.

However such cracks would find themselves oriented perpendicular to the most favorable far-field orientation once they propagated beyond the stress concentration imposed by the drifts. <u>In any case, the tensile stress concentration at the tip of the pre-existing dike would make it much more likely that the dike would propagate vertically past the drifts to the surface, rather than reach the surface via a second dike that nucleates within the drifts.</u>

6.1.3 Waste package movement

Numerical models (e.g. Woods et al., 2002) suggest that fragmented magma may flow through drifts at many meters per second during the most violent phases of the eruption. During the initial breakout of magma and gas into a drift, the passage of pyroclastic debris and shock waves could potentially pick up and damage canisters. On the other hand, if magma and gas were to be diverted through a drift, the canisters could conceivably be picked up and expelled or piled up in "log jams", during the steady-state flow of magma and gas through a drift. Whether waste canisters can be picked up and moved by the flowing magma-gas mixture depends largely on how much momentum may be transferred from the flow to the canisters.

6.1.3.1 Displacement in a drift

During *passage of a shock wave* through the drift, ANL-WIS-MD-000015 Rev 00 (p. 24-25) calculates that waste canisters may be accelerated to ~5 m/s. This high velocity is based on conservative assumptions that (a) the pressure difference across the shock (~32 MPa) is roughly twice the pressure difference between the dike and the drift, and (b) the force of the shock wave is applied across the full frontal area of the waste canisters.

During *steady-state flow* of gas and magma through the drifts, the force (F) against the waste canister would be:

$$F = \frac{1}{2}\pi r^2 \rho_m v^2 C_D \qquad (1)$$

where r is radius of the waste canister (0.83 m), ρ_m is bulk density of the mixture, v is mixture velocity, and C_D is the drag coefficient for the mixture. Taking $\rho_m=\sim1,000$ kg/m^3, $v=\sim10$ m/s, and $C_D=1.17$ for a flat circular plate at high Reynolds numbers (Hoerner, 1965, p. 3-15), the force against the front of a waste canister would be on the order of 1.3×10^5 Newtons. By contrast, the frictional strength of the waste-canister pallets is $\mu Mg=\sim2.4\times10^5$ Newtons, where μ is the coefficient of friction of the pallet (~0.6; AML, p. 24), M is the canister mass (4.23×10^4 kg; AML, p. 24), and g is gravitational acceleration (9.81 m/s^2). These numbers agree to within a factor of two, which is less than the probable uncertainty in their values. <u>Thus the flowing magma-gas mixture could, under</u>

certain circumstances, probably move the waste canisters. Woods et al. (2002) reach a similar conclusion using a similar analysis.

6.1.3.2 Lifting in a vertical conduit

In a vertical conduit, an intact waste canister will rise if the upward force imparted by the erupting magma-gas mixture equals the canister's buoyant weight. The canister buoyant weight is $(\rho_c - \rho_m) \pi r^2 L g$, where L is canister length (5.5 m) and ρ_c is canister density, equal to $(2.14 \times 10^4 \text{ kg})/(\pi r^2 L) = {\sim}3500 \text{ kg/m}^3$. The upward force on the canister due to flowing magma is:

$$F = \pi r L \rho_m v^2 C_D \qquad (2)$$

where v in this case is the velocity difference between the canister and the fluid. Setting the weight and the upward force equal, we can rearrange the equation to isolate v, the vertical velocity difference between the canister and the erupting mixture, at which the drag force against the canisters equals its weight:

$$v = \sqrt{\frac{r(\rho_c - \rho_m)g}{\rho_c C_D}} \qquad (3)$$

The drag coefficient (C_D) in this case is the representative value for a cylinder under high Reynolds-number flow, which varies between about 0.3 and 1.0 depending on its orientation relative to the flow direction (e.g. Hoerner, 1965, p. 3-9). For $\rho_m = {\sim}1,000 \text{ kg/m}^3$, the velocity required to lift the canisters is a few meters per second. If, however, the canisters were incorporated into debris that was lifted *en masse* during a single explosion, Eq. (3) would be irrelevant -- the canister would be lifted along with everything else.

These calculations support the conservative assumption that waste canisters will be moved and disrupted by flow of magma, both within drifts and in a vertical conduit.

6.1.4 Disruption of waste packages

6.1.4.1 Disaggregation of waste packages

The TSPA assessment of annual dose resulting from a volcanic eruption through the repository depends heavily on the percentage of nuclear waste in each waste package that separates from its container and is directly incorporated into the erupting magma. The TSPA-SR assumes that all waste packages in the direct path of the eruption are sufficiently damaged that they provide no further protection (e.g. Peter Swift's presentation at the May Panel meeting, slide 14).

This conservative assumption is based in part on lack of data on the performance of Alloy 22 under the temperature and other conditions of magma-gas mixtures during a volcanic eruption (Reamer, 1999).

Waste packages have a variety of forms depending on the type of waste contained. Waste from spent commercial nuclear plants, for example, is contained in 6-12 mm-diameter sealed cylindrical rods, typically of zirconium alloy, that are bundled together in arrays of ~200, held together with spacer grids of stainless steel (e.g. Fig. 3-6 of the Science and Engineering Plan). Approximately 20-40 of these arrays are then bundled in a single waste package (Fig. 3-5 of the Science and Engineering Plan). The complete removal of waste from fuel rods requires that the end caps of waste packages be removed, that the zirconium rod cladding be broken, and that the fuel pellets be pushed out of each ~5 meter-long, 6-12 mm-diameter tube.

In the scientific literature, few studies explicitly deal with effects of volcanic activity on metallic containers. At Mount St. Helens, damage to vehicles entrained in the lateral blast on May 18, 1980 amounted primarily to melting or breaking of glass, plastic, and upholstery, or battering and abrasion from flying objects (e.g. Waitt, 1981, p. 454). At Kilauea volcano, vehicles entrained in lava flows generally have non-metallic components melted or burned away with relatively less dismemberment to the metallic shell (Stapleton and Weisel, 1992). At Yucca Mountain, waste canisters incorporated into lava or pyroclastic debris could be subjected to hotter temperatures for longer periods of time than vehicles at Mount St. Helens, and to much higher flow rates than in typical lava flows at Kilauea.

Our understanding of the effects of magma on waste canisters would be greatly improved by experimental data. Experiments might address, for example (a) the conditions of heat and corrosive gas exposure required to cause the canister welds and casing to completely fail; and (b) the degree of physical disruption required to completely remove all waste from canisters and fuel rod casings.

6.1.4.2   Grain size of waste

The grain size of waste entrained in erupting magma affects such important variables as the area of dispersal (small particles travel farther than larger ones) and the fraction of waste inhaled. Spent reactor-fuel pellets that will make up most of the waste at the Yucca Mountain repository are composed of uranium oxide (UO_2) and associated fission products and are formed from pressed powders having initial particle sizes around 1 μm (Yucca Mountain Science and Engineering Report, section 3.2.1, and Reamer, 1999).

The degree to which these pellets might disaggregate into the grain size of their constituent powder is unknown, and is the subject of some debate. Early TSPA

runs (e.g. the TSPA-VA) did not consider particle-size degradation, and most TSPA runs generated grain sizes that were too large to entrain from a breached container, or too large to be lifted by the calculated eruption velocities (IRSR-KTI: Igneous Activity, Section 4.2.4.3.2). Following a technical review (Reamer, 1999), a revised TSPA analysis assumed that all waste in canisters that contact magma is entrained and fragmented to a median particle size of 20 μm.

The subject of fragmentation of nuclear waste is outside the field of expertise of members of this Peer Review panel. **The degree of fragmentation might reasonably be the subject of review by other specialists in nuclear waste or materials science.**

6.2   Surface processes during eruption

6.2.1   Deposit thickness in nearest inhabited area

During an eruption through the Yucca Mountain repository, tephra dispersal would be the most rapid and effective means of transporting waste to inhabited areas and increasing the dose rates. Although incompletely preserved, remnants of tephra blankets from the most recent volcanic eruption in the Yucca Mountain vicinity, at Lathrop Wells, are widespread enough to suggest that they were generated by violent Strombolian eruptions (e.g. IRSR-KTI: Igneous Activity, Rev. 2, 1999, p. 69). The age and lack of preservation of older basaltic centers in the region make it impossible to conclude that similar violent Strombolian activity took place during earlier eruptions; however it is conservatively assumed that future eruptions through the repository are capable of violent Strombolian activity with widespread tephra blanks.

Model Assumptions. The TSPA estimates the amount of tephra dispersed to the nearest inhabited area, 20 km south of Yucca Mountain, using a numerical model (ASHPLUME; Jarzemba, 1997) that calculates plume height by integrating ordinary differential equations for mass, momentum, and energy in vertical plumes (e.g. Woods, 1988; Sparks et al., 1997, p. p. 105), and calculates dispersal for a given wind vector using known particle-settling velocities, a conservative assumption of northerly wind direction, and wind speed data derived from measurements in the region (U.S. DOE, 1997). Model inputs include the vent diameter, eruption velocity, temperature, mass fraction gas, and atmospheric properties (e.g. thermal lapse rate). Important factors that are not considered include particle aggregation, thermal disequilibrium, condensation, rainfall, spatial and temporal variations in wind, effects of tephra fallout on plume density, and effects of short-lived buoyant thermals. Although each of these processes modifies the overall pattern of deposition, none is likely to dramatically shift the stochastic distribution thicknesses calculated using ASHPLUME (e.g., Peter Swift's talk during the May Las Vegas meeting of the Panel, slide 15).

Model Validation. ASHPLUME and other tephra models are validated by comparing their results with tephra dispersal patterns from mapped deposits. Thus one can check the TSPA estimates of ash thickness at this distance by comparing them with deposits from other violent Strombolian eruptions. Isopach maps from such deposits (e.g. Hill et al., 1998, Fig. 1; Doubik and Hill, 1999, Fig. 1; Segerstrom, 1950, Plate 1; Arrighi et al., 2001, Fig. 6b) suggest that, at 20 km distance from the source, ash thickness within 30-40 degrees of the axis of dispersal is on the order of centimeters. Outside of this sector, little or no ashfall is recorded. Thicknesses on the order of centimeters agree with ~30% of TSPA-SR realizations (red line from slide 14 from Peter Swift's talk) that assume a northerly wind direction. TSPA realizations that produce lesser thicknesses are presumably associated with scenarios in which mass flux is lower.

Input parameters. Among the input parameters the magma composition and volatile content are critiqued elsewhere in this report (Chapter 1); assumed wind velocity (magnitude and direction), are reasonably chosen based on nearby measurements or the conservative assumption of northerly wind direction. For median particle diameter of erupted debris, the TSPA assumes a log triangular distribution with a minimum of 0.01 mm, a maximum of 1 mm, and a mode of 0.1 mm (ANL-MGR-GS-000002, Rev 00, ICN 1). For the standard deviation of particle diameter (σ_ϕ), the TSPA assumes a uniform distribution between 1 and 3. These parameters are chosen to resemble measured particle-size distributions of violent Strombolian deposits elsewhere.

Overall, the range of tephra thicknesses calculated by ASHPLUME for the TSPA agrees reasonably well with observed tephra thicknesses for eruptions of the type considered likely to occur at Yucca Mountain. Input parameters are reasonably based on the best-studied analogs. A larger question, however, is the exact relevance of the original deposit thickness at 20-km distance to increases in radioactive dose to nearby inhabitants. In days or weeks after or between eruptive pulses, fine ash (which presumably contains a disproportionate fraction of the waste) may be remobilized by wind many kilometers from its original point of deposition. Below this issue is discussed in somewhat greater detail.

6.3   Remobilization of tephra

The TSPA-SR judges the primary radioactive hazard of a pyroclastic eruption through the Yucca Mountain repository to be inhalation of radioactive isotopes in airborne dust particles. In contrast to groundwater contamination from Yucca Mountain, which would primarily affect residents in Nevada's Amargosa Valley, contaminated airborne dust could affect residents throughout the southern Basin and Range. Natural airborne dust is known to travel by wind across continents and ocean basins (e.g. Prospero and Nees, 1986), though the airborne concentration at trans-continental distances arising from a relatively small tephra deposit at Yucca Mountain may be miniscule. The TSPA-SR estimates dose to

nearby inhabitants using published data on the quantity of fine particles that can be suspended in air by wind, the concentration of radionuclides in dust of various sizes, and the ingestion mechanism (e.g. direct inhalation versus accumulation in the naso-pharynx or tracheo-broncheal area) for particulates of different sizes.

As pointed out in *IRSR-TKI: Igneous Processes* (p. 79), the remobilization of tephra by wind during and following eruptions is not especially well documented, and likely varies dramatically depending on the climate (especially rainfall) and grain size distribution of erupted tephra. Silicic ash from Mount St. Helens was not heavily remobilized by wind following the eruptions of May and June 1980, largely due to spring rains that compacted the deposit (Folsom, 1986). On the other hand, historical accounts of tephra eruptions at Kilauea Volcano, Hawaii in 1790 and 1924 AD describe extensive transport of ash downwind in the weeks following eruptions (Kamakau, 1992, p. 156; Finch and Jaggar, 1924). These historical accounts are consistent with evidence for centimeters to meters of wind or surge erosion at contacts between ash layers on Kilauea (e.g. Decker and Christiansen, 1984; McPhie et al., 1990; Mastin, 1997; Swanson et al., 1998). Most of the reworking is probably accomplished quickly after deposition (weeks?); over longer periods, revegetation and compaction by rainfall (in moist areas), and accumulation of desert-pavement-like lags (in drier areas) stabilize the deposit (e.g. Folsom, 1986; Malin et al., 1983).

The issue of wind reworking is mostly outside the range of expertise of panel members. **However, based on our tangential knowledge of this subject, further review by a qualified expert would be worth considering. Additional studies of the degree and timing of wind redistribution of tephra from violent Strombolian eruptions in arid climates (Cerro Negro?) may shed additional light on this issue. This issue might also be addressed by experiments at Yucca Mountain, in which easily traceable (e.g. fluorescent), polydisperse, ashy mixtures in the Yucca Mountain region are deposited (e.g., a dump-truck full) and their distance and area of distribution are tracked.**

6.4 Summary

Among the eruptive parameters that may affect mean annual radioactive dose calculated in the Total System Performance Assessment, most are based on well-documented study of past eruptive processes in the Yucca Mountain region or of well-documented historical eruptions whose likely similarity to a future eruption at Yucca Mountain are well reasoned. Factors that produce the greatest uncertainty in TSPA calculations of dose (Table 6.1) involve processes that have not been constrained by experiment or description from analogous situations: in particular, (1) the probability that magma may be diverted through drifts to the surface; (2) the percentage of waste in entrained canisters that may be incorporated into the magma; and (3) grain size of the incorporated waste. Regarding (1), additional studies are recommended elsewhere in this report that

69

may help quantify the probability of its occurrence. Processes (2) and (3) could be better quantified by additional experiments into the response of Alloy 22, and of waste canisters in general, to heat, chemical reaction, and physical agitation by magma and magma-gas mixtures.

One other process that could be better quantified is the role of wind transport of tephra on TSPA calculations of eruptive dose. The degree of wind transport of fine basaltic ash in arid environments during and immediately after eruptions is not well quantified, but qualitative descriptions suggest that it is significant. The Department of Energy may wish to have this subject reviewed by one or more experts.

6.5   References for Chapter 6

Arrighi, S., C. Principe, and M. Rosi, Violent Strombolian and subplinian eruptions at Vesuvius during post-1631 activity, *Bulletin of Volcanology*, *63*, 126-150, 2001.

Crowe, B., S. Self, D. Vaniman, R. Amos, and F. Perry, Aspects of potential magmatic disruption of a high-level radioactive waste repository in southern Nevada, *Journal of Geology*, *91*, 259-276, 1983.

Decker, R.W., and R.L. Christiansen, Explosive eruptions of Kilauea Volcano, Hawaii, in *Explosive volcanism: inception, evolution, and hazards*, edited by National Research Council and others, pp. p. 122-132, National Academy Press, Washington, D.C., 1984.

Delaney, P.T., and D.D. Pollard, Deformation of host rocks and flow of magma during growth of minette dikes and breccia-bearing intrusions near Ship Rock, New Mexico, in *U. S. Geological Survey Professional Paper*, pp. 61, 1981.

Delaney, P.T., D.D. Pollard, J. Ziony, I., and E.H. McKee, Field relations between dikes and joints: Emplacement processes and paleostress analysis, *Journal of Geophysical Research*, *91* (B5), 4920-4938, 1986.

Doubik, P., and B. Hill, E., Magmatic and hydromagmatic conduit development during the 1975 Tolbachik eruption, Kamchatka, with implications for hazards assessment at Yucca Mountain, NV, *Journal of Volcanology and Geothermal Research*, *91*, 43-64, 1999.

Jaggar, T.A., and Finch, R.H. Monthly Reports of the Hawaiian Volcano Observatory, v. 12, no. 6, p. 57-58.

Folsom, M.M., Mount St. Helens tephra on range and forest lands of eastern Washington: Local erosion and redeposition, in Keller, S.A.C., ed., *Mount St.*

Helens: Five Years Later, Eastern Washington University Press, pp. 116-20, 1986.

Ghiorso, M.S., and R.O. Sack, Chemical mass transfer in magmatic processes IV: A revised and internally consistent thermodynamic model for the interpolation and extrapolation of liquid-solid equilibria in magmatic systems at elevated temperatures and pressures, *Contributions to Mineralogy and Petrology, 119*, 197-212, 1995.

Haar, L., J.S. Gallagher, and G.S. Kell, *NBS/NRC Steam Tables*, 320 pp., Hemisphere Publishing Corporation, New York, 1984.

Hill, B. E., C.B. Connor, M.S. Jarzemba, P.C. La Femina, M. Navarro, and W. Strauch, 1998, 1995 eruptions of Cerro Negro volcano, Nicaragua, and risk assessment for future eruptions, *Geological Society of America Bulletin, 110,* 1231-1241, 1998.

Hoerner, S.F., *Fluid Dynamic Drag*, published by the author, Vancouver, WA, 1965.

Luhr, J.F., and T. Simkin, *Paricutin, the Volcano Born in a Mexican Cornfield*, Geoscience Press, Tucson AZ, 427 pp., 1993.

Malin, M.C., D. Dzurisin, and R.P. Sharp, Stripping of Keanakakoi tephra on Kilauea Volcano, Hawaii, *Geological Society of America Bulletin, v. 94*, p. 1148-1158, 1983.

Mastin, L.G., Evidence for water influx from a caldera lake during the explosive hydromagmatic eruption of 1790, Kilauea Volcano, Hawaii, *Journal of Geophysical Research, 102* (B9), 20093-20109, 1997.

Mastin, L.G., Insights into volcanic conduit flow from an open-source numerical model, *Geochemistry, Geophysics, Geosystems, 3* (7), 10.1029, 2002.

Mastin, L.G., and M.S. Ghiorso, A numerical program for steady-state flow of magma-gas mixtures through vertical eruptive conduits, in *USGS Open-File Report 00-209*, pp. 56, U.S. Geological Survey, Vancouver, WA, 2000.

McPhie, J., G.P.L. Walker, and R.L. Christiansen, Phreatomagmatic and phreatic fall and surge deposits from explosions at Kilauea Volcano, Hawaii, 1790 A.D.: Keanakakoi Ash Member, *Bulletin of Volcanology, v. 52*, p. 334-354, 1990.

Pollard, D.D., Elementary fracture mechanics applied to the structural interpretation of dykes, in *Mafic dyke swarms; a collection of papers based on the proceedings of an international conference*, edited by H.C. Halls, and W.F. Fahrig, pp. 5-24, Geological Association of Canada, Toronto, 1987.

Prospero, J.M., Nees, R.T., Impact of the North African drought and El Niño on mineral dust in the Barbados Trade Winds. *Nature, 320,* 735-738, 1986.

Reamer, C.W., U.S. NRC memorandum MOL 1999-810.0639 concerning IRSR-KTI Igneous Activity, Revision 2, July 16, 1999.

Segerstrom, K., Erosion studies at Paricutin volcano, state of Michoacan, Mexico, U.S. Geological Survey Bulletin 965-A, 164 pp., 1950.

Stapleton, F. and D. Weisel, *Aloha o Kalapana*, Bishop Museum Press, Honolulu, 1992

Stock, J.M., J.H. Healy, S.H. Hickman, and M.D. Zoback, Hydraulic fracturing stress measurements at Yucca Mountain, Nevada, and relationship to the regional stress field, *Journal of Geophysical Research, 90* (B10), 8691-8706, 1985.

Swanson, D.A., R.S. Fiske, T.R. Rose, and C.L. Kenedi, Prolonged deposition of the Keanakako'i Ash member, Kilauea [abstr], *Eos, 79* (45), F937, 1998.

U.S. Department of Energy, *Regional and Local Wind Patterns near Yucca Mountain,* B00000000-02727-5705-00081, Washington D.C.: U.S. Department of Energy, Office of Civilian Radioactive Waste Management, 1997.

Waitt, R.B., Devastating pyroclastic density flow and attendant air fall of May 18—stratigraphy and sedimentology of deposits, *in* Lipman, P.W., and Mullineaux, D. R., eds., The 1980 eruptions of Mount St. Helens, U.S.G.S. Prof. Paper 1250, pp. 439-460, 1981.

WoldeGabriel, G., Keating, G.N., and Valentine, G.A., Effects of shallow basaltic intrusion into pyroclastic deposits, Grants Ridge, New Mexico, USA, *Journal of Volcanology and Geothermal Research, 92,* 389-411, 1999.

Woods, A.W., S. Sparks, O. Bokhove, A.-M. LeJeune, C.B. Connor, and B.E. Hill, Modeling magma-drift interaction at the proposed high-level radioactive waste repository at Yucca Mountain, Nevada, USA, *Geophysical Research Letters, 29* (13), 10.1029, 2002.

Chapter 7

Magma Breaks Through Elsewhere (Besides at Original Dike)

We consider here the fate of waste canisters in drifts that become pathways for magmatic eruptions. Much of the earlier part of this report has attempted to study the effect of the presence of drifts on eruptions that are likely to take place in the absence of the proposed repository, and of the flows that therefore arise within the drifts during such eruptions. It has already been pointed out that there is no firm theoretical explanation for all the processes that have either been observed during eruptions or been deduced to have occurred from a study of the sites of past eruptions or their eruptive products. We cannot even be sure how a flow of melt-dominated basaltic magma at a depth of several kilometers will behave as it nears the earth's surface. The situation becomes more complex at depths corresponding to the onset of fully two-phase flow in the bubbly-slug-flow-pyroclastic-flow regime applicable to the very shallow crust (i.e., at the level of the proposed repository).

The basic scenario that igneous petrologists have provided is of a near vertical deep (10's of kilometers), tabular dike of width several hundred meters approximately 1-10 m thick rising at a strike angle sub-parallel to the drift direction (a deliberately chosen design feature). We argue above that such a dike flow may have a magma front – conveniently defined as the place where melt ceases to be continuous in the magmatic two-phase (melt plus vapor) flow - sufficiently close to the dike tip that magma may flow into the drifts before the dike tip reaches the surface. <u>The way such a dike would interact with drifts depends significantly on the temperature field of the rock near the drifts, the state of back-filling and connectivity of the drifts. However for most of the 10,000-year period under consideration, it seems reasonable to assume that the drifts would act as hydrodynamical sinks of not insignificant volume, filled with gas at atmospheric pressure.</u>

Based on observations of modern basaltic fissure eruptions which commonly evolve on a rapid (hours to days) time scale from a 'curtain of fire' to localized conduit (quasi-cylindrical) flow, there is an order 1 chance of this dike flow turning into one or more localized near-cylindrical conduit flows, of Strombolian character, during Disruptive Yucca Mountain Basalt (DYMB) volcanism. There is no consensus regarding how this change comes about although heat transfer and the freezing of magma, a material with an enormous temperature-dependence of viscosity in the solidus to liquidus temperature interval is presumably a factor. The effect of drifts on this eruption-style/magma-flow transition is difficult to predict. The TSPA simply regards the two extremes as separate hazards. Dike intrusion is assumed to lead to degradation of the integrity of the canisters, leading to slow transfer into the groundwater, and a "typical" number of 7 fully-degraded canisters per drift invaded by magma is used

73

to cover the first hazard. Conduits "cutting" drifts are assumed to convert the waste of all canisters within the conduit section into part of the tephra accompanying the eruption. <u>We suggest that this approach may be the best that can be achieved given the present state of knowledge. However, further analysis of and the implications of a dog-leg scenario are clearly called for.</u>

There is no doubt that drifts would be invaded to some extent by rising tabular dikes and the quasi-cylindrical conduits into which they could develop. NRC sponsored work has raised the possibility that in certain circumstances all or much of the flow from a dike near where it intersects a drift would flow into the drift, interrupting the upward movement of the dike in that region. Furthermore they suggest that, in circumstances where the rock above the drift is fissured or otherwise weakened away from the point of intersection, the dike may resume an upward movement from the drift many meters from the original point of intersection. Little consideration seems to have been given either to how this new section of the dike would join up with that portion of the rising dike which is least influenced by the drift "sinks", or whether this is significantly probable. It has even been implied that this could be the place at which the dike flow would localize into a conduit flow, with the conduit retaining the dog-leg structure described above. Since we do not know much about the "usual" manner in which such localization develops from a tabular dike, there is little hope of giving a detailed account of what might happen in the case under discussion here. <u>Certainly fully three-dimensional forward models of mass, momentum and heat transfer incorporating a reasonable amount of the 'magma physics' could be undertaken. However, the reliability of these simulations would be difficult to test and the parameter space is not small.</u>

The flow along the drift part of a dog-leg eruption could vary from that of a wholly magmatic vapor phase of high compressibility to that of devolatilized, essentially incompressible, melt-dominated magma. Almost all eruptions produce compositionally-zoned eruptive products that evolve during the course of the eruption. It could be a laminar flow in the case of high-density melt-dominated magma but would certainly be turbulent if the vapor fraction increased sufficiently, thereby reducing the mean fluid density. For a fixed mass flow rate, characteristic of bottom-determined eruptions, the mean flow velocity U varies as the inverse of the density ρ, and so turbulent drag, proportional to ρU^2, will also vary as the inverse of density. <u>The most likely case for whole canisters to be moved and ejected would be that in which a Strombolian phase develops within the dog-leg. Under these circumstances the drift walls would almost certainly lose their integrity. In this case, flow calculations would be complex if any attempt were made to model the flow and its effect on canisters and simultaneously account for the mechanical properties of the silicic tuff wallrock. In less intense flows the canisters may be disturbed and moved, but that is unlikely to have a major influence on how and when their contents might reach the biosphere via groundwater.</u>

Chapter 8

Groundwater Transport Phenomena

8.1   Phenomena if magma breaks through to the surface
8.2   Phenomena if magma never breaks through to the surface

[Chapter 8 is missing in this Interim Report]

Appendix 1
Mathematical Formulation of Dike Problems

Appendix 2
Dike Propagation from Bottom to Top

Appendix 3
Uniformly Pressurized Penny-Shaped Fracture Parallel
to the Free Surface

Appendix 1

Mathematical Formulation of Dike Problems

(Version 1 -August 2002)

1 Introduction

This appendix deals with the mathematical formulation of several two-dimensional dike problems. The first one, denoted the base problem, deals with the ascent of a two-dimensional dike driven by an incompressible magma, taking into account the presence of the free-surface. Extensions of the model to account for compressible magma and thermal effects are then discussed. Other extensions of the model to deal with a pressure boundary condition at the inlet, bleeding of gas in the rock, and bubbly flow will be described in future versions of this appendix.

2 The Base Problem

2.1 Problem Definition

Consider a vertical dike propagating in a semi-infinite impermeable elastic medium. The dike is driven by an incompressible Newtonian magma, which is injected at the base of the dike at a constant volumetric rate q_∞ (see Fig. 1).

Several assumptions are introduced to simplify this problem:

1. plane strain conditions apply;

2. the magma is injected at infinity;

3. the dike propagates continuously in mobile equilibrium;

4. lubrication theory and linear elastic fracture mechanics are applicable.

1
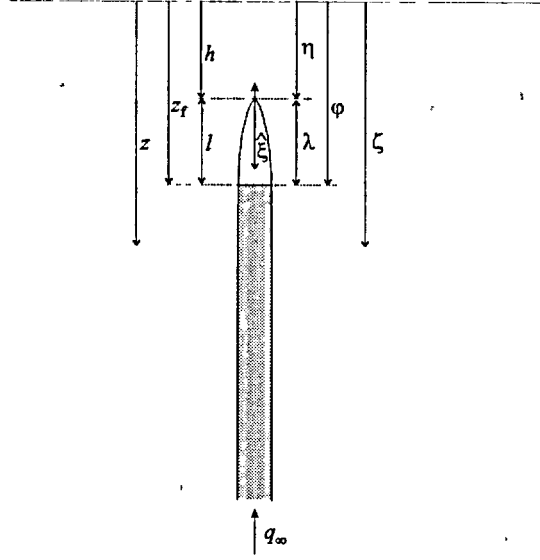
Figure 1: Problem definition

The complete formulation of this problem relies on equations from elasticity and lubrication theories, on a fracture propagation criterion from linear elastic fracture mechanics, and on boundary conditions at the inlet and at the tip of the fracture. Within this description, several parameters are used to characterize the rock, the magma, the far-field horizontal stress, and the boundary conditions. The material constants needed for the rock are Young's modulus E, Poisson's ratio ν, toughness K_{Ic}, and density ρ_r, while the relevant constants for the magma are the dynamic viscosity μ and the density ρ_f. For convenience, we introduce the reduced constants

$$E' = \frac{E}{1 - \nu^2}, \quad K' = 4 \left(\frac{2}{\pi}\right)^{1/2} K_{Ic}, \quad \mu' = 12\mu \tag{1}$$

(While E' is the plane strain modulus, the new parameters K', μ' are simply introduced to unclutter the governing equations from numerical factors.). The horizontal stress field σ_o is assumed to vary with depth z according to

$$\sigma_o = \sigma_c + \chi \rho_r g \, z \tag{2}$$

where σ_c is a constant stress, g is the acceleration of gravity, and χ a number which is typically in the range $0.3 \leq \chi \leq 1$. Finally the boundary conditions at infinity corresponds to a constant injection flow rate q_∞.

We seek to determine the fracture aperture $w(z, t)$, the magma pressure $p_f(z, t)$ and the flow rate $q(z, t)$ as a function of the depth z and the time t, as well the dependence of the

2

solution on the problem parameters. (Note that q is taken positive when directed upwards, in the opposite direction to the z-axis.) The system of equations governing w, p_f, and q are summarized in the next section.

2.2 Mathematical Formulation

Elasticity Equation. The elastic relation between the fluid pressure $p_f(z, t)$ and the fracture aperture $w(z, t)$ is expressed by a singular integral equation (Hills et al. 1996)

$$p_f(z, t) - \sigma_o(z) = E' \int_{h(t)}^{\infty} M(z, s) \frac{\partial w(s, t)}{\partial t} ds \tag{3}$$

where $M(z, s)$ is an elastic kernel which accounts for the presence of a free surface

$$M(z, s) = M_\infty(z, s) - \frac{1}{4\pi (z + s)} - \frac{2s}{4\pi (z + s)^2} + \frac{4s^2}{4\pi (z + s)^3} \tag{4}$$

with $M_\infty(z, s)$ denoting the Cauchy singular kernel for the infinite plane

$$M_\infty(z, s) = \frac{1}{4\pi (z - s)} \tag{5}$$

This formulation implies that the lateral extent of the dike is larger than its vertical extent.

We will refer to $p_f - \sigma_o$ as the net pressure p.

Poiseuille Law. According to lubrication theory, the equation governing the flow of a Newtonian fluid within the fracture is given by (Batchelor 1967)

$$q = \frac{w^3}{\mu'} \left(\frac{\partial p_f}{\partial z} - \rho_f g \right) \tag{6}$$

where ρ_f is the magma density and g the acceleration of gravity.

Fluid Mass Balance. By assuming incompressibility of the fracturing fluid, the local mass balance can be expressed as

$$\frac{\partial w}{\partial t} - \frac{\partial q}{\partial z} = 0 \tag{7}$$

3

Propagation Criterion. The propagation criterion imposes the asymptotic form of w at the tip (Rice 1968)

$$w = \frac{K'}{E'} (z - h)^{1/2}, \quad z \to h \tag{8}$$

This criterion obviously implies that $w = 0$ at $z = h$.

Condition in the Lag Zone.

$$p_f = p_{fo}, \quad h(t) \le z < z_f(t) \tag{9}$$

Condition at the Fluid Front. At the fluid front $z = z_f(t)$, the fluid pressure is the gas pressure p_{fo} in the lag zone and the velocity of the front corresponds to the average magma velocity at the front. Hence,

$$p_f = p_{fo}, \quad \frac{dz_f}{dt} = \frac{w^2}{\mu'} \left(\frac{\partial p_f}{\partial z} - \rho_f g \right) \quad \text{at} \quad z = z_f(t) \tag{10}$$

where the position of the fluid front z_f is given by

$$z_f = h + \ell \tag{11}$$

with ℓ is the length of the tip cavity.

Condition at infinity. The condition at infinity corresponds to a constant injection rate q_∞

$$q = q_\infty \quad \text{at} \quad z = \infty \tag{12}$$

It can actually be shown that this condition corresponds to a constant mean velocity v_∞.

The set consisting of the elasticity equation (3), Poiseuille law (6), fluid continuity (7), the propagation criterion (8), the conditions at the fluid front (10) and the conditions at infinity (12), forms a complete system for determining $w(z,t)$, $p_f(z,t)$, $h(t)$ and $\lambda(t)$, starting from known values of these quantities at an initial time t_o. The issue of the initial conditions will be discussed below.

2.3 Scaling

Scaling of this problem hinges on introducing the following characteristic quantities: length ℓ_*, time t_*, width w_*, pressure p_*, and flow rate q_*. Then we naturally define the dimensionless

4

depth ζ and time τ as

$$\zeta = z/\ell_* \quad \text{and} \quad \tau = t/t_* \tag{13}$$

the dimensionless crack opening $\Omega(\zeta, \tau)$, net pressure $\Pi(\zeta, \tau)$, and flow rate $\Psi(\zeta, \tau)$ as

$$\Omega = w/w_*, \ \Pi = p/p_*, \ \Psi = q/q_* \tag{14}$$

as well as the depth of the dike tip $\eta(\tau)$, the length of the tip cavity $\lambda(\tau)$, and the position of the fluid front $\varphi(\tau)$

$$\eta = h/\ell_*, \ \lambda = \ell/\ell_*, \ \varphi = z_f/\ell_* \tag{15}$$

Recall that $\varphi = \eta + \lambda$. The characteristic quantities ℓ_*, t_*, w_*, p_*, and q_* will be identified below.

Using (13)-(15), the system of equations governing $\Omega(\zeta, \tau)$, $\Pi(\zeta, \tau)$, $\Psi(\zeta, \tau)$, $\eta(\tau)$, and $\varphi(\tau)$ become

- *Elasticity equation*

$$\Pi = \mathcal{G}_e \int_\eta^\infty M(\zeta, s) \frac{\partial \Omega}{\partial s} ds \tag{16}$$

- *Poiseuille law*

$$\mathcal{G}_m \Psi = \Omega^3 \left(\frac{\partial \Pi}{\partial \zeta} + \mathcal{G}_\gamma \right) \tag{17}$$

- *Fluid continuity*

$$\mathcal{G}_w \frac{\partial \Omega}{\partial \tau} - \frac{\partial \Psi}{\partial \zeta} = 0 \tag{18}$$

- *Fracture propagation criterion*

$$\Omega = \mathcal{G}_k (\zeta - \eta)^{1/2} \ \text{as} \ \zeta \to \eta \tag{19}$$

- *Boundary condition in the tip cavity*

$$\Pi = -(\mathcal{G}_p + \mathcal{G}_t \zeta), \ \eta < \zeta \leq \varphi \tag{20}$$

- *Boundary condition at the fluid front*

$$\mathcal{G}_m \mathcal{G}_w \dot{\varphi} = -\Omega^3 \left(\frac{\partial \Pi}{\partial \zeta} + \mathcal{G}_\gamma \right) \tag{21}$$

5

- *Boundary condition at infinity*

$$\Psi = \mathcal{G}_q \text{ as } \zeta \to \infty \tag{22}$$

The eight dimensionless groups $\mathcal{G}_e$, $\mathcal{G}_m$, $\mathcal{G}_\gamma$, $\mathcal{G}_w$, $\mathcal{G}_q$, $\mathcal{G}_k$, $\mathcal{G}_t$, $\mathcal{G}_p$ are defined as follows

$$\mathcal{G}_e = \frac{E' w_*}{p_* \ell_*}, \ \mathcal{G}_m = \frac{\mu' q_* \ell_*}{w_*^3 p_*}, \ \mathcal{G}_\gamma = \frac{\delta' \ell_*}{p_*}, \ \mathcal{G}_w = \frac{w_* \ell_*}{t_* q_*}, \ \mathcal{G}_q = \frac{q}{q_*} \tag{23}$$

$$\mathcal{G}_k = \frac{K' \ell_*^{1/2}}{E' w_*}, \ \mathcal{G}_p = \frac{\sigma_c - p_{fo}}{p_*}, \ \mathcal{G}_t = \frac{\chi \rho_r g \ell_*}{p_*} \tag{24}$$

where $\delta' = \left(\chi \rho_r - \rho_f \right) g$. The particular scaling used in this problem is selected by imposing that the five dimensionless groups in (23) are all equal to one,

$$\mathcal{G}_e = \mathcal{G}_m = \mathcal{G}_\gamma = \mathcal{G}_w = \mathcal{G}_q = 1 \tag{25}$$

so as to define the five characteristic quantities ℓ_*, t_*, w_*, p_*, and q_*, which are then given by

$$\ell_* = \left(\frac{\mu' E'^3 q_\infty}{\delta'^4} \right)^{1/6}, \ w_* = \left(\frac{\mu' q_\infty}{\delta'} \right)^{1/3}, \ p_* = \left(\mu' E'^3 \delta'^2 q_\infty \right)^{1/6} \tag{26}$$

$$t_* = \left(\frac{\mu' E'}{\delta'^2 q_\infty} \right)^{1/2}, \ q_* = q_\infty \tag{27}$$

Also, the three remaining groups are renamed as

$$\mathcal{G}_e \equiv \kappa, \ \mathcal{G}_p \equiv \sigma, \ \mathcal{G}_t \equiv \gamma \tag{28}$$

where κ has the meaning of a toughness, σ of a reference stress, and γ of a relative host rock density.

$$\kappa = K' \left(\frac{1}{\mu' E'^3 q_\infty} \right)^{1/4}, \ \sigma = \frac{\sigma_c - p_{fo}}{\left(\mu' E'^3 \gamma'^2 q_\infty \right)^{1/6}}, \ \gamma = \frac{\chi \rho_r}{\chi \rho_r - \rho_f} \tag{29}$$

This scaling is an extension of the scaling used by Lister (1990) to solve the self-similar propagation of a dike, to the time-dependent case. Note that this scaling collapses if $\delta' = 0$. (For example, $\delta' = 0$ if $\chi = 1$ and $\rho_r = \rho_f$.) In that case, an appropriate scaling would correspond to

$$\mathcal{G}_e = \mathcal{G}_m = \mathcal{G}_t = \mathcal{G}_w = \mathcal{G}_q = 1, \text{ when } \mathcal{G}_\gamma = 0 \tag{30}$$

from which new expressions for ℓ_*, t_*, w_*, p_*, and q_* can easily be derived.

6

2.4 Dimensionless Formulation

In summary, the set of governing equations can be written as

$$\Pi = \int_{\eta}^{\infty} M(\zeta, s) \frac{\partial \Omega}{\partial s} ds, \quad \Psi = \Omega^3 \left(\frac{\partial \Pi}{\partial \zeta} + 1 \right), \quad \frac{\partial \Omega}{\partial \tau} - \frac{\partial \Psi}{\partial \zeta} = 0 \tag{31}$$

with the propagation criterion and the conditions in the lag zone, at the fluid front and at infinity given by

$$\Omega = \kappa (\zeta - \eta)^{1/2}, \quad \zeta \to \eta \tag{32}$$

$$\Pi = -(\sigma + \gamma \zeta), \quad \eta < \zeta \le \varphi \tag{33}$$

$$\dot{\varphi} = -\Omega^2 \left(\frac{\partial \Pi}{\partial \zeta} + 1 \right), \quad \zeta = \varphi \tag{34}$$

$$\Psi = 1, \quad \zeta \to \infty \tag{35}$$

The system of equations (31)-(35) is closed in the sense that it can be used to determine the solution $\mathcal{F}(\zeta, \tau; \kappa, \sigma, \gamma)$ where $\mathcal{F} = \{\Omega, \Pi, \Psi, \eta, \varphi\}$ given a suitable set of initial conditions.

The dependence of the solution on time arises through the boundary conditions in the tip cavity (which is changing with the depth η) and through the elastic kernel which accounts for the distance to the free surface. It is important to realize, however, that time is immaterial in this solution, if indeed the initial conditions is made to correspond to the self-similar solution of Lister (1990) for a deep dike (see discussion below). The dependence on time can then be replaced by a dependence on the depth η, once the solution has been determined (i.e. once $\eta(\tau)$ is known). The solution can thus be expressed as $\bar{\mathcal{F}}(\hat{\xi}, \eta; \kappa, \sigma, \gamma)$ with $\bar{\mathcal{F}} = \{\bar{\Omega}, \bar{\Pi}, \bar{\Psi}, \bar{\lambda}\}$, where we have chosen to use the moving coordinate $\hat{\xi} = \zeta - \eta$ rather than ζ, and the lag instead of the fluid front position. (The overbar denotes that the field quantities depend on $\hat{\xi}$ and η; also $\bar{\lambda} = \bar{\lambda}(\eta)$.)

It has been noted by various authors before that toughness is not relevant in many cases, since $\kappa \ll 1$(Spence and Turcotte 1985; Lister and Kerr 1991; Rubin 1995). Also the case $\sigma = 0$ is an appropriate case to consider. In other words, the particular solution $\kappa = \sigma = 0$ is very relevant. We denote this solution by $\mathcal{F}_o(\zeta, \tau; \gamma)$ or by $\bar{\mathcal{F}}_o(\hat{\xi}, \eta; \gamma)$; it only depends on the parameter γ. Since $\kappa = 0$, the aperture Ω behaves at the dike tip according to (Rice 1968)

$$\Omega \sim (\zeta - \eta)^{3/2}, \quad \zeta \to \eta \tag{36}$$

7

where the coefficient of proportionality is *a priori* unknown, as it is part of the solution. For this case, the condition of zero toughness is best imposed by

$$\int_\eta^\infty \frac{\Pi(s)}{s^{1/2}} ds = 0 \tag{37}$$

which uses the integral representation of the stress intensity factor. Note that the particular asymptotic behavior (36) predicates on the assumption that λ is not very small. (The term in $(\zeta - \eta)^{3/2}$ actually corresponds to the next term of the crack opening expansion when $\kappa > 0$, according to linear elastic fracture mechanics.) When $\lambda \ll 1$, the behavior (36) takes place over a region so small that it is not visible in this scaling. Under these conditions, an intermediate asymptote develops

$$\Omega \sim (\zeta - \eta)^{2/3}, \quad \zeta \to \eta \tag{38}$$

see Section 2.6 for a discussion of cases characterized by small tip cavities.

It can readily be shown (as already recognized by Lister (1990) for the self-similar case) that the solution behaves at infinity as

$$\Omega = 1, \quad \Pi = \frac{1}{4\pi\zeta}, \quad \zeta \to \infty \tag{39}$$

hence the average magma velocity $\Upsilon \equiv \Psi/\Omega = 1$ at $\zeta = \infty$. In dimensional term, the average fluid velocity at infinity, v_∞, is given

$$v_\infty = \left(\frac{\delta' q_\infty^2}{\mu'}\right)^{1/3} \tag{40}$$

It is actually convenient to formulate the boundary conditions at infinity in terms of v_∞ rather than q_∞. Hence, the characteristic quantities can be formulated as follows

$$\ell_* = \left(\frac{\mu' E'^2 V_\infty}{\delta'^3}\right)^{1/4}, \quad w_* = \left(\frac{\mu' v_\infty}{\delta'}\right)^{1/2}, \quad p_* = \left(\mu' E'^2 \delta' v_\infty\right)^{1/4}$$

$$t_* = \frac{\ell_*}{v_\infty}, \quad q_* = v_\infty w_* \tag{41}$$

and

$$\kappa = K' \left(\frac{\delta'}{\mu'^3 E'^6 v_\infty^6}\right)^{1/8}, \quad \sigma = \frac{\sigma_c - p_{fo}}{\left(\mu' E'^2 \delta' v_\infty\right)^{1/4}} \tag{42}$$

Far from the free-surface, the speed of the dike ascent is expected to be approximately equal to the far-field magma mean velocity; hence $\dot\eta = O(1)$ for $\eta \gg 1$.

8

2.5 Self-Similar Problem of a Deep Dike

Formulation of the deep dike problem solved by Lister (1990) can be deduced from the more general equations describing the base problem. First, we reformulate the equations in terms of the moving coordinates $\hat{\xi} = \zeta - \eta$. The solution is now of the form $\hat{\mathcal{F}}(\hat{\xi}, \tau; \kappa, \sigma, \gamma)$, where $\hat{\mathcal{F}} = \{\hat{\Omega}, \hat{\Pi}, \hat{\Psi}, \eta, \lambda\}$. The spatial and time derivative transform as

$$\frac{\partial}{\partial \zeta} = \frac{\partial}{\partial \hat{\xi}}, \quad \frac{\partial}{\partial \tau}\bigg|_{\zeta} = \frac{D}{D\tau}\bigg|_{\hat{\xi}} - \dot{\eta}\frac{\partial}{\partial \hat{\xi}} \tag{43}$$

In summary, the set of governing equations can be written as

$$\hat{\Pi} = \int_0^\infty \hat{M}(\hat{\xi}, \hat{s}; \eta)\frac{\partial \hat{\Omega}}{\partial \hat{s}}d\hat{s}, \quad \hat{\Psi} = \hat{\Omega}^3\left(\frac{\partial \hat{\Pi}}{\partial \hat{\xi}} + 1\right), \quad \frac{D\hat{\Omega}}{D\tau} - \dot{\eta}\frac{\partial \hat{\Omega}}{\partial \hat{\xi}} - \frac{\partial \hat{\Psi}}{\partial \hat{\xi}} = 0 \tag{44}$$

where the elastic kernel $\hat{M}(\hat{\xi}, \hat{s}; \eta)$ is now given by

$$\hat{M}(\hat{\xi}, \hat{s}; \eta) = \hat{M}_\infty(\hat{\xi}, \hat{s}) - \frac{1}{4\pi\left(\hat{\xi} + \hat{s} + 2\eta\right)} - \frac{2\hat{s}}{4\pi\left(\hat{\xi} + \hat{s} + 2\eta\right)^2} + \frac{4\hat{s}^2}{4\pi\left(\hat{\xi} + \hat{s} + 2\eta\right)^3} \tag{45}$$

with $M_\infty(z, s)$ denoting the Cauchy singular kernel for the infinite plane

$$M_\infty(z, s) = \frac{1}{4\pi\left(\hat{\xi} - \hat{s}\right)} \tag{46}$$

The propagation criterion and the conditions in the lag zone, at the fluid front and at infinity are given by

$$\hat{\Omega} = \kappa\hat{\xi}^{1/2}, \quad \hat{\xi} \to 0 \tag{47}$$

$$\hat{\Pi} = -\left[\sigma + \gamma\left(\hat{\xi} + \eta\right)\right], \quad 0 \leq \hat{\xi} \leq \lambda \tag{48}$$

$$\dot{\eta} + \dot{\lambda} = -\Omega^2\left(\frac{\partial \Pi}{\partial \zeta} + 1\right), \zeta = \varphi \tag{49}$$

$$\hat{\Psi} = 1, \quad \zeta \to \infty \tag{50}$$

The equations of the problem solved by Lister (1990) can be deduced from the general system (44)-(50) by assuming (i) that the dike is deep enough that the effect of the free surface is negligible and (ii) the solution is self-similar. It can readily be shown that the second assumption implies that the average magma velocity is constant along the dike and equal to the velocity of ascent of the dike. These assumptions imply therefore that

$$\hat{M} = \hat{M}_\infty, \quad \frac{D\hat{\Omega}}{D\tau} = 0, \quad \dot{\lambda} = 0, \quad \dot{\eta} = -1 \tag{51}$$

9

The solution is now of the form $\hat{\mathcal{F}}_{ss}(\hat{\xi}; \kappa, \sigma, \gamma, \eta)$, where $\hat{\mathcal{F}}_{ss} = \{\hat{\Omega}, \hat{\Pi}, \hat{\Psi}, \lambda\}$ and is governed by

$$\hat{\Pi} = \int_0^\infty \hat{M}_\infty(\hat{\xi}, \hat{s}) \frac{d\hat{\Omega}}{d\hat{s}} d\hat{s}, \quad \hat{\Omega}^2 \left(\frac{d\hat{\Pi}}{d\hat{\xi}} + 1 \right) = 1 \tag{52}$$

and

$$\hat{\Omega} = \kappa \hat{\xi}^{1/2}, \quad \hat{\xi} \to 0; \quad \hat{\Pi} = - \left[\sigma + \gamma \left(\hat{\xi} + \eta \right) \right], \quad 0 < \hat{\xi} \le \lambda; \quad \hat{\Omega} = 1, \quad \zeta \to \infty \tag{53}$$

Note, however, that a strictly self-similar solution does not exist, since the depth η enters into the problem formulation via the boundary condition in the lag zone. So within the assumption of self-similarity, the evolution problem is actually seen as a sequence of self-similar solutions.

Numerical solution of the system of equations (52)-(53) is given by Lister (1990)[1]. This solution could actually be used as a suitable initial condition for the base problem, i.e.

$$\mathcal{F}(\zeta - \eta_o, 0; \kappa, \sigma, \gamma, \eta) = \mathcal{F}_{ss}(\hat{\xi}; \kappa, \sigma, \gamma, \eta_o) \tag{54}$$

where $\eta_o >> 1$ (but in practical terms $\eta_o \simeq 2$, as the free-surface effect is negligible at those depths).

2.6 Discussion

2.6.1 Preliminary results

Figure 2 shows the results of preliminary calculations of the base problem, obtained by tracking the lag explicitly. This figure shows that the length of the tip cavity is increasing and that the pressure gradient behind the fluid front decreases as the tip of the dike is approaching the free-surface.

2.6.2 Tip considerations for small tip cavity size

Preliminary calculations for the particular case $\sigma = 0$ and $\kappa \ll 1$ indicate that there are regions in the parametric space (γ, η) where λ is very small; for example, when both γ and

---

[1]Lister use $\hat{x}$, $\hat{h}$, $\hat{p}$ to denote the characteristic quantities used to scale distance, half-aperture, and net pressure, respectively. These quantities are related to the those defined here according to $\hat{x} = \ell_*/2$, $\hat{h} = w_*/2$, $\hat{p} = p_*/2$.
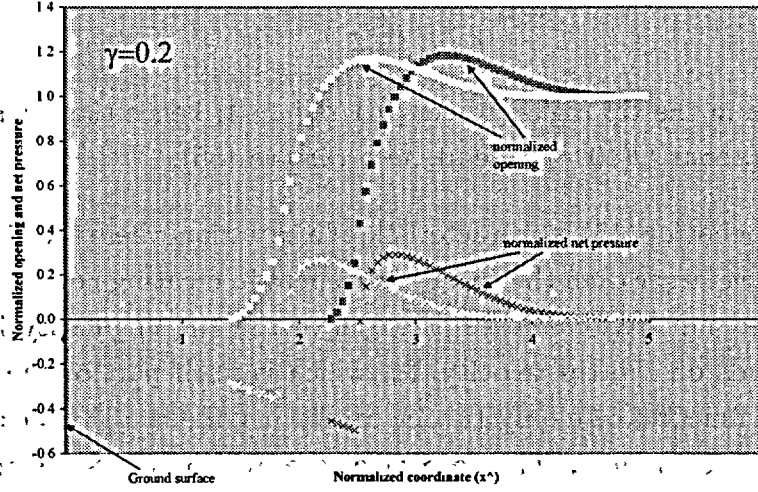
Figure 2: Net pressure and opening for $\gamma = 0.2$ and $\kappa = 10^{-2}$ at two different depths for the base problem (Calculation perfomed by X. Zhang, CSIRO).

η are $O(1)$ or larger. This suggests that the lag and the region of rapid change of the fluid pressure scale by a lengthscale other than ℓ_* when $\lambda << 1$. (In other words, $\lambda \simeq 0$ does not imply that $\ell = 0$.) The need to rescale the lag when the far-field stress is "large" and the toughness is "small" is also a feature of the solutions for hydraulic fractures where gravity effects are neglected (Detournay 2001).

Under conditions when a small lag exists, another strategy for computing the solution is needed, in view of the near impossibility to discretize numerically the lag region and at the same time capturing the global solution.

Asymptotically when $\lambda \ll 1$ for $\kappa \ll 1$, the solution is characterized by the presence of a boundary layer. The solution at the length scale ℓ_* (the "outer" solution) has a tip asymptote for opening and pressure given by

$$\Omega = \beta_{mo}\Upsilon_o^{1/3}(\zeta - \eta)^{2/3}, \quad \Pi = \delta_{mo}\Upsilon_o^{1/3}(\zeta - \eta)^{-1/3}, \tag{55}$$

where $\beta_{mo} = 2^{1/3}3^{5/6}$, $\delta_{mo} = -6^{-2/3}$, and Υ_o is the dimensionless tip velocity $\Upsilon_o = v_o/v_\infty$ (also $\Upsilon_o = -\dot\eta$). The asymptotes (55) are determined by rescaling the autonomous solution for zero toughness given by (Desroches et al. 1994)

$$\hat\Omega_{mo} = \beta_{mo}\hat\xi_m^{2/3}, \quad \hat\Pi_{mo} = \delta_{mo}\hat\xi_m^{-1/3} \tag{56}$$

where $\hat\Omega_{mo} = w/\ell_m$, $\hat\xi_m = (z-h)/\ell_m$, $\hat\Pi_{mo} = p/E'$, with the viscosity length scale ℓ_m defined

11

as

$$\ell_m = \frac{\mu' v_o}{E'} \tag{57}$$

Note that (55) applies in the tip region where $|\partial \Pi / \partial \zeta| \gg 1$; hence the asymptotic region is expected to be small (about $O(10^{-2})$ or less), according to (55).

The tip asympotic behavior (55) is characteristic of a situation where the viscous dissipation in the tip region is much larger than the energy rate spent in creating new surface in the rock. Unlike the toughness-dominated case, the strength of the tip singularity in the viscosity-dominated case depends on the tip velocity Υ_o, which is itself part of the solution. Note, however, that Υ_o is a function of η only (under conditions of "small" tip cavity), i.e., $\Upsilon_o = \Upsilon_o(\eta)$ and that $\Upsilon_o = 1$ for η large. The deep dike case, which is self-similar, was solved by Lister (1990).

The lag and the region of rapid change of the fluid pressure scale by ℓ_{ms} when $\lambda \ll 1$

$$\ell_{ms} = \left(\frac{E'}{\sigma_o}\right)^3 \frac{\mu' v_o}{E'} \tag{58}$$

where v_o is the tip velocity and σ_o is the effective confining stress in the lag zone ($\sigma_o \simeq (\sigma + \gamma \eta) p_*$, for zero gas pressure in the tip cavity). The solution at the length scale ℓ_{ms} (the "inner" solution) corresponds to the solution of a semi-infinite crack moving steadily at the velocity $v_o(\eta)$, without gravity effect. This solution is in fact similar to the solution obtained by Garagash and Detournay (2000), but for the elastic kernel which accounts for the presence of the free-surface. This inner solution is characterized by $\hat{\Omega} \sim \hat{\xi}^{2/3}$ and $\hat{\Pi} \sim \hat{\xi}^{-1/3}$ at infinity. This viscosity singularity, which provides the matching between the inner and outer solution, is actually an intermediate asymptote (Barenblatt 1996).

The maximum lag ℓ_{max} occurs when $K' = 0$ and is given by $\ell_{max} \simeq 0.36 \, \ell_{ms}$. Consider, for example, the case $\mu' = 10^{-6}$ MPa·s, $E' = 10^4$ MPa, $v_o = 1 \text{m/s}, \sigma_o = 10$ MPa. Then $\ell_{ms} = 0.1$ m and $\ell_{max} \simeq 3.6$ cm. Note that for this set of parameters and $\delta' = 2 \cdot 10^3$ N/m^3, the outer solution length scale $\ell_* \simeq 300$ m. Since $\ell_*/\ell_{ms} = O(10^4)$, the tip cavity can clearly not be discretized in the solution of the large scale problem, for this particular set of parameters.

3 Extension to Compressible Magma

Extension of the formulation to compressible fluid requires a modification of the fluid mass balance equation (7), which now becomes

$$\frac{\partial w}{\partial t} - \frac{\partial q}{\partial z} + \frac{1}{\rho}\left(w\frac{\partial \rho}{\partial t} - q\frac{\partial \rho}{\partial z}\right) = 0 \tag{59}$$

where ρ is the fluid density. Assume that the magma equation of state is a known function of n state variable S_i, $i = 1, n$

$$\rho = \rho(S_1, .., S_n) \tag{60}$$

Taking into account (60), (59) can be rewritten as

$$\frac{\partial w}{\partial t} - \frac{\partial q}{\partial z} + \frac{1}{\rho}\sum_{i=1}^{n}\frac{\partial \rho}{\partial S_i}\left(w\frac{\partial S_i}{\partial t} - q\frac{\partial S_i}{\partial z}\right) = 0 \tag{61}$$

where S_i is a function of both the depth z and time t.

The two most important state variables are the fluid pressure p_f and the gas bubble fraction ϕ, which are both part of the solution; i.e. $p_f(z,t)$ and $\phi(z,t)$. To the first order, the state equation (60) can then be written as

$$\rho = (1 - \phi)\rho_f(p_f) \tag{62}$$

where ρ_f is the density of the magma without gas bubbles. Since

$$\frac{1}{\rho}\frac{\partial \rho}{\partial p_f} = \frac{1}{k_f}, \qquad \frac{1}{\rho}\frac{\partial \rho}{\partial \phi} = -\frac{1}{1-\phi} \tag{63}$$

where k_f is the bulk modulus of the magma with $\phi = 0$ (and here assumed to be constant), the mass balance equation (61) can be rewritten as

$$\frac{\partial w}{\partial t} - \frac{\partial q}{\partial z} + \frac{1}{k_f}\left(w\frac{\partial p_f}{\partial t} - q\frac{\partial p_f}{\partial z}\right) - \frac{1}{1-\phi}\left(w\frac{\partial \phi}{\partial t} - q\frac{\partial \phi}{\partial z}\right) = 0 \tag{64}$$

After some manipulations, the fluid mass balance (64) can finally be rewritten in dimensionless form as

$$\frac{\partial \Omega}{\partial \tau} - \frac{\partial \Psi}{\partial \zeta} + \beta\left(\Omega\frac{\partial \Pi}{\partial \tau} + \gamma\Omega - \Psi\frac{\partial \Pi}{\partial \zeta}\right) - \frac{1}{1-\Phi}\left(\Omega\frac{\partial \Phi}{\partial \tau} - \Psi\frac{\partial \Phi}{\partial \zeta}\right) = 0 \tag{65}$$

where β is the dimensionless fluid compressibility

$$\beta = \frac{p_*}{k_f} \tag{66}$$

13

and Φ is the bubble fraction ϕ, function of the dimensionless variables ζ and τ, i.e., $\Phi(\zeta, \tau)$.

It can generally be expected that the compressibility number β is small and thus (65) can be simplified as

$$\frac{\partial \Omega}{\partial \tau} - \frac{\partial \Psi}{\partial \zeta} - \frac{1}{1 - \Phi} \left(\Omega \frac{\partial \Phi}{\partial \tau} - \Psi \frac{\partial \Phi}{\partial \zeta} \right) = 0 \tag{67}$$

which obviously degenerates into the incompressible fluid form (7) when $\Phi = 0$. When $\Phi > 0$, additional equations governing the exsolution of gas from the fluid and the diffusion of gas within the magma are needed to close the system of equations to be solved for Π, Ω, Ψ, Φ, η, and λ.

4 Extension to Thermal Effects

This section is provided as is. It needs to be completed by a set of equations to account for magma freezing.

4.1 Mathematical Formulation

The temperature field $T(z, t)$ (averaged over the fracture aperture) is governed by

$$C_f \left(w \frac{\partial T}{\partial t} - q \frac{\partial T}{\partial z} - A_L q^2 w \frac{\partial^2 T}{\partial z^2} \right) = Q \tag{68}$$

where C_f is the volumetric specific heat, A_L is a dispersion coefficient, and Q is the heat loss to the rock. The third term in the LHS of (68) accounts for the dispersion effect associated with the parabolic velocity profile that causes part of the heat to be transported ahead of a point moving at the average velocity. The dispersion coefficient A_L is given by (Taylor 1953)

$$A_L \simeq \frac{\alpha_L}{D_f} \quad \text{with} \quad \alpha_L \simeq \frac{1}{210} \tag{69}$$

where $D_f = K_f/C_f$ the thermal diffusivity of the magma, with K_f denoting the thermal conductivity of the magma. (Note that the usual longitudinal dispersion coefficient D_L is given by $D_L = A_L q^2$.)

It can be shown that heat transport in the rock adjacent to the dike can approximated by the one-dimensional heat diffusion equation, at the relevant time scale t_*

$$D_r \frac{\partial^2 T}{\partial x^2} = \frac{\partial T}{\partial t} \tag{70}$$

14

where x is coordinate perpendicular to the dike and $D_r = K_r/C_r$ is the thermal diffusivity of the rock with K_r the thermal conducticity and C_r the volumetric specific heat of the rock.

Hence the heat loss $Q(z,t)$ from the magma to the host rock can be computed using the Green's function for the one-dimensional diffusion equation in a semi-infinite domain, i.e.

$$Q = \frac{2K_r}{(\pi D_r)^{1/2}} \left[\frac{T - T_r}{(t - t_o)^{1/2}} + \int_{t_o}^{t} \frac{\partial T}{\partial u} \frac{du_z}{(t - u)^{1/2}} \right] \tag{71}$$

where $t_o(z)$ is the time of arrival of the dike tip at depth z and $T_r(z)$ is the initial temperature in the rock

$$T_r = T_s + a z \tag{72}$$

where a is the geothermal gradient.

The boundary conditions are taken to correspond to a fixed temperature at a reference depth $\bar{z}$

$$T = T_o, \quad z = \bar{z} \tag{73}$$

and a mixed condition at the fluid front (*needs to be discussed*)

$$C_f T q + K_f \frac{\partial T}{\partial z} = 0, \quad z = z_f \tag{74}$$

4.2 Scaling

The characteristic temperature T_* is taken equal to the magma temperature T_o at the reference depth $\bar{z}$. Then, the dimensionless temperature $\Theta(\zeta, \tau)$ is defined as

$$\Theta = T/T_* \tag{75}$$

Using (75), the governing equations (68), (73), (74) for the temperature become

$$\Omega \frac{\partial \Theta}{\partial \tau} - \Psi \frac{\partial \Theta}{\partial \zeta} - \mathcal{G}_d \frac{\partial^2 \Theta}{\partial \zeta^2} = \mathcal{G}_h \Gamma \tag{76}$$

$$\Theta = 1, \quad \zeta = \bar{\eta}; \quad \Theta \Psi + \mathcal{G}_h \Omega \frac{\partial \Theta}{\partial \zeta} = 0, \quad \zeta = \varphi \tag{77}$$

with the three dimensionless groups $\mathcal{G}_d$, $\mathcal{G}_h$, $\mathcal{G}_b$ given by

$$\mathcal{G}_d = \frac{\alpha_L q_*^2 t_*}{D_f \ell_*^2}, \quad \mathcal{G}_h = \left(\frac{\pi D_r}{t_*} \right)^{1/2} \frac{C_f w_*}{2K_r}, \quad \mathcal{G}_b = \frac{t_* D_f}{\ell_*^2} \tag{78}$$

In (76), $\Gamma(\zeta, \tau)$ denotes the dimensionless heat flux loss Q/Q_* where

$$Q_* = \frac{2K_r T_*}{(\pi D_r t_*)^{1/2}}$$ (79)

Hence

$$\Gamma = \frac{\Theta(\zeta, \tau_o(\zeta)) - \Theta_r(\zeta)}{(\tau - \tau_o(\zeta))^{1/2}} + \int_{\tau_o}^{\tau} \frac{\partial \Theta}{\partial u} \frac{du}{(\tau - u)^{1/2}}$$ (80)

with $\tau_o = t_o/t_*$ and $\Theta_r(\zeta) = \Theta_s + \varrho\zeta$, with $\Theta_s = T_s/T_*$ and $\rho = a\ell_*/T_*$.

4.3   Dimensionless Formulation

Let us rename $\mathcal{G}_h = \alpha$, $\mathcal{G}_b = \chi$, and $\mathcal{G}_d = 1/\mathcal{P}$ where $\mathcal{P}$ is the Peclet number

$$\mathcal{P} = \frac{t_* D_f}{\alpha_L w_*^2}$$ (81)

The Peclet number appears to be small, thus the dispersion effect are likely to be important. The equations for the thermal problem can thus be summarized as

$$\Omega \frac{\partial \Theta}{\partial \tau} - \Psi \frac{\partial \Theta}{\partial \zeta} - \frac{1}{\mathcal{P}} \frac{\partial^2 \Theta}{\partial \zeta^2} = \alpha \Upsilon, \quad \varphi < \zeta < \bar{\eta}$$ (82)

References

Barenblatt, G. (1996). *Scaling, Self-Similarity, and Intermediate Asymptotics*, Volume 14 of *Cambridge Texts in Applied Mathematics*. Cambridge UK: Cambridge University Press.

Batchelor, G. K. (1967). *An Introduction to Fluid Dynamics*. Cambridge UK: Cambridge University Press.

Desroches, J., E. Detournay, B. Lenoach, P. Papanastasiou, J. R. A. Pearson, M. Thiercelin, and A. H.-D. Cheng (1994). The crack tip region in hydraulic fracturing. *Proc. Roy. Soc. London, Ser. A Serie A*(447), 39–48.

Detournay, E. (2001). Propagation regimes of fluid-driven fractures in impermeable rocks. In C. Desai, T. Kundu, S. Harpalani, D. Contractor, and J. Kemeny (Eds.), *Proc. 10th Int. Conf. on Computer Methods and Advances in Geomechanics*, Volume 2, Rotterdam, pp. 1277–1288. Balkema.

Garagash, D. I. and E. Detournay (2000). The tip region of a fluid-driven fracture in an elastic medium. *ASME J. Appl. Mech. 67*, 183–192.

Hills, D., P. Kelly, D. Dai, and A. Korsunsky (1996). *Solution of Crack Problems. The Distributed Dislocation Technique*, Volume 44 of *Solid Mechanics and its Applications.* Dordrecht: Kluwer Academic Publ.

Lister, J. R. (1990). Buoyancy-driven fluid fracture: The effects of material toughness and of low-viscosity precursors. *J. Fluid Mech. 210*, 263–280.

Lister, J. R. and R. C. Kerr (1991). Fluid-mechanical models of crack propagation and their applications to magma transport in dykes. *J. Geophys. Res. 96*(B6), 10,049–10,077.

Rice, J. R. (1968). Mathematical analysis in the mechanics of fracture. In H. Liebowitz (Ed.), *Fracture, an Advanced Treatise*, Volume II, Chapter 3, pp. 191–311. New York NY: Academic Press.

Rubin, A. M. (1995). Propagation of magma-filled cracks. *Annu. Rev. Earth Planet Sci. 23*, 287–336.

Spence, D. and D. Turcotte (1985). Magma-driven propagation crack. *J. Geophys. Res. 90*, 575–580.

Taylor, G. I. (1953). Dispersion of soluble matter in solvent flowing slowly through a tube. *Proc. Roy. Soc. London Ser. A 219*, 186–203.

Appendix II – Dike propagation from bottom to top

The following appendix was written prior to the current Chapter 2 and early in the evolution of thinking about this problem. For the non-specialist, Chapter 2 of the interim report should be sufficient. For the specialist, some claims are made in Chapter 2 that are supported only here, and more details about particular problems that may be of interest can be found here. Given sufficient time, this Appendix would have been substantially edited to reflect the most current status of the interim report. Instead, at the start of each lettered section are italicized annotations that describe the content of that section, for the convenience of interested readers.

A. Introduction

1. Although field observations can provide information concerning distributions of dike thicknesses and lengths, dike propagation and magma flow directions, ascent velocity, and magma composition (relevant to estimates of viscosity, density, volatile content, and perhaps the depth of dike origin), many important aspects of dike ascent from the mantle to the surface are inaccessible to direct observation and must be deduced from continuum mechanical models. Some basic predictions of dike propagation models are consistent with observations of shallow dikes in Iceland, Hawaii, and Japan, where the lengths and widths of the dikes can be determined from geodetic data, the propagation velocity from the migration velocity of the fronts of induced earthquake swarms, and the viscosity from observed surface flows (if an eruption occurs) or experiments on relevant magma compositions. The predictions of the same models have been compared to data collected from oil-industry hydrofracture experiments, where pumping pressure, volumetric flow rate, fluid viscosity, and fracture size can be monitored.

2. Aspects of dike propagation that are absent from existing numerical models at the level that might be important for assessing igneous hazards at Yucca Mountain include (1) compressible flow of bubbly magma with gas exsolution/resorption, (2) aspects of non-Newtonian flow, for example if bubbles concentrate near the walls and give rise to "plug-like" flow near the tip, (3) the mechanism(s) by which bubbles near the magma front expel (or not) their gas into the "lag zone" near the dike tip (discussed later), (4) large-scale inelastic deformation of the host rock due to the near-failure ambient stress at Yucca Mountain, (5) the mechanical effects of the Earth's surface, and (6) the full 3-dimensionality of dike propagation. Some of these (such as (1)) should be easy to include within a timeframe of several months. For others this might not be feasible. Assessing the effects of these other processes can be carried out to some (limited) extent by using intuition gained from existing solutions or future approximate solutions.

B. A basic model

Numbered paragraphs 1-2 etc. of this section discuss in slightly more general terms and less mathematical detail issues that are covered in Appendix 1. Readers already familiar with this subject will find Appendix I easier to digest. Paragraphs 3 etc. give a fuller discussion of rock fracture issues than can be found in Chapter 2 or Appendix 1.

0. <u>Definitions</u>: For convenience we take compressive stresses and pressures to be positive. We use "thickness" to refer to the separation between the dike walls and reserve "width" for the horizontal extent of vertical dikes. "Length" may refer to the dike width or height as appropriate.

1. <u>Elasticity</u>: Away from the dike tip, strains in the host rock are small (on the order the dike thickness:length ratio, roughly 1:1000), so it is reasonable to assume that (in the absence of thermal or mechanical erosion of the host rock) the dike thickness is determined by elastic deformation (for validation see Delaney and Pollard, 1981). Then the thickness $2w$ of a dike is of order

$$2w \sim \frac{P - \sigma_n^o}{\mu/(1-\nu)} 2l \equiv \frac{\Delta P}{M} 2l \ ,$$
(1)

where the excess pressure ΔP is the amount by which the magma pressure P exceeds the compressive stress normal to the dike σ_n^o; M is the elastic stiffness, where μ is the elastic shear modulus and ν is Poisson's ratio; and $2l$ is the short in-plane dimension (e.g., the horizontal extent of a dike rising mostly vertically from the mantle). Thus ΔP can be estimated from observations of dike thickness and length, provided the observed length $2l$ is the relevant (short) in-plane dimension, and provided the elastic properties of the rock are known. In practice, the greatest uncertainty in such estimates of ΔP results from poor knowledge of the large-scale in-situ elastic shear modulus of the host rock. Lab values of M for Yucca Mountain tuffs are ~15 Gpa, but it is well known that in-situ values can be quite less, even by more than an order of magnitude. For typical dike thickness:length ratios of ~1:1000 and an elastic stiffness M of a few GPa, ΔP is a few MPa. For non-uniform excess pressures this estimate represents some average over the dike surface (weighted most heavily towards pressures applied away from the dike ends). Models of dike propagation must explicitly account for the dependence of elastic thickness at each point upon an integral of the pressure over the entire dike face.

2. Viscous flow: For typical basaltic magmas moving through dikes up to a few meters in thickness, flow is expected to be laminar. Assuming Newtonian viscous behavior (a good approximation for bubble- and crystal-poor basalts), the local mean velocity $\bar{u}$ averaged across the dike thickness has horizontal (x) and vertical (z; positive downward) components given by

$$\bar{u}_x = -\frac{1}{3\eta} w^2 \frac{dP}{dx}$$
(2a)

$$\bar{u}_z = -\frac{1}{3\eta} w^2 \left(\frac{dP}{dz} - \rho_m g \right)$$
(2b)

where η is magma viscosity and ρ_m is magma density.

Note that because the rock density ρ_r enters neither equation (1) nor (2), dikes do not sense the host-rock density directly but only the ambient dike-normal stress σ_n^o. In this sense dike propagation in elastic rock is fundamentally different from the rise of one viscous fluid in a more dense viscous host. When combining the fluid flow and elasticity equations it is often convenient to write P in terms of the excess pressure and the dike normal stress, as $P = \sigma_n^o + \Delta P$. Then defining the "tectonic" stress $\Delta \sigma_n$ to be the difference between the ambient dike-normal stress and the vertical stress ($\Delta \sigma_n \equiv \sigma_n^o - S_v$), the pressure gradients driving viscous flow in (2) may be written

$$\frac{dP}{dx} = \left(\frac{dS_v}{dx} + \frac{d\Delta \sigma_n}{dx} \right) + \frac{d\Delta P}{dx}$$
(3a)

$$\left(\frac{dP}{dz} - \rho_m g \right) = \left(\Delta \rho g + \frac{d\Delta \sigma_n}{dz} \right) + \frac{d\Delta P}{dz} \ ,$$
(3b)

where $\Delta \rho \equiv \rho_r - \rho_m$ and it is assumed that $dS_v/dz = \rho_r g$. In practice the $d(S_v + \Delta \sigma_n)/dx$ term in (3a) is often assumed zero and the ($\Delta \rho g + d\Delta \sigma_n/dz$) term in (3b) may be treated as an "effective" magma buoyancy $\Delta \rho g'$. In the lower crust it is expected that ductile creep maintains $\Delta \sigma_n \sim 0$ so $\Delta \rho g' \approx \Delta \rho g$; however, within the brittle crust in regions undergoing tectonic extension, $d\Delta \sigma_n/dz$ is negative (becomes more tensile with depth) and has a magnitude several times that of $\Delta \rho g$. This makes

unvesiculated magma "effectively negatively buoyant" regardless of the intrinsic density contrast with the host rock.

For an incompressible fluid, mass balance requires that the net flux into or out of a section of the dike be accommodated by a local change in dike thickness. This leads to the statement that the time derivative of the thickness equals (minus) the spatial derivative of the flux:

$$\frac{dw}{dt} = -\nabla \cdot (w\overline{u}) \qquad (4)$$

For a compressible (bubbly) magma, the same equation applies if $\rho_m w$ is substituted for w. In this case, an equation of state is required to relate ρ_m to P. One option is to assume that pressure changes slowly enough to maintain equilibrium between liquid magma and exsolved volatiles. For basaltic liquids this is likely to be a valid approximation even near the dike tip, where the pressure varies rapidly. Even so, equations (2) might be inadequate to describe such a flow since they do not account for (1) viscous resistance of the magma to bubble expansion, (2) non-Newtonian flow at the high bubble fraction expected at shallow depths or near the dike tip, and (3) possible segregation of the liquid and gas phases. All numerical models of dike propagation of which we are aware assume incompressible flow (models of fluid flow during dike propagation are generally less sophisticated than models of fluid flow in erupting conduits because in the latter case either the conduit thickness or pressure distribution is stipulated, whereas in dike propagation models these quantities are treated as unknowns to be solved for by coupling the flow to elasticity). *Future calculations should include the effects of gas exsolution and compressibility in the fluid flow law.*

3. <u>Rock fracture</u>: It is traditional to treat rock fracture during dike propagation as being governed by Linear Elastic Fracture Mechanics (LEFM), in which the resistance to fracture is characterized by the rock fracture toughness K_c (units of MPa m$^{1/2}$) or fracture energy G_c (units of J m^{-2}); the latter is proportional to the square of the former. A crack propagates if its stress intensity factor $K > K_c$ or mechanical energy release rate $G > G_c$. K is a measure of the strength of the stress concentration near the crack tip, which in LEFM increases without bound as the distance r to the tip decreases (as $r^{-1/2}$). Rock cannot withstand infinite stresses and instead deforms inelastically near the crack tip (e.g., by grain-scale fracturing); nonetheless, abundant engineering experience shows that provided the region of inelastic deformation is very small compared to the crack length, it is permissible to neglect the details of the fracture process and embody the resistance to fracture in a single parameter K_c (or equivalently G_c). In laboratory experiments on rock the zone of inelastic deformation at the crack tip is only centimeters in length, whereas dikes are kilometers; hence the traditional reliance on LEFM as a dike propagation criterion.

The "nominal" stress intensity factor of a dike is of order

$$K \sim \Delta P \sqrt{l} \qquad (4)$$

where ΔP may be taken from estimates of the dike thickness-to-length ratio. Equation (4) gives the exact value of K for a uniform excess pressure in a 2-D dike. In practice, viscous flow produces a magma pressure drop that ensures that $K = K_c$ during propagation, but this pressure drop is concentrated very near the tip and is much more effective in reducing K than it is in reducing the dike thickness. For typical estimates of the excess pressure (a few MPa) and dike half-lengths l of 1 km, the "nominal" K exceeds laboratory values of K_c for rock (~1 MPa m$^{1/2}$) by two orders of magnitude. Coupled elastic/fluid mechanical models invariably show that under such conditions the rock fracture toughness does not influence dike propagation and may be neglected (Lister and Kerr, 1991, and others). That is, nearly all the energy is dissipated in viscous flow rather than in rock fracture. Another way of viewing this result is that the confining pressure is much more important than any internal cohesive stresses within the crack-tip damage zone in keeping the tip closed. As

the dike approaches the surface and the confining pressure approaches zero, these internal cohesive stresses may become relatively more important in determining when the dike breaches the surface.

Rubin (1993) showed that at confining pressures that exceed the magnitude of the failure stresses at the crack tip (roughly comparable to measured tensile strengths), the notion of a "stress intensity factor" becomes poorly defined. The fracture energy remains well-defined, provided the zone of inelastic deformation at the tip is small compared to crack length, but it may now depend upon the crack size and loading configuration as well as rock type. Delaney et al. (1986) demonstrated that dike intrusion into sandstone on the Colorado Plateau was accompanied by the formation of ~100 dike-parallel joints; similar (although usually less abundant) joints are common in granites, gneisses, limestones, etc. Assuming that each joint consumed the energy of a typical laboratory fracture ($\sim 10^2$ J m^{-2}), this is evidence of a fracture energy two orders of magnitude larger than lab values; or a fracture toughness 1 order of magnitude larger than lab. Estimates of the inelastic energy expended by earthquakes that accompany dike intrusion (Rubin, 1995) range from higher to lower than this. Thus, there is ample evidence that the fracture energy of dikes could be 2 orders of magnitude larger than that of laboratory samples. However, the implied order of magnitude increase in K_c is still an order of magnitude less than the estimate of K from (4), and numerical models indicate that under such conditions the influence of rock fracture on dike propagation remains small. The possibility of even larger fracture energies cannot be ruled out; however, outcrop-scale observations of host-rock deformation adjacent to dikes shows that pervasive small-scale inelastic deformation is nearly always quite limited in extent. In this case, inelastic deformation leading to a "fracture energy" sufficient to influence propagation is likely to occur on widely-spaced faults with offsets that are a significant fraction of the dike thickness. It would be more appropriate to incorporate such faults into models explicitly than to treat them as simply an increased small-scale fracture energy.

4. Coupled elasticity and fluid flow, and the origin of the magma lag zone: Magma flow and host rock deformation are coupled in that the changing dike thickness (dw/dt) in equation (4) must be consistent with both viscous flow of the fluid (equation 2), and changes in dike thickness due to the changing dike length and excess pressure distribution (a generalized equation 1). Near the dike tip (and, in two-dimensional models, along the entire dike), the average flow velocity in the propagation direction is very nearly the propagation velocity. From equation (2), this implies that the pressure gradient for flow varies approximately as w^{-2}. Because the dike thickness (in elastic rock) slowly approaches zero near the crack tip, the magma runs out of pressure before it reaches the tip, and there is a gap between the tip and the magma front (Barenblatt 1962). If magma and rock were the only phases present, this lag zone would be a vacuum. In the Earth, it is presumably filled at some low pressure by volatiles exsolving from the magma (Lister 1990a), or by pore fluids infiltrating from the host rock (Rubin 1993). Above the water table exsolving volatiles are the only option.

Numerical models show that if the lag zone is a small fraction of the dike length, as is expected to be the case at great depth, details such as the lag length or underpressure exert little influence on bulk properties of the dike such as thickness and propagation velocity (just as was the case when the nominal dike stress intensity factor was much larger than the fracture toughness) (refs). In sections C and D we discuss aspects of dike propagation that are thought to be insensitive to the details of the lag zone. At shallow depth the lag zone may grow to become quite large. We consider the properties of the lag zone in greater detail in sections E and F.

C. Dike ascent from the mantle

Sections C and D discuss the "paradox" of the short along-strike length of analog dikes in considerable detail. Section C examines the case of constant "effective" buoyancy.

1. Relevance:

i. The lateral extent of near-surface dikes affects the probability of an igneous event impacting the repository.

ii. The characteristics of dike ascent provide a "bottom boundary condition" for modeling interaction of a dike with the repository.

2. Lister (1990b) considered the lateral extent of buoyant dikes fed by a constant-flux source of magma at depth. Analogy is drawn with the flow of a viscous fluid down a slope: The fluid runs primarily downhill under the influence of gravity, but also spreads in the cross-stream direction because the pressure is greater along the flow centerline (where the flow thickness is greatest) to edge (where the thickness dwindles to zero). For a constant fluid flux Q, the lateral extent of the flow reaches a steady value after the leading edge has passed.

3. In a dike, the pressure gradient for lateral flow is induced not by gravity but by the excess pressure ΔP required to prop open the dike walls. Because ΔP is expected to be small the pressure gradient for vertical flow is approximated as $\Delta \rho g'$, and the pressure gradient for lateral flow at a distance z above the source (this is the one section of this document where z is reckoned positive upward) is $\Delta P/l(z)$, where $2l(z)$ is the dike width (lateral extent). By adding the steady-state mass balance constraint that (well behind the leading edge of the dike) the vertical flux through any horizontal cross-section equals the source flux, the dike width (well above the source and below the leading edge) is found to be

$$2l(z) \approx 5.2 \left(\frac{Q\eta M^3}{(\Delta \rho g')^4} \right)^{1/10} z^{3/10} \tag{5}$$

For $\Delta \rho g' \sim \Delta \rho g$ and $\Delta \rho = 300$ kg m^{-3}, $M=10$ GPa, $\eta=10$ Pa s, and $Q=10^3$ m^3 s^{-1} (e.g., a 1 km by 1 m fissure with a flow rate of 1 m s^{-1}), the prediction of (5) is that $2l$ reaches 12 km and 17 km at distances of 30 km and 100 km above the source (Lister, 1990b). This distance range brackets the likely ascent distance of alkali basalts in this region. These widths are an order of magnitude greater than the median for this region inferred from the outcrop lengths of nearby analog dikes. Note that $2l$ is quite insensitive to reasonable variations in nearly all the relevant parameters, so within the framework of this model lengths as small as 1-2 km seem very difficult to achieve. A factor of 10 decrease in Q or η results in only a 26% decrease in l; a factor of 10 decrease in M results in only a factor of 2 decrease in l.

4. The following comments might help account for this discrepancy; however, it is not obvious that (even in combination) they are sufficient:

4A. Lister approximates the 2-D flow/3-D elasticity problem by combining (using mass balance) 1-D flow/2-D elasticity in horizontal and vertical cross-sections. For this reason the model has an unquantified uncertainty attached to it. However, a similar model apparently does a good job of describing viscous flow down an inclined plane. While the similarities between the two processes are only qualitative, this would seem to justify the conceptual approach.

4B. The rock fracture toughness, which is ignored, will begin to limit the lateral flow with increasing height above the source as the dike gets longer and narrower in a horizontal section. This seems unlikely to limit dikes to half lengths of 1 km. Combining equations (1) and (3), the "nominal" stress intensity factor at the lateral edge of the dike is $\Delta P l^{1/2} \sim w M l^{-1/2}$. For $w=1$ m and $l=1$ km this is 30 times laboratory values of the fracture toughness even for M of only 1 GPa, indicating that (if lab values of the fracture toughness are anything close to appropriate in situ) rock fracture should not limit the lateral spreading of these dikes (Lister, 1990b). Even if larger-than-lab values of K_c are hypothesized, one cannot hypothesize an indefinite reduction in length because the nominal stress intensity factor at the dike top (where propagation is presumably still occurring)

8/23/2002   5

exceeds that at the lateral edges by a factor of only roughly $(\Delta \rho g' l^{3/2} + wMl^{-1/2})/wMl^{-1/2}$ $=1+(\Delta \rho g' l/wM)l^2$. For reasonable values of the parameters in parentheses and $l=1$ km this factor is not too much larger than 1.

4C. Magma freezing is not accounted for in the model and will be most effective at limiting growth at the lateral edges where the dike is narrow and velocities slow (Lister, 1990b). Again, however, it is not clear if this could limit dike half-lengths to as little as 1 km, because in this case (for the reasons outlined in paragraph [4B]) it is not much easier to avoid freezing at the upper edge than at the lateral edges as l becomes smaller (note that most of the material at the lateral edges first got there by flowing up nearer the center of the dike where the thickness and flow rate are greater).

4D. The magma source could become depleted (that is, Q at depth could drop to ~0) long before the dike breached the surface. This is plausible in that an erupted volume of 0.1 km³ could be contained in a dike 2 km long by 2 m wide by 25 km tall. When fixed volumes of air or buoyant liquid are injected into gelatin blocks, they typically rise as ~penny-shaped cracks with roughly constant diameters. Note, however, that the ascent velocities of such cracks are so low as to imply that they are rate-limited by the gelatin fracture toughness and not viscous flow, placing these experiments in an inappropriate dynamical regime relative to the earth (unless the in-situ fracture toughness is orders of magnitude larger than lab values). We are unaware of any analyses or experiments designed to address the question of whether fixed-volume batches of magma would increase, maintain, or decrease their lateral extent during ascent when K_c is unimportant. For a fluid film on a slope the batch would presumably continue to spread laterally because the pressure is tied only to the local flow thickness, which is greatest along the centerline. In a dike, however, the non-local nature of the elastic pressure/thickness relationship could alter this. Analog dike models can also be carried out by injecting fluid between clear acrylic and foam rubber, using a thin rubber membrane over the foam to prevent fluid infiltration (Fialko and Rubin, 1998), but more experiments would have to be done to show that surface tension does not play a major role.

4E. Because in 3-D the dike top is somewhat rounded, the crack that first breaches the surface will not be as long as the main part of the dike below. If intersection with the surface somehow reduces the magma pressure sufficiently, the dike might soon cease propagating and funnel magma up the existing crack, and the dike length would increase with depth. In view of the results of section E that the first portion of the dike to breach the surface is at near atmospheric pressure anyway, it is not clear that a mechanism that relied on a pressure reduction could work.

5. A cartoon prevalent in the literature shows "tadpole" dikes of fixed volume that rise by fracturing the rock at their tip and squeezing shut at their base. Weertman (1971) showed that the minimum height and thickness of a crack with $K=K_c$ at the top (to overcome the rock fracture toughness) and $K=0$ at the bottom (to close) are given (in 2-D) by $2h=2(K_c/\Delta \rho g')^{2/3}$ and $2w=K_c^{4/3}/\Delta \rho g'^{1/3}M$. The gelatin models suggest that in 3-D such dikes might have more-or-less penny-shaped heads. However, for lab values of K_c these cracks are so small (height of order 100 m; thickness of order millimeters) that they would carry little magma and freeze before going anywhere. Dikes large enough to traverse the lithosphere must have a magma supply that does not shut off until the dike is considerably larger. (Note also that Stevenson (1982) showed that the tails of such dikes would freeze before closing completely because of the difficulty in forcing a viscous fluid out of a closing slot).

6. An aside concerning 2-D models: Several models of dike ascent have coupled 1-D fluid flow to 2-D, plane strain deformation of the dike walls (Lister, 1990a; Rubin, 1998; Meriaux and Jaupart, 1998). In the fixed-flux model of Lister and the fixed-volume model of Rubin, the dike has a long tail where the excess pressure is essentially zero and a wider bulbous nose near the top where the excess pressure is positive. This nose is of doubtful relevance to dikes in a 3-D earth (at least those that traverse the lithosphere). For dike tails thinner than the Weertman crack of paragraph [5], the nose height and thickness are the minimum required to reach the rock fracture toughness. However,

for lab values of the fracture toughness this thickness is so low that such dikes would freeze immediately. For meter-wide dikes, the bulbous nose arises not to meet the rock fracture toughness but for the elastic thickness produced by the nose excess pressure to reach the thickness dictated by mass balance within the tail. If the dike narrowed monotonically towards the tip, the pressure gradient for flow would increase monotonically towards the tip, generating a magma underpressure everywhere along the dike and (mathematically) interpenetration of the dike walls. An increased thickness in the nose implies a reduced pressure drop, consistent with a local excess pressure that generates the widening. In 3-D, there is an excess pressure even within the dike "tail" that in fact determines the tail thickness (unlike the 2-D case, pressures applied near the dike top are insufficient to keep the tail propped open to the requisite thickness). Thus there is no obvious mechanism for generating a bulbous nose in a 3-D earth (assuming the dike is taller than it is wide) until the magma supply cuts off (at which point the entire dike above this level becomes the "nose").

7. A more relevant comment concerning 2-D models: Because of the coupling of fluid flow to long-range elasticity and a fracture criterion, 2-D elastic models (with 1-D fluid flow) are very convenient to work with. For processes restricted to near the dike tip, considering a 2-D cross section orthogonal to the tip is probably adequate. However, when dealing on a larger scale with the approach to the surface of a dike that is taller than it is wide, this approach presents something of a dilemma. To account for vertical flow and the free surface a vertical cross-section is required, but the relevant (short) dike dimension appears only in a horizontal cross-section. The simplest "fix" is to examine a vertical cross-section where the dike "height" is taken to be the width of the natural dike that is the subject of the modeling. However, this is not ideal because in 2-D the dike thickness increases significantly as the tip approaches the surface (for a given pressure distribution; alternatively the pressure decreases considerably for a given magma volume). In 3-D the thickness is controlled largely by the horizontal dimension and may not increase much as the dike top approaches the surface. One option may be to model a "pseudo" 3-D problem in which 1-D (vertical) flow is coupled to 3-D elasticity in which the dike width is stipulated a priori.

D. Dike propagation through the crust

Sections C and D discuss the "paradox" of the short along-strike length of analog dikes in considerable detail. Section D examines the additional tendency for lateral propagation in a region of tectonic extension.

1. Relevance:
    i. The ascent of mantle-derived basalt through extending crust in dikes only a few kilometers wide presents something of an enigma, the understanding of which might impact our assessment of volcanic hazards at Yucca Mountain.

2. In actively extending regions, the greatest compressive stress is vertical (S_v) and the least is horizontal (S_h). It is believed that $S_v = \rho g z$ and that S_h is controlled by the frictional strength of optimally-oriented normal faults. In rock stressed to the failure envelope the ratio of the least to greatest compressive stresses is

$$\frac{S_h - p_p}{S_v - p_p} = \frac{S_h^*}{S_v^*} = \left(\sqrt{\mu_f^2 + 1} + \mu_f\right)^{-2} \tag{6}$$

where p_p is the pore pressure, stars denote "effective" stresses, and μ_f is the coefficient of friction. For $\mu_f = 0.6$ this ratio is $\sim 1/3$, so for a Yucca Mountain rock density of 2×10^3 kg m^{-3}, S_h increases at about 13 MPa/km beneath the water table and at about 15 MPa/km for a rock density of 2.5×10^3 kg m^{-3}. Measured values of S_h at repository depths seem to show even slightly lower stress

gradients, perhaps 8-14 MPa/km (document Dike Propagation Near Drifts, ANL-WIS-MD-000015 REV00, ICN1).

3. The assumption that in actively deforming regions $dS_v/dz \approx \rho_r g$ while the horizontal stress is controlled by the rock failure envelope (with laboratory values of the coefficient of friction) is consistent with in-situ stress measurements made worldwide (with the apparent exception of the San Andreas fault). This includes shallow measurements at Yucca Mountain and measurements to 9 km depth in the KTB borehole, Germany (refs).

4. At higher temperature, rock will creep in response to geologic strain rates at negligible differential stresses, and $S_h \approx S_v$. For quartz-bearing rock in the presence of water the transition between the brittle and ductile regimes is thought to occur at ~300°C, or at a depth of ~10 km in the Basin and Range, broadly consistent with the maximum depth of recorded earthquakes. In the earth the transition between the two regimes might be spread over a few kilometers.

5. These considerations indicate that for magma with an intrinsic density of 2.5×10^3 kg m^{-3}, the host rock shallower than 8-12 km is "effectively" less dense than the magma unless the magma bubble fraction exceeds ~40% (assuming negligible bubble density). For excess pressures (relative to S_h) of a few MPa the magma pressure at these depths would be 120-180 MPa (at such pressures somewhat larger bubble fractions are required because the density of the gas, assumed to be CO2, is roughly 20% of the magma density). Alkali basalts with 3-4% dissolved H2O reach bubble fractions of only ~0-15% at 120 MPa, and so are "effectively neutrally buoyant" at the brittle/ductile transition (Figure A2-1).

6. When magma rising buoyantly encounters the "effective" level of neutrally buoyancy ('LNB'), the dike tip slows down, magma "ponds" at this depth (still in a vertical dike), and ΔP increases locally (Figure A2-2). The increasing ΔP provides a pressure gradient for lateral flow of order $\Delta P/l$, where l is the dike width, and a mechanism for driving magma above the 'LNB' (lateral flow dominates because the excess pressure decreases with height above the 'LNB' even for a static column of magma). Lister and Kerr (1991) analyzed this case by approximating the magma input from the mantle as a source of specified flux at the 'LNB'. The dike height and thickness were determined locally by examining vertical cross-sections orthogonal to the dike, assuming negligible fracture toughness and viscous pressure losses due to vertical flow (relaxing the last two assumptions would reduce the height). For $\Delta \rho g'$ symmetric about the 'LNB' the half-height h is of order $\Delta P/|\Delta \rho g'|$; for $K_c=0$ it is larger by a factor of $\pi/2$. Lateral growth was driven by $d\Delta P/dx$ and the system of equations was closed using mass balance. For a constant flux Q Lister and Kerr found

$$h = a_1 \left(\frac{\eta M^4 Q^2 t}{(\Delta \rho g')^5} \right)^{1/11} \qquad l = a_2 \left(\frac{(\Delta \rho g')^4 Q^5 t^8}{\eta^3 M} \right)^{1/11} \qquad (7)$$

where the constants a_1 and a_2 were determined numerically. Anything that tends to increase ΔP for a given volume (for example, increasing η, M, or Q) will increase h relative to l. For $\eta=100$ Pa s, $M=20$ GPa, $Q=10^3$ m^3 s^{-1}, $|\Delta \rho g'|=3$ MPa/km, and $t=10^4$ s, h and l are 4.5 and 14 km, respectively (Lister and Kerr, 1991, Figure 17). For $|\Delta \rho g'|$ twice as large (more appropriate for an 'LNB' produced by the brittle/ductile transition) and $\eta=10$ Pa s (also appropriate for alkali basalts), h and l are 2.6 and 35 km at the same value of t.

7. It is well known from seismic and geodetic data that in Iceland, and perhaps Hawaii, dikes only a few kilometers high can propagate laterally for tens of kilometers or even 100 km. It is thought that this reflects lateral propagation at the 'LNB' of the sort discussed above (refs). The

shallow depth of propagation is consistent with the known density structure of these rift zones and the large thermal gradient, which is expected to result in a shallow brittle/ductile transition. The primary differences between this case, where the immediate magma source is itself near the 'LNB', and that discussed in paragraph [6], where the source lies in the mantle, are that: (1) In Iceland and Hawaii it is probably more appropriate to think of the source as being at constant pressure rather than constant flux, so that h quickly approaches a limiting value (although both the constant-pressure and constant-flux cases are simplifications and the constant-pressure case is identical to a particular flux-vs.-time that could be computed). (2) In Iceland and Hawaii there is likely to be an extra pressure gradient driving lateral flow – the dS_v/dx term in equation (3a) that results from downrift gradients in topography, and the $d\Delta\sigma_n/dx$ term that may result from the prior intrusive history (more intrusions near the magma source decreasing the magnitude of $\Delta\sigma_n$). (3) Magmas in Iceland and Hawaii become saturated with volatiles only at very shallow depth.

8. These considerations, together with those of section C, suggest that a gap in our understanding of magma ascent from the mantle must be filled if we are to explain how mantle-derived dikes can have widths of order 1 km at shallow depth. The following are possibilities:

8A. The stress "hole" at the 'LNB' in Figure A2-1 can be "filled" by prior dikes. That is, early dikes can spread laterally at the 'LNB', and then "freeze in" a stress gradient dS_v/dz at least as large as $d\rho_m/dz$ over their height $2h$. This means that $\Delta\rho g' \approx 0$ locally, so subsequent dikes can ascend to shallower depth (assuming that intrusion occurs more rapidly than the intrusion-related stresses can be relaxed by ductile flow of the crust). That this scenario is plausible is supported by the behavior of the 20 or so dike intrusions from 1975-1984 at Krafla in Iceland, which progressed from primarily subsurface intrusions prior to 1980 to primarily eruptions thereafter. The interpretation is that the early dikes could be intruded at low enough pressure that the magma head was below the surface, while later dikes required pressures sufficient to erupt in order to intrude. The inference of increasing magma pressure is also supported by the geodetically-observed general increase in reservoir elevation from intrusion to intrusion. That the location of dike intrusion may be determined by the stresses imparted by previously frozen dikes is also supported by seismic and geodetic observations that the 1975-1984 intrusions "fill up" different portions of the rift along strike (refs); similar behavior has been observed for dikes off the Izu peninsula, Japan (refs). While this mechanism can ultimately lead to eruption, such dikes would be expected to have a lateral extent comparable to the initial depth of the 'LNB'. One implication of this scenario is that if numerous cinder cones are clustered at the surface, they might represent a large fraction of the dikes that rose to produce that volcanic field, but if only a few are observed, there may be many more dikes below that "paved the way" for the last few that made it.

8B. If the dike top reaches depths where the magma bubble fraction exceeds 40% (at ~2-4 km depth for 2-4 wt% H_2O and $P \sim S_h$), then magma at the dike top would again become buoyant and perhaps a finger of the dike could propagate upward as the main dike continues to propagate laterally at depth. This mechanism might work well in conjunction with that in 8A. It is not known what the lateral extent of such a finger would be; modeling this 3-D process would be quite challenging.

8C. Because near the dike tip P may be considerably less than σ_n^o, the mechanism of 8B could possibly operate at even greater depth. Existing models indicate that low pressures occur only over a relatively small depth interval behind the tip, and depth intervals of at least the "Weertman" height are probably required for such an instability to occur, so this mechanism probably will not operate effectively except at depths approaching that discussed in 8B. However, gas expansion and exsolution would aid such an instability, so this possibility is worth exploring (useful insight could probably be gained from 2-D models with compressible flow).

9. Delaney and Gartner (1997) describe potentially analogous dikes in the San Rafael swarm on the Colorado Plateau that appear to have arisen directly from the mantle (although the stress state

beneath the Colorado Plateau is expected to be more nearly lithostatic). The inferred depth of exposure is 0.5-1.5 km. Most dikes are less than 2 km in lateral extent (the longest is 9 km). Of relevance to this discussion is that the dikes appear to become shorter and thicker upward. Delaney and Gartner suggest that this is due to volatile exsolution at shallow depth. This suggestion bears some resemblance to the scenarios outlined in paragraphs [8B] and [8C] (see also paragraph [4E] of section C), but whether these observations are the predicted consequence of those scenarios is unknown.

10. From the orientation of offsets between dike segments and steps on dike margins, Delaney and Gartner (1997) conclude that the dike propagation direction was often within 30° of horizontal even on these km-wide mantle-derived dikes. Estimates of magma flow directions (as opposed to crack propagation directions) can often be obtained from the orientation of anisotropy of magnetic susceptibility or elongated vesicles. *Such measurements made on analog dikes, ideally as a function of distance from the dike wall, could prove to be useful in constraining models designed to explain how mantle-derived dikes can have lateral extents of only a few kilometers.*

E. The dike tip cavity

Section E discusses the tip cavity in considerably more detail than Chapter 2. It also includes the calculation of the cavity pressure that can be maintained by a balance between volatile exsolution from the magma and leak-off into the adjacent host rock. The implications for the most appropriate boundary condition to apply in the vicinity of the magma front are extensively discussed.

1. Relevance:
    i. The gap between the crack tip and the magma front is the first part of the dike to impact the repository. The pressure within this lag zone determines the explosivity of this initial interaction and the initial mass flux into a drift.
    ii. The lag length determines where the dike tip may be when magma first encounters a drift.
    iii. It has been proposed in the literature that sufficiently large gas cavities at dike tips might "pinch off" from the main dike and ascend on their own (Crawford and Stevenson; Lister, 1990a; Rubin, 1995; Menand and Tait, 2001).

2. Although modeling of the lag zone has become accepted practice in the dike propagation and hydrofracture communities, this has not been addressed in sufficient detail for purposes of hazards assessment at Yucca Mountain. Most often the pressure within this zone has been stipulated rather than determined as part of the solution. Processes overlooked include (1) mass flux of magmatic volatiles into and out of the lag zone; (2) cooling and possible condensation of water vapor in the lag zone, and (3) the approach to the earth's surface.

3. A bare-bones cartoon of a lag zone is shown in Figure 2-1 of this report. The magma pressure exceeds the dike-normal compressive stress over the bulk of the dike. There is a source of magma far from the tip. The magma pressure decreases towards the tip, most steeply near the magma front where the crack is thinnest (Figure 2-2). As noted in section B, eventually the magma runs out of pressure. Between the magma front and the crack tip is a "cavity" or "lag zone" filled with a low-viscosity fluid (exsolving CO_2 and/or H_2O gas; at great depth the cavity fluid might be water infiltrating from the host rock but this need not concern us). The pressure is continuous across the magma front. Because the cavity fluid moves roughly at the speed of the magma (*this should be verified a posteriori for a leaky lag zone*) but has a viscosity many orders of magnitude less, any viscous pressure drop within the cavity is neglected. At crustal depths the density of the cavity phase is also negligible (unlike eruptive conduits where the density of the gas-supported phase includes that of the entrained liquids and solids, prior to eruption the velocities in the tip cavity are probably low enough, of order 1-10 m/s rather than 100 m/s, that most of the liquid phase is left behind at the magma front).

4. At the tip of the lag zone is a zone of inelastic deformation where the crack faces are separating; in the lab this region is typically centimeters long and extends a few millimeters to either side of the crack. This is the region where fracture energy is consumed and, as discussed in section B, it exerts little overall influence over the dike. The location of the crack tip is such that the positive contribution to K from the excess pressure over bulk of the dike cancels the negative contribution to K from the underpressure within the cavity and the cohesive stresses within the inelastic zone at the tip (but for the most part the cohesive stresses may be neglected). The crack tip can adjust its location at essentially elastodynamic speeds to local variations in stress or fracture toughness. In contrast, the magma flow is rather sluggish, being rate-limited by viscosity. For fracture energies anywhere near lab values, the pressure in the lag zone P_λ must be less than the ambient compression σ_n^0 if the crack tip is to move at less than dynamic speeds; thus we have $0 < P_\lambda < \sigma_n^0$.

5. Field observations: Dike tips (other than the tips of en-echelon segments) are exposed only rarely. They range from empty tensile cracks extending beyond frozen magma fronts, reminiscent of the model discussed above, to blunt fingers with radii of curvature of tens of centimeters. The latter are a clear sign of inelastic deformation of the host rock on at least the length scale of the radius of curvature, and tend to be restricted to easily deformed rock such as tephras or (when the intrusion is parallel to bedding) finely-laminated shales. In crystalline rock or well-indurated sediment dike walls can be followed for kilometers without obvious signs of inelastic deformation other than dike-parallel joints or broken rock bridges between en-echelon dike segments. This lack of inelastic deformation is consistent with the passage of a tip cavity but not a blunt dike tip. Where dike tips are observed to be blunt, it is not always possible to determine if this was a characteristic of dike propagation or only of dike arrest.

6. In published models, either the cavity pressure or length is specified and the other is determined as part of the solution. Ideally one would solve for both parameters using a physical model of the mass flux into and out of the lag zone. It is instructive to first summarize how the lag length λ and the half-thickness at the magma front δ_{mf} depend upon the underpressure within the tip cavity $\Delta P_\lambda = \sigma_n^0 - P_\lambda$ (defined to be positive). From paragraph (4), $0 < \Delta P_\lambda < \sigma_n^0$. Most existing results assume a uniform ΔP_λ and either steady-state or self-similar dike growth (the latter two assumptions do not yield very different results and both should be adequate guides to time-dependent propagation provided ΔP_λ does not vary significantly as the tip propagates over short spatial scales). In general, there is a one-to-one correspondence between the ratio $\Delta P_\lambda / \Delta P$ and the ratios λ/l and δ_{mf}/w. Figure 2-3 shows the self-similar, no-buoyancy, zero-toughness numerical results of Rubin (1993); more analytical results for steady-state propagation, including for non-zero fracture toughness, are given by Garagash and Detournay (2000). In the limit of large $\Delta P_\lambda / \Delta P$, $\lambda/l \approx (\Delta P_\lambda / \Delta P)^{-3}$ and $\delta_{mf}/w \approx 0.5(\Delta P_\lambda / \Delta P)^{-2}$; as an example, for a dike half-length of 1 km and half thickness of 1 m, $\lambda \sim 10$ m and $\delta_{mf} \sim 2$ cm for $\Delta P_\lambda / \Delta P = 4$ (a small enough value to show 50% deviations from the large $\Delta P_\lambda / \Delta P$ limit). Figure 2-3 also shows that the dike thickness and velocity are very insensitive to λ/l for $\lambda/l < 0.1$.

7. Lister (1990a) suggested that the lag zone pressure might be equated with the equilibrium vapor pressure of the magma. This does not account for the fact that the volume of exsolved gas at this pressure is infinitesimal, and that further pressure reduction is required to fill a (leaky) lag zone of finite volume. The remainder of section E is devoted to outlining a self-consistent description of the lag zone.

8. A highly idealized physical picture might be the following: In a steady-state reference frame moving with the dike tip, magma flows up the dike center and down the walls (in a fixed reference frame, for laminar Newtonian flow the velocity is zero at the dike wall and exceeds the propagation velocity by 50% at the dike center). We assume that bubbles are small enough that their ascent velocity relative to the surrounding fluid is negligible (*this should be verified given the bubble fraction and the high rate of depressurization near the tip*). Fresh bubble-bearing magma flows down the dike center, vents between 0 and 100% of its gas content to the lag zone when it reaches

the magma front, and then turns to the wall where it develops a velocity less than that of the tip. Any gas not vented to the cavity it is gradually resorbed by the magma flowing away from the tip in the tip reference frame. That is, despite the fact that the magma near the dike wall continues to ascend, the low-pressure tip region leaves any entrained bubbles in this magma behind so they see increasingly large pressures. We assume no subsequent mixing of this degassed magma with undegassed magma moving up the dike center.

9. Gas will leak out of the lag zone if the lag pressure exceeds the pore water pressure in the adjacent host rock $p_w{}^\lambda$. For propagation velocities U such that $U \ll \omega/\lambda$, where ω is the rock hydraulic diffusivity, the host rock is essentially "drained" on the length scale of the lag zone and $p_w{}^\lambda$ equals the ambient pore pressure $p_w{}^o$. For $U \gg \omega/\lambda$, the rock behaves as "undrained" on the length scale of λ, and there is a large reduction of the local pore pressure (Ruina, 1978). For reasonable poroelastic parameters $p_w{}^\lambda$ may be reduced to near zero or at least by a very large fraction of ΔP_λ, such that for $P_\lambda \leq p_w{}^\lambda$ the lag zone is very small indeed. Typical rock properties are such that for U from 1 to 10 m/s the surroundings could behave as either drained or undrained on the length scale of λ (see discussion in Rubin, 1993). While this distinction is important in general, it need not concern us at repository depths unless the properties of the lag zone at ~1 km depth affect its properties at ~300 m depth (it appears that the repository rocks are permeable enough that this is not the case).

10. To estimate the vapor flux into the lag zone Q_{in} we take as given an expression for the equilibrium volumetric bubble fraction of the magma ϕ_b as a function of pressure (see, e.g., Figure 2, p. 38, of the document "Characterize eruptive processes at Yucca Mountain"). We assume further that the magma pressure varies sufficiently slowly that equilibrium is achieved, and also that there is negligible difference in pressure between both (1) the bubbles and the surrounding magma, and (2) the bubbles at the magma front and the lag pressure P_λ (i.e., negligible surface tension).

11. To proceed further, one must account for the fraction of the flow near the magma front that approaches the tip. For example, for plug-like flow in which the magma moves at essentially the tip speed, no gas would enter the lag zone except insofar as the bubbles rose faster than the surrounding magma. For Poiseuille flow, valid a few conduit thicknesses behind the magma front, the flow profile is parabolic (assuming an incompressible Newtonian fluid) and the velocity exceeds the tip velocity out to $w/3^{1/2}$ from the dike centerline. Assuming that this flow profile remains approximately valid up to the magma front and integrating the flux (in the reference frame of the moving tip) between the dike centerline and $w/3^{1/2}$ yields

$$Q_{in} \approx 0.19 \phi_b(P_\lambda) \delta_{mf} U \qquad (8)$$

where $\phi_b(P_\lambda)$ is the bubble fraction at the magma front. Equation (8) implies that for each increment of propagation, ~20% of the material progressing past the old magma front (in a reference frame fixed to the dike wall) consists of magma moving faster than the tip that reached the magma front and had the opportunity to degas, while the remainder is either moving faster than the tip but has not yet reached the magma front, or is moving slower than the tip because it already reached the magma front and is now seeing a pressure increase. Equation (8) also assumes that 100% of the bubbles reaching the magma front vent their gas. This seems likely and maximizes Q_{in}; if a fraction α of the bubbles do not vent, then the r.h.s. of (8) should be multiplied by $(1-\alpha)$. *The factor 0.19 is model-dependent and could be refined by carrying out a steady-state 2-D calculation for flow of a compressible fluid up a vertical slot. However, this may be unnecessary if Q_{in}/Q_{out} is so low that $P_\lambda \sim 0$ even for a factor of 1 (the maximum possible).*

12. The lag zone could lose volume through gas diffusion into the host rock and cooling or condensation of volcanic gases in the lag zone. Considering diffusion only, an estimate of the gas flux out of one wall of the lag zone (in m^3 s^{-1} per meter of dike length, or m^2 s^{-1}) is

$$Q_{out} = (P_\lambda - p_w{}^\lambda) \sqrt{\frac{k}{\eta_v} \frac{\phi}{K_b} U\lambda} \tag{9}$$

where k is the rock permeability, η_v is the vapor viscosity, ϕ is the host rock porosity, and K_b is the vapor bulk modulus. Linearizing the bulk modulus around the reference pressure P_λ and assuming an ideal gas yields $K_b = P_\lambda$. (Equation (9) is strictly valid only for small deviations of density about the reference state. *More precise numerical calculations could be carried out that treat the gas compressibility fully and that consider density variations due to cooling.* Below the water table one must also account for gas diffusion into water-saturated rock. Note also that if $p_w{}^\lambda$ is reduced because of poroelastic effects it will depend upon P_λ.)

13. Before solving for P_λ by setting (8)=(9), we take as illustration the case in paragraph [6] above with l=1 km, w=1 m, λ=10 m, and δ_{mf}=2 cm. For ΔP=3 MPa and $\Delta P_\lambda/\Delta P$=4, ΔP_λ=12 MPa. For P_λ we initially suggest a value of 10 MPa, because for 2% H2O this is the pressure at which (at equilibrium) ϕ_b=0.75, and this seems to be the consensus volume fraction at which erupting conduit flows transform from isolated bubbles in a viscous matrix to isolated solid and liquid fragments in a gas matrix. To estimate $p_w{}^\lambda$, note that $\sigma_n^0 = P_\lambda + \Delta P_\lambda$=22 MPa so the depth is ~1.8 km (assuming $d\sigma_n^0/dz \approx 12$ MPa/km). At this depth the ambient pore pressure is ~12 Mpa for a water table at 600 m, but assuming undrained deformation and accepting errors of tens of percent we can set $p_w{}^\lambda$ to zero. For rocks near the repository depth we take k=10^{-12} m^2 and ϕ=10^{-2}. Reasonable values for U and η_v are 1 m s^{-1} and 10^{-5} Pa s. Plugging these values into (9) yields Q_{out}~0.3 m^2 s^{-1}, or more than 1 cavity volume in the time it takes to propagate only 0.1λ. Plugging the same values of ϕ_b, δ_{mf}, and U into [8], Q_{in}≈0.003 m^2 s^{-1}, or only ~0.01Q_{out}. Q_{in}≈Q_{out} would require roughly a four order-of-magnitude increase in $k\phi$ or a two order-of-magnitude increase in U, both of which are unrealistic at shallow depth. Clearly the gas influx is insufficient to maintain P_λ=10 MPa.

14. To solve for P_λ we set (8) equal to (9), substituting ϕ_b=1, $K_b = P_\lambda$, and (using the small λ/l approximation from paragraph [6]) $\lambda = (\Delta P_\lambda/\Delta P)^{-3}l$ and δ_{mf}=0.5$(\Delta P_\lambda/\Delta P)^{-2}w$. This yields

$$P_\lambda \frac{\Delta P_\lambda}{\Delta P} \left(1 - \frac{p_w{}^\lambda}{P_\lambda}\right)^2 \approx 10^{-2}\frac{wU\eta_v}{k\phi l} \tag{10}$$

For parameter values as in paragraph [13], the r.h.s. of (10) is 10^4 Pa. If P_λ is to be of order MPa, then either $\Delta P_\lambda/\Delta P \ll 1$ or $(1-p_w{}^\lambda/P_\lambda)^2 \ll 1$. $\Delta P_\lambda/\Delta P \ll 1$ (i.e., an underpressure near zero) is not physically reasonable; in fact this option relies on a wildly inappropriate extrapolation of the small λ/l approximations. Shrinking λ from the 10 m value in paragraph [13] is not an option because even though this reduces Q_{out}, it reduces Q_{in} even more (through the mutual dependence of λ and δ_{mf} on $\Delta P_\lambda/\Delta P$). Thus satisfying (9) requires $(1-p_w{}^\lambda/P_\lambda)^2 \ll 1$; that is, that the lag pressure be only very slightly greater than the adjacent pore water pressure so as to reduce Q_{out} by orders of magnitude relative to the estimate from paragraph [13]. (This need not be the case at great depth where $k\phi$ could be much larger. Note also that k may increase by orders of magnitude as the relevant length scale is reduced to the cm range. However, lag zones so short require very large $\Delta P_\lambda/\Delta P$. Because $\Delta P_\lambda \le \sigma_n^0$, at <2 km depth σ_n^0 is too small to allow sufficiently large ΔP_λ to generate such small lag zones, and $(1-p_w{}^\lambda/P_\lambda)^2 \ll 1$ applies).

15. In water-saturated rock this result is not patently absurd. For some range of ambient pore pressures relative to the dike-normal stress and poroelastic properties, one can have $P_\lambda \sim p_w{}^\lambda$ and both in the range of several MPa (Rubin, 1993, see eq. 18). For a possibly larger range of parameters, however, $p_w{}^\lambda$ will drop until the pore water vaporizes at near atmospheric pressure, and satisfying $(1-p_w{}^\lambda/P_\lambda)^2 \ll 1$ in this case (and of course in the unsaturated rock at the repository depth as well) requires P_λ to be essentially atmospheric. At such pressure the "bubbly magma" behind

the "magma front" would be more than 99% gas by volume, and one would expect that the bubbles would have long since connected.

16. Because imposing the condition $Q_{in} \approx Q_{out}$ while hypothesizing a well-defined front separating viscous magma (with isolated bubbles) from an essentially inviscid gas results in a P_λ so low that the "isolated bubbles" would almost certainly be interconnected, we conclude that a simple magma front of the form envisioned cannot exist when $p_w^\lambda \sim 0$. Instead, one must imagine a foamy region at the tip where bubbles are connected, allowing free flow of gas both down the dike channel and into the host rock. Given that the ease of gas flow into the rock maintains P_λ near atmospheric pressure at repository depths, if the pressure at which the bubbles become interconnected significantly exceeds this there must be some pressure drop between this "interconnected bubble front" (hereafter termed simply the "magma front") and the dike tip. This pressure drop is available to drive the foam forward. A "foam front" might occur where this pressure gradient drops below hydrostatic for the magma/gas mixture, plausibly when the pressure approaches atmospheric (the foam could not be maintained as a steady-state feature unless there were a pressure drop across it in excess of hydrostatic). This foam front now marks the (perhaps gradational) transition to the lag zone of pressure P_λ.

17. Note that in this scenario the value of P_λ derived from balancing Q_{in} and Q_{out} may be larger than would be estimated from equation (10) because of the pressure drop between the magma and foam fronts. Equation (9) for Q_{out} is unchanged (of course the functional dependence of λ on $\Delta P_\lambda / \Delta P$ may change because the flow law in the foam is different from that in the magma), but equation (8) (with "δ_{mf}" now interpreted as the thickness at the foam front) will underestimate Q_{in} because U should now be interpreted as the gas velocity, and this may significantly exceed the tip velocity (because of gas diffusion out of the lag zone). The maximum possible increase in Q_{in}, occurring if the foam region were impermeable to gas diffusion into the host rock (highly unlikely) and had a pressure close to that at the foam front, would be the ratio of the equilibrium gas volume per unit mass at the foam front to that at the magma front, times the ratio of the thickness at the magma front to that at the foam front. For a magma front pressure of 10 MPa and P_λ near atmospheric these combined factors could easily exceed 100. However, the fact that the gas permeability into the host rock probably varies from near the intrinsic value at the foam front to near zero at the interconnected front will reduce this number considerably, as will the fact that a gradual pressure drop between the magma and foam fronts ensures that some of the excess flux at the magma front goes into widening the dike between the two fronts. *We suspect that gas diffusion in the presence of a foamy region will still maintain P_λ at near atmospheric values at repository depths, but this should be verified.*

18. An alternative model: If gas diffusion into the host rock is easy on the timescale of dike propagation but very difficult relative to gas flow through a basaltic foam, the gas pressure could be essentially uniform between the magma front and the dike tip. In this case there is no pressure drop to maintain a steady-state foam, but by supposition there would be a pressure discontinuity (arising from surface tension or viscous resistance of the magma to bubble expansion) between the isolated bubbles behind the magma front and the lag zone. In this case one could again estimate P_λ by balancing Q_{in} and Q_{out} after accounting for gas expansion across the magma front. While this scenario is much easier to model than a foamy region, it seems very unlikely that pressure drops of several MPa (a reasonable value for the pressure at which bubbles become interconnected) could be sustained across the magma front, so we discard this.

19. To summarize paragraphs [7]-[18]: There is no self-consistent constitutive law for determining P_λ in the published literature. A continuous pressure across a simple boundary between two homogeneous flow regimes (magma-supported upstream and gas-supported downstream), as assumed in previous treatments, seems untenable when the pore pressure in the adjacent host rock is near zero (either because the tip is in unsaturated rock or in rock at depth with a large poroelastic reduction in pore pressure). We propose that in such cases a foamy region with

an interconnected gas phase that sustains a pressure drop separates these two "homogeneous" regions. The lag zone pressure P_λ may be approximated as nearly uniform and should be determined by mass balance. Preliminary calculations in this section suggest that P_λ will exceed $p_w{}^\lambda$ only very slightly for permeabilities of 10^{-12}–10^{-13} m^2, implying that at near-repository depths P_λ is essentially atmospheric. *These calculations could be improved by including the effects of (1) nonlinear gas compressibility and variable viscosity during diffusion into the host rock; (2) gas cooling and (possibly) condensation within the lag zone and host rock; (3) gas expansion and exsolution between the "interconnected bubble" and foam fronts; and (4) gas diffusion into the host rock between the interconnected bubble and foam fronts.* But it is likely that the inference of a very low P_λ will stand.

20. Many processes not considered in existing models of dike propagation, for example a flow law for a foam, would be required for a full description of the tip region envisioned above. Probably many of these processes will not be well understood in a several-year timeframe. Before enumerating these, it is important to point out that it is nonetheless possible to develop a coherent modeling strategy. Existing solutions (with and without magma freezing) indicate that the lag zone affects the bulk characteristics of the dike only when λ is a significant fraction of the dike length. It is likely that (because of sufficiently large host rock permeabilities) more refined calculations will still show $P_\lambda \sim p_w{}^\lambda$. $p_w{}^\lambda$ can range from 0 to $p_w{}^o$, so for typical values of ΔP of a few MPa, $\Delta P_\lambda / \Delta P$ is quite large and λ quite small at depths of more than 2 km. Even if the adopted constitutive law in the region of very high bubble fraction is in error, the very steep drop in pressure near the magma front in existing models (e.g., Figure 2-2) suggests that the region suffering from these errors is confined to very near the lag zone, so the lag zone should remain a very small fraction of the dike length and not significantly affect its bulk properties.

21. At depths shallower than 1 km, and certainly at repository depths, σ_n^o is sufficiently low that $\Delta P_\lambda / \Delta P$ is no longer large and properties of the lag zone may affect the dike propagation. In this case it is worth bearing in mind that even for incompressible Newtonian flow, the value of λ is uncertain to the extent that it is proportional to l and ΔP^3. Thus a sensible strategy for modeling the dike tip is to incorporate those "novel" processes in the paragraph below that are easily accommodated, and to account for uncertainty in the remainder by considering a suitably large range of bulk dike properties such as l, ΔP, $\Delta \rho g'$, etc.

22. *The novel processes alluded to above include: (1) an estimate of the magma viscosity as a function of bubble fraction and strain rate; (2) proper accounting of compressible flow and an equation of state for the magma/gas mixture; (3) consideration of non-Newtonian flow regimes at the very high bubble fractions and strain rates appropriate near the magma front; (4) an estimate of the (shear and/or volumetric strain-rate dependent?) pressure at which bubbles become interconnected; that is, the pressure at the magma/foam transition; (5) consideration of possibly different pressures in the gas and liquid phases due to surface tension or viscous resistance of the magma to bubble expansion (that is, the pressure exerted by the magma/gas mixture on the dike walls could be less than the bubble pressure); (6) a flow law for the foamy region with the continuous gas phase; and (7) gas diffusion into the host rock within the foamy region. One might also wish to consider developing (or looking up?) a generic model of 2-D flow near the fluid front to aid in estimating the gas flux into the foamy region or lag zone.*

23. A possibly relevant observation regarding a flow law for a magmatic foam is that many very silicic dikes contain a pervasive linear fabric near the margin, presumably parallel to the flow direction, that may be an indication of stretched vesicles and perhaps plug-like flow. To our knowledge basaltic dikes do not exhibit similar features.

F. Approach to the surface

This section discusses possible instability of the dike tip as it approaches the surface. Paragraphs 1-4 address this analytically. Paragraphs 6-10 give numerical examples, but these have been largely superceded by results discussed in Appendix 1. Paragraphs 11-16 consider the implications of these results for a Yucca Mountain repository and for understanding observations of the onset of the 1943 Paricutin eruption.

0. Using the results of section E, we assume in the following that $P_\lambda \sim 0$ (and hence $\Delta P_\lambda \approx \sigma_n^o$) at depths shallower than the water table. Calculations are carried out with a well-defined magma front and no foamy region.

1. Section E assumes that ΔP_λ within the lag zone is uniform. At the top of a rising dike, P_λ is ~uniform but σ_n^o decreases towards the tip at a rate $d\sigma_n^o/dz$. When the lag zone is small enough that $\lambda[d\sigma_n^o/dz] \ll \Delta P_\lambda$, gradients in the host rock stress are unimportant and the results of section E still apply. However, a major difference arises when this condition is not met. As the dike top approaches the surface, the decrease in σ_n^o ensures that the corresponding decrease in ΔP_λ and increase in λ lead to $\lambda d\sigma_n^o/dz \sim \Delta P_\lambda$.

2. Recall that λ responds on very short timescales to maintain a balance between the two major contributors to the dike-tip stress intensity factor K: The excess pressure acting over the bulk of the dike, and the underpressure within the lag zone. For a uniform ΔP_λ the (negative) contribution from the latter increases monotonically with λ (proportionally to $-\Delta P_\lambda \lambda^{1/2}$ in the limit of small λ/l). This means that as ΔP_λ for a given dike decreases, λ becomes longer and longer so as to maintain $K = K_c$. For a uniform ΔP_λ there is a one-to-one correspondence between ΔP_λ and λ.

3. For $\lambda(d\sigma_n^o/dz) \sim \Delta P_\lambda$, λ cannot increase monotonically with decreasing ΔP_λ because eventually K increases with λ. This can be seen by writing the contribution to K from the lag zone ($\equiv K_\lambda$) as the superposition of that due to a uniform underpressure ΔP_λ and that due to an overpressure that increases linearly from zero at a distance λ behind the tip to $\lambda(d\sigma_n^o/dz)$ at the tip. Integrating the point force solution (e.g., Lawn, 1993) over this region and taking the limit of small λ/l yields:

$$K_\lambda = -\frac{\sqrt{8}}{\pi}\Delta P_\lambda \lambda^{1/2} + \frac{16}{3\pi 2^{3/2}}\frac{d\sigma_n^o}{dz}\lambda^{3/2}$$

$$\approx -0.9\Delta P_\lambda \lambda^{1/2} + 0.6\frac{d\sigma_n^o}{dz}\lambda^{3/2} \quad . \tag{11}$$

For small λ the first term in (11) dominates and the results of the section E apply; for large λ the second term dominates. Differentiating with respect to λ yields

$$\frac{dK_\lambda}{d\lambda} \approx \left(-0.45\Delta P_\lambda + 0.9\lambda\frac{d\sigma_n^o}{dz}\right)\lambda^{-1/2} \tag{12}$$

Setting (12) to zero shows that K_λ reaches a minimum for $\Delta P_\lambda = 2\lambda(d\sigma_n^o/dz)$. This means that as λ increases from small values, K_λ first decreases but then increases when the suction at the tip ΔP_{tip} is only one-half that at the base of the lag zone; that is, long before the tip develops an overpressure. (Even though the net suction force within the lag zone increases with λ beyond this critical value, K_λ decreases because the Green's function for K is heavily weighted towards those stresses applied very near the tip, and these stresses decrease with λ.)

4. The implication of equation (12) for rising dikes is that once λ grows to the point that $\Delta P_{tip} \sim 0.5\Delta P_\lambda$, the tip will go unstable. If this happens at considerable depth and $p_w^\lambda \neq 0$, the rapidly

increasing volume of the lag zone may reduce P_λ, increasing ΔP_λ and helping to stabilize the tip. Near the surface, however, $P_\lambda \sim 0$ so rapid expansion of the lag zone will not significantly impact ΔP_λ and the dike tip is likely to propagate elastodynamically. Plugging $\Delta P_{tip} \sim 0.5 \Delta P_\lambda$ into equation (11) indicates that the lag zone at the time of instability is 2.25 times longer than the lag zone for $d\sigma_n^0/dz=0$ at the same value of ΔP_{tip}.

5. The criterion $\Delta P_{tip} \sim 0.5 \Delta P_\lambda$ for instability may be inaccurate for dikes because (1) it does not account for how the contribution to K at the dike tip from viscous flow also varies with λ; (2) equation (12) assumes the small λ/l limit, which may be a poor approximation for lag zones large enough to become unstable; and (3) the mechanical influence of the free surface and the three-dimensionality of the dike are not accounted for.

6. To help assess (1) and (2), numerical calculations were carried out for steady-state propagation of a dike with a source of unit excess pressure ΔP applied a unit distance l behind the tip of a semi-infinite crack (note to modelers: The Green's functions used were actually those for a symmetrically-loaded crack of half-length l, but this need not concern us). The magma was assumed incompressible and to have zero density contrast with the host rock. A well-defined magma front was assumed with a constant P_λ, so the gradient of the excess pressure within the lag zone was $d\sigma_n^0/dz$. Calculations were carried out for normalized values of $d\sigma_n^0/dz$ (normalized by $\Delta P/l$) of 0, 2, 4, 8, 16, and 32 (for example, a normalized $d\sigma_n^0/dz$ of 4 might correspond to $d\sigma_n^0/dz=12$ Mpa/km, $\Delta P=3$ MPa, and $l=1$ km). There are of course several questions to be asked concerning how this 2-D calculation corresponds to the 3-D earth, but assuming the dike is taller than it is wide it is most appropriate to equate the length scale l to the dike half-width.

7. Figure A2-3 shows both $\Delta P_\lambda/\Delta P$ and δ_{mf} (normalized by the thickness at a distance l behind the tip) as a function of λ/l for two values of the rock fracture toughness: $K_c/\Delta P l^{1/2}=0.01$ (appropriate for ~lab values of K_c) and $K_c/\Delta P l^{1/2}=0.1$ (K_c ten times larger). Several results are noteworthy. First, for $d\sigma_n^0/dz=0$ (dashed lines) the tip suction ΔP_λ is a monotonically decreasing function of λ (as in paragraph [2]). Second, the results for nonzero $d\sigma_n^0/dz$ are very close to those for $d\sigma_n^0/dz=0$ when λ is small enough that $\lambda[d\sigma_n^0/dz]<<\Delta P_\lambda$ (as in paragraph [1]). Third, ΔP_λ passes through a minimum and then increases as λ increases, so $\lambda(\Delta P_\lambda)$ is double-valued over some range of ΔP_λ (as in paragraph [3]). Fourth, as λ increases beyond the minimum in ΔP_λ, the dike walls within the lag zone eventually interpenetrate, an unphysical result that marks where the curves for the various $d\sigma_n^0/dz$ in Figure A2-3 end.

8. Previous investigations of linear gradients in the lag underpressure have focused on this interpenetration of the dike walls for large λ (Lister and Kerr, 1991). It has been suggested that at this point the lag zone might pinch off and run rapidly upward, leaving the magma behind (Rubin, 1995; Menand and Tait, 2001). However, this is not the proper interpretation of this result. At great depth, λ is sufficiently small that the solution does not differ significantly from the $d\sigma_n^0/dz=0$ case, and the appropriate $\lambda(\Delta P_\lambda)$ lies to the left of the minimum. As the dike top shallows, $\Delta P_\lambda \approx \sigma_n^0$ decreases and eventually reaches its minimum (we assume for the sake of argument that the steady solution is an adequate representation of the time-dependent case here even though this is questionable when the steady-state lag length varies rapidly for small changes in ΔP_λ, i.e., depth). At this point the dike continues to rise and ΔP_λ decreases further. However, there is no stable λ for lower ΔP_λ; numerical solutions that stipulate a larger λ (as was done to produce Figure A2-3 and in Lister 1990a) find a solution by increasing ΔP_λ. Because this is not an option for a rising dike with $P_\lambda \sim 0$ and $\Delta P_\lambda \approx \sigma_n^0$, the curves in Figure A2-3 to the right of the minimum are physically unrealizable.

9. The prediction of equation (12) that instability occurs when $\Delta P_{tip} \sim 0.5 \Delta P_\lambda$ is quite consistent with the calculations in Figure A2-3. In Figure A2-3a, $\Delta P_{tip}/\Delta P_\lambda=0.52$ and 0.49 at the minima in ΔP_λ for those minima that occur for $\lambda/l<0.1$. This suggests that the changing contribution to K due to the changing magma pressure distribution as a function of λ is indeed negligible (although this is

but one realization of the flow and things could conceivably change for a time-dependent calculation, compressible flow, or nonzero $\Delta \rho g'$). ΔP_{tip} gradually decreases to $0.4\Delta P_\lambda$ for normalized $d\sigma_n^0/dz=2$, presumably due to violation of the small λ/l approximation in equation (11) ($\lambda/l\approx0.25$ in this case) but still not far from the simple analytical estimate of $0.5\Delta P_\lambda$. In addition, in all cases the value of λ/l at instability is 2.22 ± 0.03 times the value for $d\sigma_n^0/dz=0$ at the same ΔP_λ, as predicted.

10. Computing the fate of the lag zone beyond the minima in Figure A2-3 would require time-dependent models. As was noted in paragraph [4], for $P_\lambda\sim0$ rapid expansion of the lag zone cannot be called upon to help stabilize the tip. In elastostatic models with incompressible magma, rapid propagation of the tip will result in a pressure drop behind the magma front which could promote stability. However, at shallow depths the magma is expected to be highly vesicular even well behind the magma front and this will help maintain pressure as λ increases, suggesting that the tip would run to the surface without the lag zone pinching off. For purposes of hazards assessment, elastostatic models (in which the entire dike sees the current position of the moving crack tip instantaneously) might be adequate to compute the location of the dike tip as a function of the magma front depth, including when it would jump to the surface. However, if it is thought that dynamic crack propagation itself (above or below the repository) could alter interaction with the drifts in a substantial way then it would be necessary to resort to an elastodynamic code. It is not clear why this would be necessary.

11. It is of great interest to determine the depth at which the dike tip goes unstable, because if this occurs before the magma front reaches the repository then the tip would be expected to breach the surface before there was any mass flux into the drifts (because the lag zone is at essentially the repository pressure and this is all the drifts have seen). For our "reference" dike with $\Delta P=3$ MPa and $l=1$ km, the normalized $d\sigma_n^0/dz=4$ for $d\sigma_n^0/dz=12$ MPa/km. The minimum stable $\Delta P_\lambda/\Delta P$ for this case is ~1.4, or $\Delta P_\lambda=4.2$ MPa, which for $d\sigma_n^0/dz=12$ MPa/km occurs at a depth of 350 m. To the extent that these calculations are appropriate, the tip is expected to go unstable when the magma front is some tens of meters below the repository. For $\Delta P=1.5$ MPa and $l=2$ km, yielding the same dike thickness and normalized $d\sigma_n^0/dz$, the tip would not go unstable until the magma front reached a depth of 175 m. At the repository depth of 300 m ($P_\lambda\approx\sigma_n^0\approx4.2$ MPa), $\Delta P_\lambda/\Delta P$ would be 2.4 in this case and from Figure A2-3a $\lambda/l\approx0.3$ (essentially the same as for $d\sigma_n^0/dz=0$) so $\lambda\approx60$ m. For $\Delta P=1.5$ MPa and $l=1$ km, yielding the same dike thickness for an elastic modulus a factor of 2 lower and a normalized $d\sigma_n^0/dz$ of 8, the tip would not go unstable until the magma front reached a depth of 225 m. At the repository depth, λ/l would be about 0.3 (again) so $\lambda\approx30$ m. Finally, using the results of paragraph [9] to interpolate between the curves shown in Figure A2-3, for $l=1$ km the tip would go unstable when the magma front was deeper than 300 m for $\Delta P\geq2.4$ MPa.

12. These results might be altered substantially by the free surface. In general, stresses applied far from the dike tip are more sensitive to the presence of the surface than those applied close to the tip. This means that the surface increases the positive contribution to K from the bulk of the dike more than it increases the negative contribution to K from the lag zone. Thus, to match $K=K_c$ the lag length must increase (for a given excess pressure and dike length), pushing the instability to greater depth. 2-D boundary-element calculations, that approximate the dike excess pressure as constant except within the zero-pressure lag zone, indicate that (for $l=1$ km) the free surface reduces by $\sim1/3$ the maximum value of ΔP that can be sustained without the tip going unstable before the magma front reaches 300 m. This would reduce the value of 2.4 MPa in paragraph [11] to 1.5 MPa. However, in 3-D the dike width helps limit the dike thickness and stabilize the tip. 3-D calculations with a square dike of half-length 1 km and constant excess pressure suggest that the combination of the free surface and 3-D elasticity could increase by $\sim20\%$ the maximum value of ΔP for the tip to be stable with a magma front at 300 m, increasing the above value of 2.4 MPa to about 2.8 MPa.

13. Despite their limitations, these calculations suggest that for some reasonable range of parameters the dike tip will go unstable for magma fronts deeper than the repository, and for some

reasonable range it would go unstable at shallower depth. *Future calculations should include (1) time-dependent propagation, (2) gas exsolution/expansion, and (3) the effect of the free surface.* The latter might be difficult to assess in a meaningful way without also addressing the 3-D nature of the problem. One might gain some insight by solving a "pseudo-3-D" problem, for example by coupling 1-D vertical flow through a 3-D elastic boundary element model in which the lateral extent of the dike is stipulated a priori.

14. <u>Observations</u>: Few fissure eruptions have been observed from the time the dike tip first breached the surface. Duffield et al. (1982) report that during the 1971 eruption in the Southwest Rift of Kilauea, a line of lava fountains moved downrift at about 0.15 m/s, ahead of which new ground cracks opened and preexisting cracks widened. "Then in rapid succession, volcanic fume combined with condensing steam from vaporized ground water (?) issued from the cracks, clots of molten lava were ejected in Strombolian fashion to heights of a few meters, dense dark fume billowed forth, and finally lava fountaining began." The paper is not quantitative about the timing, but Duffield (pers. commun., 2002) states "The sequence of action immediately before lava fountaining probably lasted no more than a minute or two at a fixed site. It may have been less than a minute." Since vertical flow rates are likely to have been less than horizontal flow rates for this dike, the tip may have been no more than 10 m beneath the surface when the cracks appeared. However, for low-gas eruptions in Hawaii the magma may be effectively "negatively buoyant" nearly to the surface, and in this case the crack tip can be stabilized with a lag zone so short that the instability discussed above does not occur (because of the magmatic underpressure over much of the upper portion of the dike).

15. More pertinent observations may come from the onset of the eruption of Paricutin in 1943 (Foshag and Gonzales, 1956). After about 2 weeks of seismic activity, a fissure ~50 m long and ~5 cm wide opened up, followed about 8 hours later by vigorous fountaining thought to mark the arrival of the magma column. The depth of the magma front at the time of fissure formation is unknown, but if it propagated steadily for 8 hours at the slow pace of 1 cm/s it would have been 300 m. 2-D boundary element calculations for $d\sigma_n^0/dz = 12$ MPa/km and a magma front at 300 m at the time of instability indicate that the surficial thickness of the crack to first breach the surface is only ~5% of the maximum dike thickness, so 5 cm is not an unreasonable value for this scenario. The strike length of this crack appears to be roughly equal to the depth of the magma front.

16. Two processes that could restrict instability of the tip to much shallower depths should be mentioned here. If thermal stresses increase σ_n^0 to (for example) 12 MPa at repository depths, then $\Delta P_\lambda/\Delta P = 4$ for $\Delta P = 3$ MPa and at these depths the lag zone would be only ~10 m for $l=1$ km and ~1 m for $\Delta P=1$ MPa. Thus, a full accounting might require consideration of lag zones ranging from ~1 m to those that reach the surface before the magma front reaches the repository. Second, large-scale inelastic deformation ahead of the dike tip could increase σ_n^0, although perhaps not by as much as in the "hot repository" scenario. Large-scale inelastic deformation between the dike tip and the magma front could effectively do the same, although in this case a discontinuous lag-zone thickness would also result. *Observations of analog dikes in rock types and at depths similar to the repository, particularly in vertical sections, could shed light on the nature and likelihood of such inelastic deformation.*

G. Inelastic deformation before the dike arrival

The content of this section is adequately covered by paragraphs 1 and 2 below.

1. Relevance:

i. In the tectonic environment of the repository inelastic deformation is virtually certain to occur before the dike reaches the drifts. This deformation may be the first to directly impact the repository.

ii. Normal faulting ahead of the dike is likely to increase the horizontal compressive stress at the depth of the repository, thus shortening the lag zone and damping possible instability of the tip.

iii. Faulting that cuts one wall of the cavity will affect the properties of the lag zone and, if this occurs below the repository, the timing of events as seen by the repository.

iv. There is a chance that significant cracks will grow downward from the surface into the repository even before magma arrives at repository depths, setting up a potential magma pathway up the dike, through the drifts, and up the cracks to the surface. This possibility needs to be evaluated.

2. Two styles of inelastic deformation seem ubiquitous during shallow dike propagation: Earthquakes/faulting and ground cracking.

3. In Iceland, Afar, and Hawaii, geodetic data and field observations show that inward-facing normal faults can be activated up to several kilometers from dikes, with offsets that reach a substantial fraction of the dike thickness (see references in Rubin, 1992). Rubin and Gillard (1998) summarize observations indicating that earthquake size during dike intrusion tends to increase with elapsed time since the prior intrusion, up to the magnitude ~5.5 earthquakes produced during the 1874 intrusion at Askja, the first to enter that rift zone in 400 years. The inference is that the longer it has been since the prior intrusion increased S_h to the level of the magma pressure, the longer tectonic extension has had to bring the rock back to near the failure envelope. If dikes are intruded into regions that are already close to failure, large-scale fault slip can occur out to considerable distances (of the order of the dike length).

4. Because typical dike excess pressures are comparable to typical earthquake stress drops, and stress changes of this magnitude extend out to a sizeable fraction of the dike length, a dike-triggered magnitude 6 earthquake in the Basin and Range should not be a surprise. Because earthquakes this size are not thought to represent a hazard to the repository directly, we discuss them only in the context of how they may affect the dike.

5. Because of the low confining pressure at shallow depths and the stress-concentrating ability of the free surface, shallow normal faulting can occur while the dike tip is still at considerable depth. The primary effect of such faulting will probably be to alter the "ambient" stress field as seen by the dike when it arrives. Stress changes due to normal fault slip are spatially variable, but in general there is an increased horizontal stress adjacent to the fault that is a substantial fraction of the stress drop (Figure A2-4). As was noted above, this could increase σ_n^o at the level of the repository and shorten the lag zone. However, it might also be possible for faulting to decrease σ_n^o at the level of the repository, if thermal stresses are large enough to suppress normal faulting at that depth but faulting occurs above or below (in general the horizontal stress is decreased above the top or below the bottom of a normal fault). In this case the stresses will most likely not be reduced to pre-repository levels (because then the mechanism for suppressing faulting would be lost).

6. In normal faulting regimes the differential stress might increase at ~8-10 MPa/km, so at depths of >1 km stress changes of a few MPa should not alter the principal stress directions substantially. At repository depths this is not so clear but this can be checked (if the principal stress changes due to faulting are mostly horizontal and vertical at repository depths, then the principal stresses will not rotate but may interchange at sufficiently shallow depth).

7. If the dike tip hits a normal fault and induces slip on the updip side, or if such slip occurs after the dike tip has passed, this can effectively isolate the rock above from the dike-induced tensile stresses that would otherwise have promoted continued propagation of the tip. Propagation could temporarily be halted, and the magma front would approach the dike/fault intersection. This increases the tensile stress locally, to which the rock could respond by renewing propagation of the dike tip, by increasing the fault slip, or both. If fault slip completely closes the cavity above the intersection, the magma front eventually hits the fault, continued flux from below increases the magma pressure, and propagation might (at least locally) cease entirely or proceed up along the

fault. Inelastic deformation of this sort is something of a "wildcard", and could interfere with the tip instability described in section E. Note, however, that (at least away from the surface) reducing the horizontal stress by ΔP_λ within the lag zone also reduces the vertical stress by the same amount (Rubin, 1993). That is, even though passage of the lag zone brings the adjacent rock closer to failure, it does not do so by as much as one might expect using the intuitive notion that the vertical stress remains unchanged. In fact, the near-tip stress field is such that it is difficult to form "new" faults in competent rock (as opposed to producing slip on existing faults) during propagation (Rubin and Gillard, 1998). The common observation that dikes cutting cinder cones result in a "keystone block" dropping into the dike cavity and apparently blocking the flow might reflect a very shallow phenomenon.

8. The other common form of inelastic deformation to accompany shallow dike intrusion is the creation of tensile cracks at the surface. These often take the form of paired crack sets that are either quasi-parallel and located symmetrically on both sides of a fissure eruption, or that diverge from the ends of a fissure eruption (Pollard et al., 1983; Mastin and Pollard, 1988; Rubin, 1988; Greely et al., 1977). Pollard et al. (1983) noted that because of the free surface, the horizontal surface stress directly above a vertical dike is zero, and that maxima in the surface tensile stress occur on either side of the dike. The separation between these maxima decreases and their magnitude increases as the dike tip approaches the surface. For a uniform excess pressure, the tension exceeds the excess pressure when the depth of the top is less than ~1/4 of the dike height. That crack sets are observed to diverge from the ends of eruptive fissures was interpreted by Pollard et al. to be indicative of the increasing depth to the dike top with increasing distance from the eruptive portion of the dike.

9. When the dike top is much shallower than the dike bottom, the distance from the computed tensile maximum to the dike plane very nearly equals the depth of the dike top (the agreement appears to be exact for a dislocation extending to minus infinity from a given depth beneath the surface of a half-space). Using analog models consisting of a flour/sugar "crust" and cardboard "dike", Mastin and Pollard (1988) observed the spacing between the cracks to range from the expected value of twice the depth to the dike top to as little as 20% of that value. They interpreted this as indicating that inelastic deformation effectively reduced the depth of the dike top. A lag zone between the magma front and the dike tip represents one idealized manifestation of such inelastic deformation. Boundary element models show that for a constant pressure "dike" with an underpressured "lag zone" such that $K=0$, the separation between the tensile maxima is equal to that expected for a constant-pressure dike with a top somewhere between the magma front and the crack tip (as might have been anticipated). Thus, for a more-or-less constant excess magma pressure below a lag zone/zone of inelastic deformation, the numerical and analog models suggest that the depth of the magma front when the tensile cracks form is at least half the crack separation.

10. The ~constant pressure dike may be a reasonable quick approximation for a dike rising beneath Yucca Mountain, but the case of a laterally-propagating dike might be more relevant to the interpretation of existing observations. For laterally-propagating dikes a more appropriate loading configuration might be an excess pressure that decreases linearly from the dike center to an underpressure at the dike top and bottom sufficient to drop K to zero. Boundary element models show that the separation between the tensile maxima in this case is 4.4 times the depth to the dike top, so the depth to the magma front/dike tip at the time of crack formation might be only ~20-25% of the crack separation. This substantial difference from the results in paragraph [9] may be rationalized by recognizing that a constant-pressure dike has a rather uniform thickness except near the ends, so the dislocation solution is not a bad approximation, while a peaked excess pressure at the dike middle effectively adds some deeper dislocations, spreading the tensile maxima apart.

11. Paired crack sets above the 1984 dike intrusion at Mauna Loa diverge from the ends of the eruptive fissure and reach a maximum separation of 300 m (Rubin, 1988), suggesting that they formed when the magma front was ~70 m deep (assuming a pressure distribution appropriate for lateral propagation). Paired crack sets surrounding an eruptive fissure in the King's Bowl Lava

Field on the Snake River Plain are separated by 1.6 km, suggestive of formation when the magma front was ~350 m deep (for the laterally-propagating case) or ≥800 m deep (for the constant magma pressure case). (Because the growth of these cracks was not witnessed, there is some small chance that they were not produced by the dike they parallel. They are partially covered by lava from the eruptive fissure, so clearly they predate that flow and postdate the flow in which they are located. *We assume that such cracks in the surrounding flows are rare enough that their association with the fissure eruption is unlikely to be fortuitous; this could be checked.*)

12. Above a rising dike the expected scenario is the following: Because the surface has both low confining pressure and maxima in tensile stress changes due to the dike, cracks initiate at the surface and propagate downward. As a dike rises the tensile stresses at the surface ultimately reach the tensile strength of the rock, at which point crack growth begins. This growth actually imparts a significant compression to the region between the crack sets (Mastin and Pollard, 1988; Rubin, 1988). This compression suppresses the formation of new cracks, providing a partial explanation for why fissure eruptions often occur between well-defined crack sets, rather than within a region of continuous cracking produced as the dike tip rises. A related result is that the tensile cracks preserve most of their initial thickness as the dike top rises to quite shallow depth, even in elastic models that would allow them to close. Compression between the paired crack sets was the explanation provided by Mastin and Pollard (1988) for the small surficial pressure ridge they sometimes observed above the dike in their flour/sugar models, and the explanation provided by Rubin (1988) for why large preexisting fractures between the paired crack sets formed by the 1984 Mauna Loa intrusion did not widen during that event (based upon their undisturbed fill). Both the observations of paired crack sets and the evidence of compression between them represent non-intuitive features whose consistency with elastic models increases the credibility of those models.

13. Of primary interest from the standpoint of a hazards analysis is the depth to which the tensile cracks extend. Rubin (1988) examined the particular case of a dike with a top at 100 m, bottom at 2.9 km, and a peaked driving pressure increasing linearly from -0.2 MPa at the dike top and bottom to 4 MPa at the dike center. The cracks, which were constrained to be vertical, were found to grow to a depth of 250 m (assuming negligible fracture toughness). Given the depth of the dike top inferred from the King's Bowl crack sets, the possibility of tensile cracks growing deeper than the dike top could be viewed as alarming, as this would generate a potential magma pathway up the dike, along many drifts for possibly hundreds of meters, and then up to the surface via the tensile cracks. However, the boundary conditions considered by Rubin (1988) were inappropriate in that the stress intensity factor at the dike top was so large that the dike top would not have been stable at the specified depth. On other words, if one is willing to artificially restrict the dike top from propagating, arbitrarily large (but unphysical) tensile stress concentrations can be produced at the surface. A corollary is that it is possible that tensile cracks are more a feature of laterally-propagating dikes rather than of vertically-propagating dikes. That is, having the magma be effectively negatively buoyant near the surface, with an underpressure over much of the dike top, could help stabilize the top while the excess pressure at depth produces quite large thicknesses that in turn impart considerable tension to the surface. For such thicknesses and more uniform stresses, the dike tip might have gone unstable at much greater depth, when the surface tensions were less.

14. To estimate the depth to which cracks may extend, we note that the dike-induced stress changes beneath the tensile maxima are rather uniform at depths shallower than the dike top (Figure A2-5). Assuming that this tension is added to an ambient compression that increases linearly with depth, cracks that do not extend as deep as the dike top are expected to propagate to a depth where the ambient compression is ~1.6 times the applied tension (assuming negligible fracture toughness) (Lachenbruch, 1961; Rubin, 1988). Recall from paragraph [11] of section F that for $l=1$ km the dike tip could be stable when the magma front was at 300 m depth for $\Delta P=2.4$ MPa. Recall also from paragraph [8] of this section that the tensile maxima exceed the dike excess pressure for tops shallower than roughly 25% of the dike half-height. For a tensile maximum of 2.4 MPa, the crack could be driven to a depth where the ambient compression was 3.8 MPa, or deeper than the

repository for $d/dz=12$ MPa/km. However, as was noted in paragraph [12] of section F, the free surface reduces the maximum stable ΔP, perhaps to 1.5 MPa, which would limit crack growth to lesser depths.

15. 2-D boundary-element calculations that include the free surface and that approximate the excess pressure as uniform except within the (zero-pressure) lag zone show that the maximum stable excess pressure for $l=1$ km and a magma front at 300 m is 0.76 MPa (for $d\sigma_n^0/dz=12$ MPa/km). (Similar calculations without the free surface show the maximum excess pressure for stability at 300 m is 1.2 MPa. The difference between this estimate of 1.2 MPa and the estimate of 2.4 MPa from paragraph [11] of section E is due to the neglect of viscous pressure losses in the boundary element calculation). The resulting change in horizontal stress is shown in Figure 8. The tensile maximum of 1.4 MPa (1.8 times the excess pressure) is located 330 m from the dike plane. When (vertical) crack growth is permitted, the cracks extend to 160 m depth, deep but not deep enough to impact the repository (fracture toughness neglected). Accounting for a viscous pressure drop would reduce the stress concetration at the dike tip more than the tensile maxima at the surface. This would allow for a larger tensile maximum for (larger ΔP) dikes on the verge of instability, so in the fully coupled problem the cracks could be expected to grow somewhat deeper.

16. *Future calculations of the growth of the tensile cracks from the surface should use the stress field computed from a calculation that includes (1) time-dependent propagation, (2) the effects of gas exsolution/expansion, and (3) the effect of the free surface*, as outlined in section E. Future calculations could also use a "maximum circumferential tension" or other criterion for crack growth that allows the cracks to choose their own path (although near-vertical growth is expected). In addition, it might be important to account for a reduction in the elastic stiffness of the rock at shallow depth (the surface strains are probably limited by the dike thickness, and since for a given pressure this is controlled largely by the elastic stiffness at several km depth, if the elastic stiffness is significantly less at shallow depth the tensile stresses will be less). Such a reduction in elastic stiffness might also inhibit the dike-tip instability discussed in section F.

17. As with the potential instability of the dike tip as it approaches the surface, the growth of deep tensile cracks could be "short-circuited" by dike-induced normal faulting. Because normal faults are expected to be near to failure to considerable depth, slip might be induced long before the dike tip gets close enough to the surface for the tensile maxima to exceed the rock tensile strength. At the surface of the foot-wall block (the block below the dipping fault), normal faulting produces compression ranging from over twice the fault stress drop where the fault cuts the surface to about 75% of the stress drop roughly one fault length from that intersection (Figure A2-4). For stress drops of a few MPa this could suppress surface tensions above a dike altogether. On the other hand, at the surface of hanging-wall block the horizontal stress (continuous with that of the foot-wall block at the fault intersection) decreases to zero about 1/3 of the fault length away from the intersection, and has a tensile maximum of more than 50% of the stress drop about 2/3 of the fault length away from the intersection. In the absence of secondary faulting, such tensions would assist the growth of any dike-induced tensile cracks in this region.

18. Modeling inelastic deformation away from the dike becomes tricky because the sequence of events affects the development of later events. While viscous flow provides a natural timescale for dike propagation, once fault slip or tensile crack growth begins only time-dependent failure mechanisms can prevent elastodynamic crack growth. One option using an elastostatic code is to propagate the dike, check the surroundings to see if a failure law is exceeded, and if so allow for growth of that feature to completion before checking the next failure law (e.g., $K=K_c$ at the dike tip), and finally allowing magma flow to continue. However, at shallow depths the magma may be so compressible that elastodynamic codes would be required to faithfully adhere to all the adopted failure laws. Given the large uncertainty in failure laws and boundary conditions (in both the rock and the magma), a more reasonable strategy would be to just examine a range of failure laws and boundary conditions.
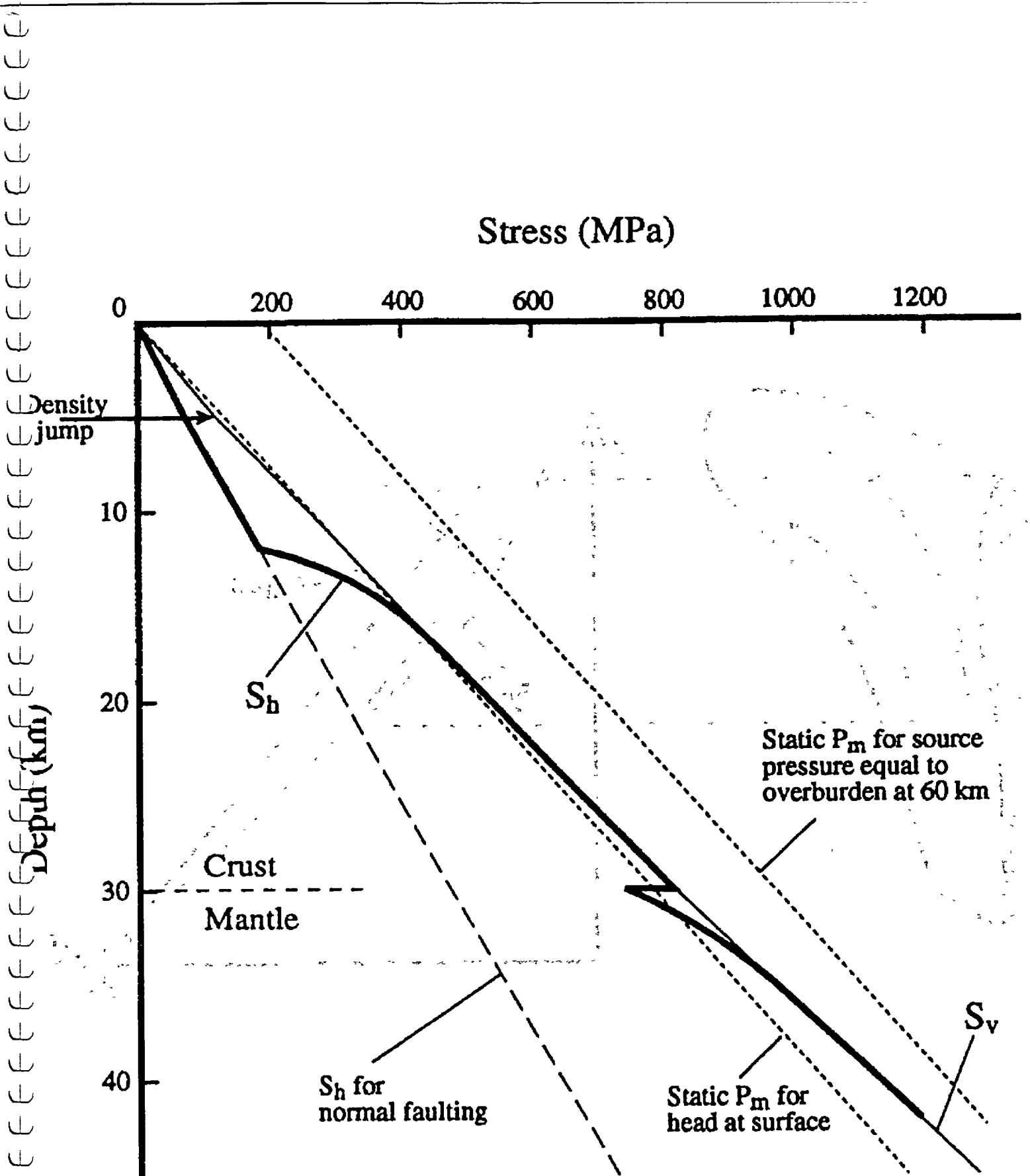
Figure captions

Figure A2-1. Hypothetical stress state, drawn to scale, for region undergoing horizontal extension. S_v, vertical stress; S_h, horizontal stress. Host rock density $\rho_r=2.3\times10^3$ kg m^{-3} above 5 km depth, 2.8×10^3 kg m^{-3} below 5 km depth, 3.1×10^3 kg m^{-3} within mantle. Reference magma pressure curves P_m are for magma density $\rho_m=2.6\times10^3$ kg m^{-3} . It is assumed that normal faults dipping at 60° are in state of incipient slip above brittle/ductile transition at 12 km depth, and that pore pressure is hydrostatic. Within middle to upper crust and at crust/mantle boundary, gradients in tectonic stress may be much more significant than magma buoyancy in determining dike propagation direction. From Rubin (1995a).

Figure A2-2. Cartoon showing lateral propagation of three-dimensional dike encountering the "effective" level of neutral buoyancy (LNB). Unvesiculated magma is effectively less dense than the host rock below the effective LNB but more dense above. The amount of overshoot (in the absence of sufficient vesiculation) increases with the excess pressure at the effective LNB, which for given material properties increases with the source flux.

Figure A2-3. Various dike attributes as a function of the tip cavity length normalized by the dike length. The dike has a unit excess magma pressure applied one unit length below the dike tip, but no magma buoyancy. Calculations assume quasi-steady propagation. Left panels are for a rock fracture toughness (normalized by the excess pressure and dike length^1/2) of 0.01 (roughly appropriate for laboratory values of the rock fracture toughness); right panels are for a normalized fracture toughness ten times larger. Dashed curves are for no vertical gradient in the dike-normal stress, solid curves are for gradients in the dike-normal stress (normalized by the excess pressure divided by the dike length) of 2, 4, 8, 16, and 32. In a time-dependent calculation the dike tip would be expected to go unstable at about the minima in the curves in the upper panel. See text for scaling. Curves end where interpenetration of the dike walls is implied.

Figure A2-4. Change in horizontal stress adjacent to a normal fault extending from the surface to unit depth. Stresses are normalized by the (uniform) fault stress drop. Stresses are generally compressive near the surface but tensions exceeding 50% of the fault stress drop occur at shallow depth within the hanging wall ~1 fault length from the fault trace.

Figure A2-5. Change in horizontal stress above a buried "dike" with a uniform excess pressure of 0.76 MPa from 0.3 to 2.3 km depth. The dike tip is barely stable (a pressure increase of 0.01 MPa would drive it to the surface) at 0.14 km depth. The tensile maximum at the surface occurs ~300 m from the dike plane and exceeds the dike excess pressure by ~40%.
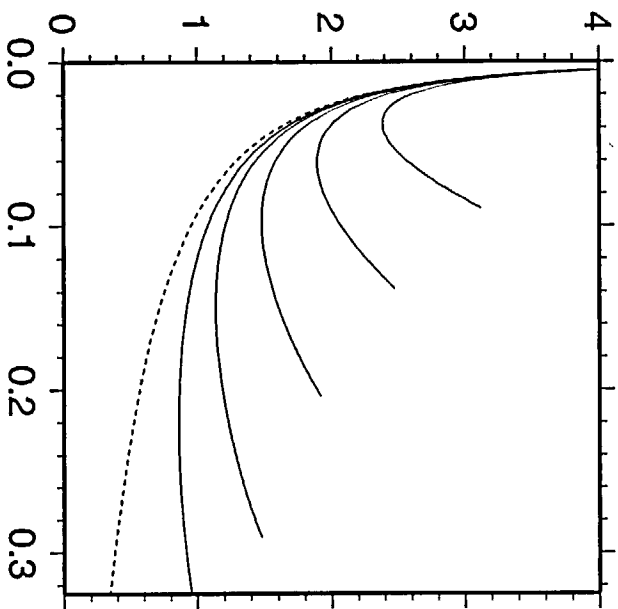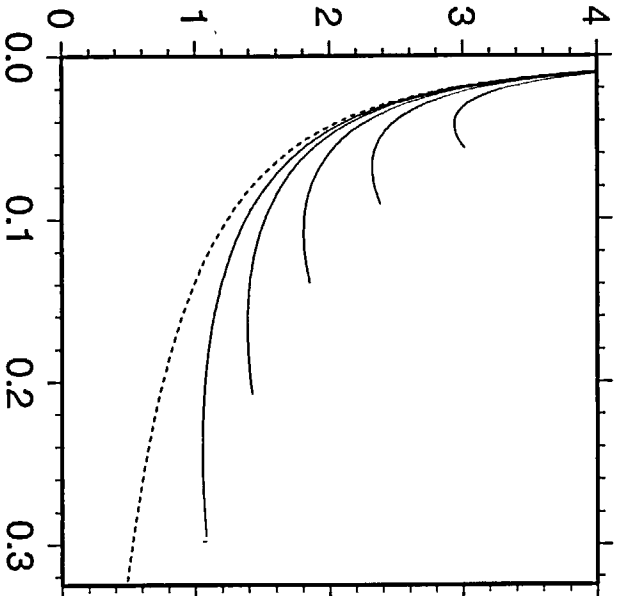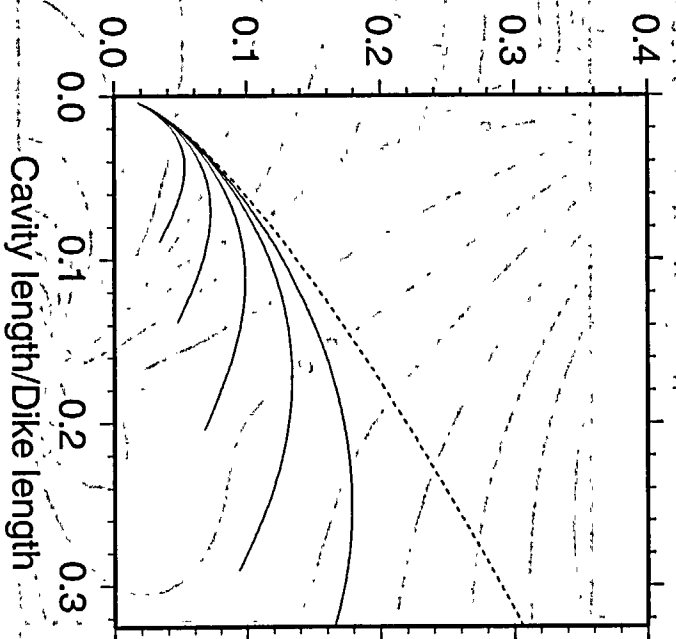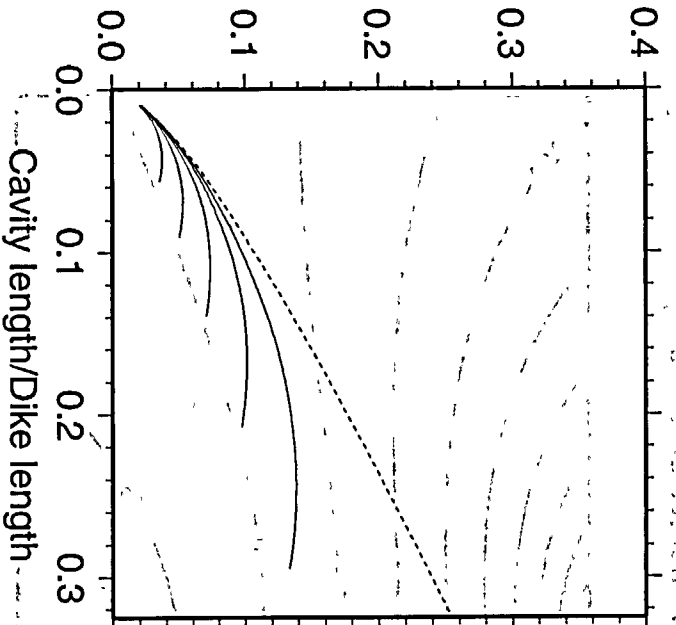
Figure A2-3

Magma front thickness/Dike thickness

Magma front suction/Source overpressure

Kc/DP.sqrt(l)=0.01

Kc/DP.sqrt(l)=0.1

Cavity length/Dike length

Change in horizontal stress (compression positive)

Figure A2-4
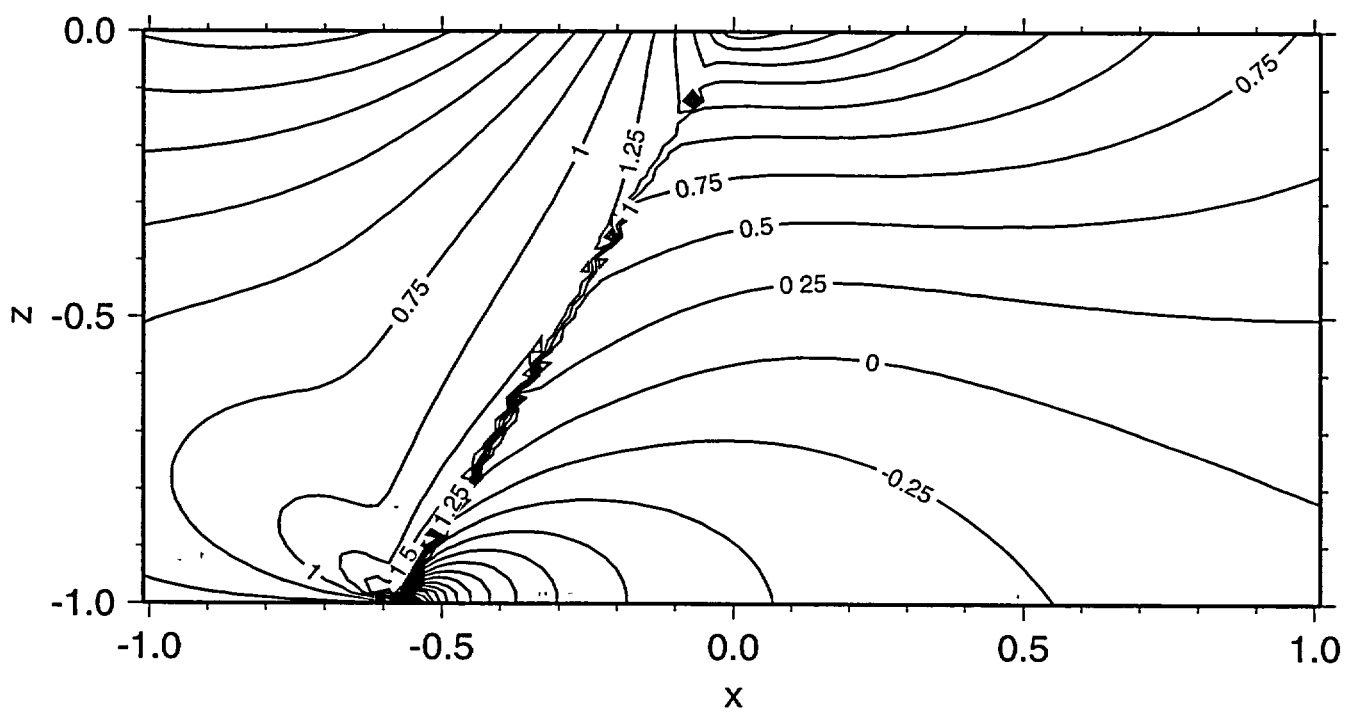
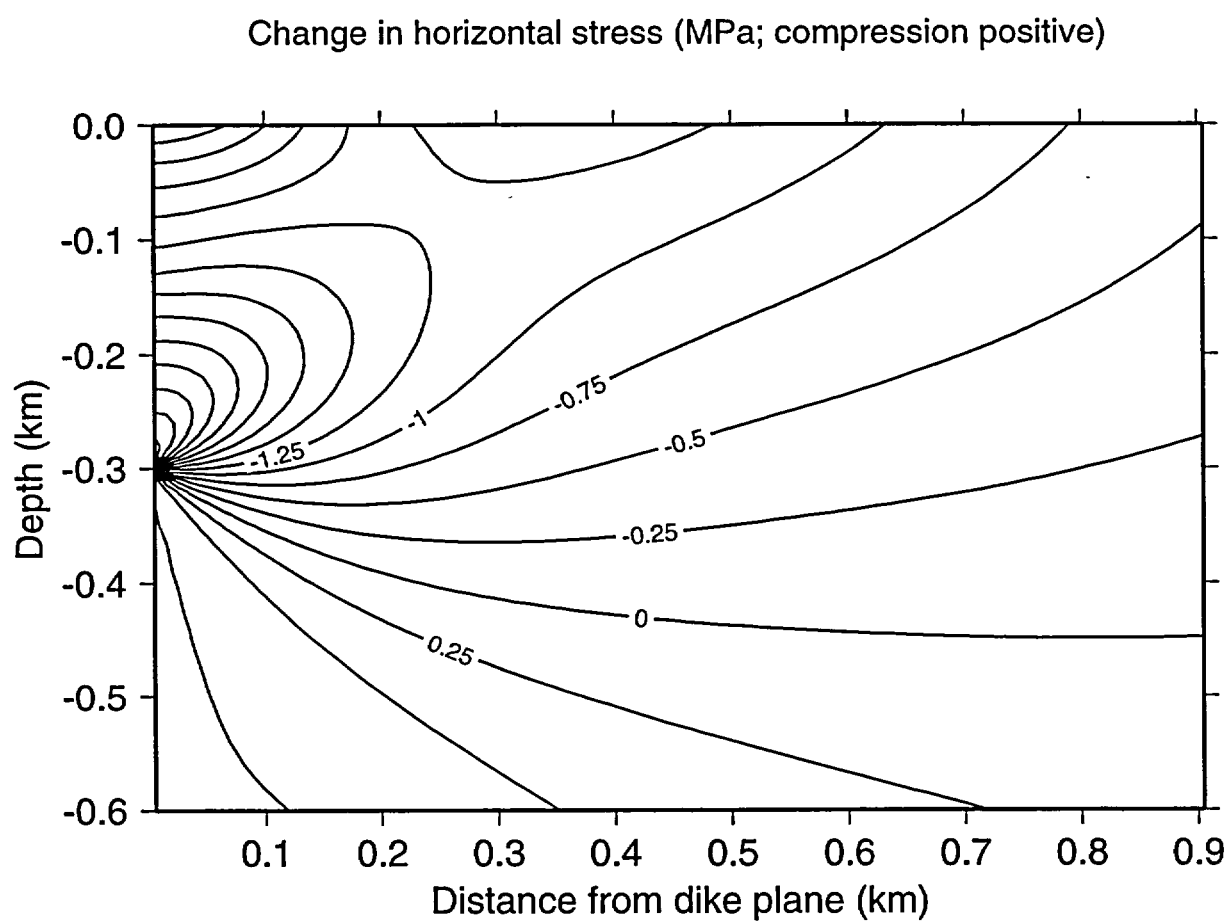Change in horizontal stress (MPa; compression positive)

Figure A2-5

Appendix 3
Uniformly Pressurized Penny-Shaped Fracture Parallel to the Free-Surface

(Version 1 -August 2002)

Consider a fluid-filled penny-shaped crack of radius R parallel to the free-surface of a semi-infinite elastic rock mass. Let σ_o denote the vertical normal stress at the depth H of the fracture. It is assumed that the fluid in the fracture is at a uniform pressure p_f, and that the crack is in limit equilibrium.

This appendix describes the equations needed to calculate the radius R and the net pressure $p = p_f - \sigma_o$, given the volume of fluid V_o inside the fracture and the following material constants of the rock: Young's modulus E, Poisson's ratio ν, and toughness K_{Ic}. Details of the analysis behind these equations is given by Zhang et al. (2002).

First, it is convenient to introduce the plane strain modulus E' and a toughness K', respectively proportional to E and K_{Ic}

$$E' = \frac{E}{1 - \nu^2} \qquad K' = 4 \left(\frac{2}{\pi} \right)^{1/2} K_{Ic} \tag{1}$$

Next, we introduce the toughness scaling (Detournay 2001) for the net pressure p, and the radius R

$$p = \varepsilon_k E' \Pi(\mathcal{R}), \quad R(t) = L_k \, \gamma(\mathcal{R}) \tag{2}$$

where ε_k a small parameter and L_k a lengthscale respectively given by

$$\varepsilon_k = \left(\frac{K'^6}{E'^6 V_o} \right)^{1/5} \qquad L_k = \left(\frac{V_o E'}{K'} \right)^{2/5} \tag{3}$$

and where $\mathcal{R}$ is the crack radius scaled by the depth H

$$\mathcal{R} = \frac{R}{H} \tag{4}$$

Let Π_o, γ_o, and $\mathcal{R}_o$ denote the solution for a fracture in stable limit equilibrium. It can be shown that $\mathcal{R}_o$ is obtained by solving the implicit equation (Zhang et al. 2002)

$$\frac{\mathcal{R}_o}{\gamma_*^{6/5}(\mathcal{R}_o) K_*^{2/5}(\mathcal{R}_o)} = \frac{L_k}{H} \tag{5}$$

1

and that

$$\Pi_o = \gamma_*^{-3/5}(\mathcal{R}_o)K_*^{-6/5}(\mathcal{R}_o), \quad \gamma_o = \gamma_*^{6/5}(\mathcal{R}_o)K_*^{2/5}(\mathcal{R}_o) \tag{6}$$

where γ_* and K_* are two known functions of $\mathcal{R}$ only, see Figs. 1 and 2. Polynomial fits of $\gamma_*(\mathcal{R})$ and $K_*(\mathcal{R})$, which are not known in closed form, are given by Zhang et al. (2002).

References

Detournay, E. (2001). Propagation regimes of fluid-driven fractures in impermeable rocks. In C. Desai, T. Kundu, S. Harpalani, D. Contractor, and J. Kemeny (Eds.), *Proc. 10th Int. Conf. on Computer Methods and Advances in Geomechanics*, Volume 2, Rotterdam, pp. 1277–1288. Balkema.

Zhang, X., E. Detournay, and R. Jeffrey (2002). Propagation of a penny-shaped hydraulic fracture parallel to the free-surface on an elastic half-space. *Int. J. Fracture 115*, 125–158.
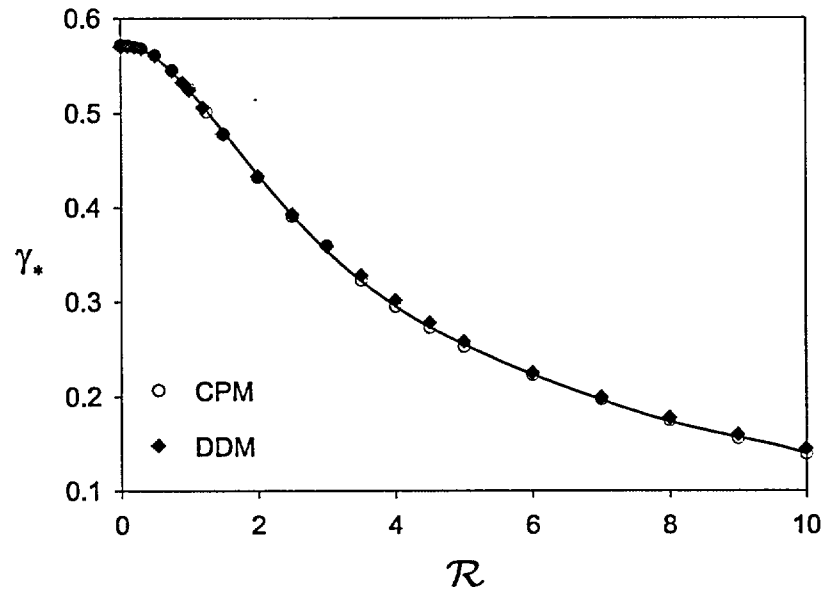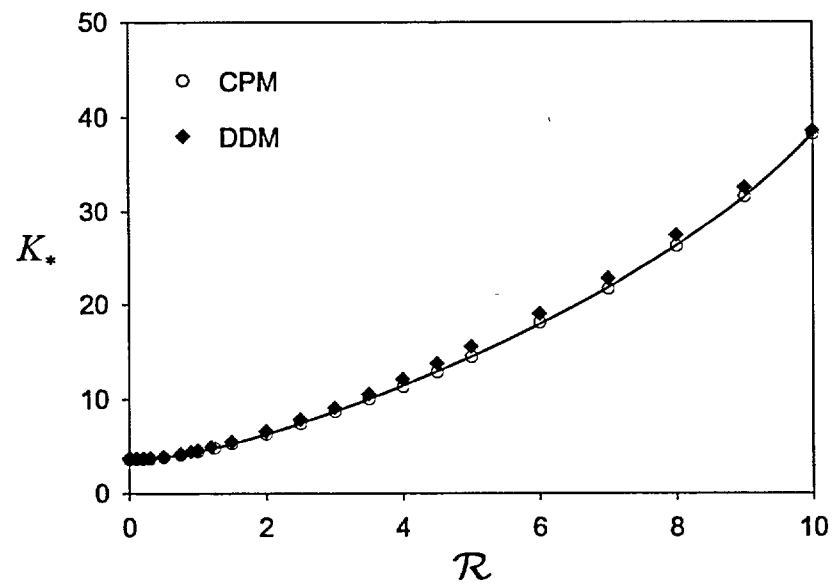
Figure 1: Function $\gamma_*(\mathcal{R})$

Figure 2: Function $K_*(\mathcal{R})$

3